SECONDARY FLOW IN A CASCADE OF AIRFOILS

Thesis by

Richard H. Briceland

In Partial Fulfillment of the Requirements

For the Degree of

Doctor of Philosophy

California Institute of Technology

Pasadena, California

1959

ACKNOWLEDGEMENTS

The author wishes to acknowledge with gratitude the encouragement and advice which were received from Professor W. D. Rannie during the course of this research project.

Special thanks are also due to Mr. F. Tyler Linton for his assistance both in collecting experimental data and in preparing the drawings for this report.

I also wish to express my appreciation to Mrs. Ingrid Stenberg for aiding with the computations and to Mrs. Roberta Duffy for typing the manuscript.

The project was sponsored by the Office of Naval Research, under Navy Contract Nonr-220(23).

ABSTRACT

Secondary flows were studied experimentally in a diffusing cascade. A family of screens were installed ahead of the blade row at the midspan position to produce a controlled distortion of the upstream velocity profile. In this way it was possible to focus attention on those regions of the flow field which were distant from the tunnel walls and to thereby restrict the investigation to a study of small disturbance phenomena.

It was found that the general behavior of the flow at the cascade exit plane was satisfactorily described by a modified channel-theory analysis in which a simple iterative correction was included to account for the spanwise self-transport effects of the induced secondary flows.

Two methods are proposed for evaluating the spanwise distribution of blade loading when the approach velocity into the cascade is non-uniform; these methods were tested experimentally and were found to give results which were in good agreement with measured data.

TABLE OF CONTENTS

SUMMARY

In early experimental investigations dealing with axial flow compressors, it was found that performance could be significantly influenced by the boundary layers along the internal surfaces of the inlet flow passages. More specifically, it was observed that low energy boundary layer fluid in moving through a blade row tended to cause flow distortions which were not necessarily confined to the boundary layers themselves. To study these effects experimentally, a two-dimensional cascade of airfoils was used to simulate a row of compressor blades. The particular problem of interest is to attempt to predict the flow perturbations which occur in and downstream of the cascade when the velocity profile ahead of the blades is distorted by a shear disturbance from its normal pattern. These flow perturbations emanating from upstream velocity disturbances are referred to as "secondary flows", and it is with their determination that the thesis deals.

Although the detailed quantitative behavior of secondary flows can best be studied by working directly with the vorticity equations, the general physical interpretation of these flows can be visualized most readily from the following simplified analysis. Consider a given cascade of airfoils and assume that the upstream flow field is initially uniform, i.e., that the velocity profile is not distorted by boundary layers or by external disturbances.

As this flow passes through the blade row and is turned, a pressure field is established in accordance with the condition for irrotational motion; for example, the pressure gradient necessary to balance the centrifugal force set up by the cascade turning is given

by $\frac{\partial p}{\partial n} = \frac{\rho q^2}{R}$ where "n" is the direction normal to the streamline, "q" is the magnitude of the velocity, and "R" is the local streamline radius of curvature. Suppose now that the velocity is reduced upstream over a small fraction of the blade height, but that the extent and magnitude of the change are not sufficient to substantially alter the pressure distribution that was established previously. As a mass of this low velocity fluid moves through the cascade vanes, its response to the prescribed pressure gradient is such that it is turned through a larger angle than is the surrounding flow. Consequently, the streamlines of the restricted flow may be significantly different from those of the undisturbed flow; the corresponding perturbations which are superposed on the original fluid motion represent an example of secondary flows.

Secondary flows in cascades have been investigated experimentally in the last two decades by studying the flow perturbations which result when boundary layers from the tunnel walls pass through the turning vanes. Early attempts to analyze these effects dealt primarily with the so-called "airfoil-theory" approach in which the individual blades of the cascade were treated as isolated airfoils represented by lifting lines. This procedure was not satisfactory, and little success was achieved in predicting the quantitative behavior of the induced secondary motion prior to the introduction of the "channel-theory" model by Squire and Winter in 1948. In this approach the authors chose to treat each blade passage as an independent channel by supposing that the turning vane surfaces were extended downstream of the actual trailing edge plane. Attention was then focused on the distribution of vorticity in the straight channel far downstream of the blade row; in particular, when the flow ahead of

the cascade has a component of vorticity normal to the mainstream direction, such as might be found along the upstream tunnel wall boundary layers, then a streamwise component of vorticity is produced as the flow passes through the turning vanes. It is this generated vorticity which is responsible in the channel-theory model for the existence of the induced secondary flows.

Squire and Winter used linearized techniques to determine the magnitude of the distributed streamwise component of vorticity; they subsequently found approximate solutions for the corresponding induced velocity field and then carried out experimental studies to test the validity of the proposed model. The secondary flows that were investigated in this program were those emanating from boundary layer distortions of the upstream velocity profile, and, while sufficient agreement was achieved between theoretical and experimental results to indicate that the analysis was indeed useful, the method was nevertheless not entirely satisfactory from a quantitative point of view. A primary objection to the experimental work of Squire and Winter, and later Hawthorne and Armstrong, is that their investigations were restricted to studies of boundary layer flows. Because the non-uniformities in the upstream velocity profile are generally quite severe in the boundary layers along the tunnel walls, the resultant induced flows tend to be considerably larger than perturbation quantities and, as such, are not directly amenable to analysis by a linearized theory.

In the current investigation, the secondary flows were deliberately isolated from the large disturbance boundary layer effects by using a family of screens to produce distortions in the upstream velocity profile at the mid-span position. By varying the density and

the size of the screen obstruction elements, it was possible to produce controlled variations in the approach flow and to thereby obtain an important degree of flexibility which was not previously available. The screen strips which were used in these studies extended completely across the tunnel and covered approximately the center ten per cent of the blade height. Extensive tests were made for screen configurations which produced maximum velocity deficiencies at the center of the wake equal to 11, 31, and 53 per cent respectively of the undisturbed freestream velocity.

The usefulness of the channel-theory model as a means for predicting the behavior of small disturbance secondary flows was studied by comparing the measured and the calculated distributions of the induced spanwise component of velocity downstream of the cascade. It was found that good agreement was achieved between theory and experiment only when the self-transport properties of the secondary flows were included in the analysis. A simple iterative method of incorporating these effects is proposed; this suggested approach was found to be adequate as long as the induced velocities remained small.

An important assumption in the linearized channel-theory analysis is that upstream fluid surfaces which are originally perpendicular to the spanwise direction tend to remain horizontal planes as they move through the blade row. This hypothesis was tested and was found to be valid when the secondary velocities were small; for those cases in which the induced velocities become somewhat larger than perturbation quantities, a simple method is given for predicting the amount of streamsurface warpage.

The good agreement found between the experimental and the theoretical results indicates that the channel-theory model is indeed a useful concept for the quantitative study of secondary flows. Moreover, because the behavior of the induced flow was described satisfactorily by the linearized analysis, it is possible to derive two methods for predicting the spanwise variation in blade loading when the approach velocity upstream of the cascade is non-uniform.

In the first derivation, the distribution in bound circulation is evaluated and the blade lift is then calculated by assuming that the flow is locally two-dimensional along the span. This approach was found to be somewhat sensitive to the self-transport effects of the secondary flows; however, comparison of experimental and theoretical results shows that it is a useful analysis if the induced velocities are sufficiently small. In the second derivation, the linearized channel-theory analysis is first used to define the velocity field downstream of the cascade, and the variation in blade loading is then calculated by finding the change in momentum of the fluid as it moves through the turning vanes. This method was also tested experimentally, and good agreement was again found between the measured and the predicted results.

SYMBOLS

c	Blade chord
F	Blade force
g	Blade gap
h	Spanwise half-width of screen element
p_s	Static pressure
$P_{atm.}$	Atmospheric pressure
P_t	Total pressure
q	Velocity magnitude
$q_{wake_{max}}$	Minimum value of the upstream velocity in the wake of the screen
R	Streamline radius of curvature
U	Primary flow velocity
s, n, z	Orthonormal coordinates in the streamwise, radial, and spanwise directions respectively
u, v, w	Secondary velocity components in the s, n, z directions respectively
x, y	Coordinate directions perpendicular and parallel to the cascade axis respectively
v_x, v_y	Components of total velocity in the x, y directions respectively
v_s, v_n	Components of total velocity in the s, n directions respectively
α, β, τ	Dimensionless coordinates parallel to the s, n, z axes respectively
γ	Angle that the velocity vector makes with the x-axis
Γ	Circulation
Γ_v	Bound circulation along the cascade vanes
ρ	Air density
ϕ	Velocity potential

ϕ, ψ, z	Orthoginal coordinates parallel to the s, n, z axes
$\omega_1, \omega_2, \omega_3$	Components of vorticity in the s, n, z directions respectively
$\vec{\Omega}$	Vorticity vector
$\vec{q}$	Velocity vector
$\vec{i}, \vec{j}, \vec{k}$	Unit vectors in the s, n, z system

Subscripts

0	Upstream reference station
1	Upstream point
2	Downstream reference station

I. INTRODUCTION

1:1 DEFINITION OF SECONDARY FLOW

In the literature dealing with the flow of fluids around bends and through blade rows, the term "secondary flow" has been used extensively to describe the flow perturbations which result from such diversified phenomena as viscous and non-viscous boundary layers, moving walls, non-uniform temperature and entropy distributions, separation, and tip clearance flows. Therefore, it is desirable to indicate exactly how this term will be employed in the following discussion.

In this report, the term "secondary flow" will be used in connection with the flow of air through a subsonic, rectangular, diffusing cascade; in particular, it will be used to describe the changes which occur in the cascade flow field when the velocity profile upstream of the blade row is distorted from its normal shape by installing strips of screening ahead of the turning vanes. In keeping with this definition, the term "primary flow" will be introduced to describe the flow field that exists in the absence of all externally produced upstream velocity distortions.

1:2 ORIGIN OF SECONDARY FLOWS

The origin of secondary flows can be shown qualitatively as follows: consider first the two-dimensional flow of an incompressible, non-viscous fluid through the rectangular cascade illustrated in figure 1. Suppose that the velocity profile far upstream is initially uniform and that a mean streamline is turned by the cascade through some flow angle $\theta_1^* - \theta_2^*$, (figure 2). In accordance with the condition for equilibrium in the "n" direction, there then exists a pressure gradient

perpendicular to the mean streamline given by:

$$\frac{\partial p^*}{\partial n} = -\rho q^* \frac{\partial q^*}{\partial n} = -\frac{\rho q^{*2}}{R^*} \qquad (1.1)$$

where R* is the radius of curvature of the streamline.

Suppose that the velocity profile far upstream is then distorted to the form shown in figure 3 by installing a strip of screening which extends parallel to the cascade; here it is assumed for simplicity that this profile shape is functionally dependent only on "z", and does not vary at successive stations in the "n" direction. Let it further be assumed that both the magnitude and the spanwise extent of the velocity distortion is small enough so that the pressure field remains everywhere independent of "z". Consider then a slug of fluid from the wake region as it passes through the cascade. The normal equilibrium condition for this flow is given by:

$$\frac{\partial p}{\partial n} = -\rho q \frac{\partial q}{\partial n} = -\frac{\rho q^2}{R} \qquad (1.2)$$

But $\frac{\partial p}{\partial n} = \frac{\partial p^*}{\partial n}$ by assumption; thus

$$\frac{q^2}{R} = \frac{q^{*2}}{R^*} \qquad (1.3)$$

from equations 1.1 and 1.2.

Moreover, since $\frac{\partial p}{\partial n} = \frac{\partial p^*}{\partial n}$ in the wake, equation 1.3 implies that the radius of curvature of a typical wake mean streamline is less than that of a streamline in the two-dimensional flow, and, therefore, that the flow in the wake region tends to be turned more than the two-dimensional

flow (figure 4). Furthermore, this "overturning" of the wake flow as it passes through the cascade tends to produce a circulatory type of motion because of the wall-like boundary restrictions of the blade elements. Viewed from a station just aft of the trailing edge and looking upstream, the nature of this motion is shown in figure 5.

The circulatory flow sketched in figure 5 is characteristic of the fluid motion that is superposed on the two-dimensional cascade flow as a result of the upstream velocity profile distortion, (figure 3). This induced motion is, therefore, the secondary flow which corresponds to the simplified qualitative model under consideration.

1:3 ANALYTIC MODELS FOR SECONDARY FLOW STUDIES

In examining the work which has been done in the study of secondary flows, it is convenient to discuss separately those analyses which deal with real fluid theory and those which are based on perfect fluid models. In the real fluid category, the contributions of Herzig and Hansen (1) and Mager (2) are noteworthy; here, attention is focused on the role of viscous effects in the boundary layer regimes of the flow field as the fluid is turned by the cascade. In the second category, a flow with a non-uniform upstream velocity field is assumed to proceed through the turning vanes in accordance with non-viscous perfect fluid theory. Here the problem of secondary flows has been studied on the basis of both airfoil-theory and channel-theory; the characteristics of these two conceptually different models are described in the following paragraphs.

1:3.1 THE AIRFOIL THEORY

Consider again the rectangular cascade of figure 1, and suppose

that the velocity profile far upstream is of the type illustrated in figure 3. In the airfoil-theory model, the individual vanes of the cascade are treated as isolated airfoils and a trailing vortex lattice corresponding to a spanwise variation in blade circulation is assumed to be shed in accordance with classical lifting line theory. The secondary flow is then regarded as the velocity field which is induced by this vortex array. The fundamental disadvantage with this approach is that neither the blade circulation nor loading is known a priori, and that the contribution to the trailing vortex sheet from this source is therefore undetermined. Also significant is the fact that this method fails to give quantitative information about the details of the flow in the cascade passages.

1:3.2 THE CHANNEL THEORY

The channel-theory model for the determination of secondary flows was first introduced by Squire and Winter (3) in 1948. Because of the fact that the fundamental ideas presented in their paper have been used extensively by various authors in attempting to predict the quantitative behavior of secondary flows, it is worthwhile to discuss the important features of this model. In the channel-theory approach, the boundary of the passage which is formed by two adjacent blades is thought of as being extended both upstream and downstream of the vanes along mean streamlines of the primary flow as is shown in figure 6. The problem is to determine the velocity field throughout this hypothetical channel when the upstream flow is prescribed and when the extended walls, which are defined by the streamsurfaces of the primary flow, are also assumed to be streamsurfaces for the secondary

motion. Two basic methods of solving this problem have been proposed: the first of these was given by Squire and Winter (3) and was based on a perturbation scheme utilizing the linearized vorticity equations; the second approach was introduced by Preston and involved following a vortex filament kinematically through the blade row. The essential features of these two methods of solution are described in the following paragraphs; also included are pertinent remarks concerning some particular modifications which have been advanced by other authors.

1:3. 2. 1 Solution by Linearized Vorticity Equations

Consider the hypothetical channels shown in figure 6 and assume that the upstream flow contains a velocity gradient in the spanwise direction only. Squire and Winter first wrote the vorticity equations in linearized form and then integrated along streamlines to find expressions for the components of vorticity as functions of the turning angle and the upstream rotation. The secondary flow velocities were assumed to be so small that they did not influence the primary flow, and the undisturbed streamlines were assumed to be concentric circular arcs which remained parallel to the plane of the channel. Under these restrictions, it was found that the streamwise component of vorticity at the exit of the cascade was equal to $-2\epsilon \frac{dU_o}{dz}$, where "$\epsilon$" is the turning angle of the vanes and $\frac{dU_o}{dz}$ is the strength of the upstream vorticity. Squire and Winter assumed that the streamwise vortex lines were carried down the extended channel by the primary flow, and the authors subsequently determined an approximate solution for the secondary flow from this distributed vortex array.

Hawthorne (8) later employed the linearized vorticity equations to give a three-dimensional theory which was applicable to isolated airfoils and curved channels as well as to cascades.

Loos (6) presented a modified version of the Squire and Winter type of linearized channel theory by incorporating self-transport effects of the perturbation velocities into the model; this approach was made in an attempt to describe an analytical system which accounted for the so-called "vortex roll-up" which was often found in conjunction with the boundary layer regimes of cascade flows.

1:3. 2. 2 Solution by Vortex Filament Kinematics

A second method of solution of the channel-theory problem was introduced by Preston (4) and is discussed extensively by Hawthorne (5), Soundranayagan (9), and Smith (10). In these analyses, the upstream flow is again assumed to have a velocity gradient only in the spanwise direction and consequently to have vortex lines extending perpendicular to the mainstream flow as is shown in figure 7. The movement of a particular vortex filament is then followed kinematically through the blade row under the assumption that the perturbation velocities do not affect the mainstream flow. Preston observed that the magnitude of the velocity along the outer "pressure surface" wall was less than that along the inner "suction surface" wall and thereby reasoned that the vortex-filament is distorted as it is carried through the channel, (figure 7). Because of this distortion which accompanies a turning of the primary flow, a component of vorticity is generated in the streamwise direction. It has been shown that the magnitude of this vorticity is approximately the same as is its value when computed by the Squire and Winter type of channel analysis which was discussed

previously; the secondary velocities which correspond to the distributed vorticity in this extended channel are, therefore, the same in both cases.

An additional significant feature of the kinematical analysis is that it provides a means of obtaining information about the vortex sheet which exists just downstream of the cascade trailing edge. In particular, it is possible to estimate, under certain rather stringent restrictions, the contribution to the vortex sheet which is due to a shedding of bound vorticity from the blades and also the contribution which arises from the distortion of the vortex filament (see b'b'' in figure 7). This feature of the analysis is considered further in a later section.

1:4 RESULTS OF PREVIOUS EXPERIMENTAL INVESTIGATIONS

Although the effects of secondary flows have been observed for many years in both cascades and compressors, very little systematic experimental data was published prior to the report of Squire and Winter (3) in 1948. Since that time, numerous other authors have carried out extensive investigations in attempting to verify particular secondary flow theories and hypotheses. Before outlining the objectives of the present paper, a partial review of the results of past experimental studies will be given.

Squire and Winter tested the basic channel-theory model by comparing the magnitudes of the measured and the analytically calculated spanwise components of velocity near the exit of a rectangular cascade. The upstream vorticity was first evaluated from velocity measurements in the boundary layer of the approach flow, and the streamwise component of vorticity at the trailing edge was determined from the theory; the spanwise velocity corresponding to this vorticity was then computed.

The velocity field so determined was compared with the measured spanwise velocity near the trailing edge; while not completely satisfactory, the agreement between theory and experiment appeared to be sufficiently adequate to verify the validity of the linearized analysis.

Hawthorne and Armstrong (5) also considered the validity of the channel-theory model by carrying out an investigation using a turbine nozzle cascade. Here the secondary flows corresponding to both a thin and an artificially thickened boundary layer were studied. As in the earlier Squire and Winter experiments, Hawthorne and Armstrong tested the channel-theory model by comparing the computed values of spanwise velocity with the values which were measured experimentally. In addition, the authors used the previously outlined kinematical approach of Preston to determine the contribution to the trailing edge vortex sheet which resulted from distortions of the upstream vortex filaments. They then estimated the variation of shed bound vorticity along the span and thereby attempted to calculate the distribution of blade loading on the basis of two-dimensional lifting line principles. In their work with a thin upstream boundary layer, Hawthorne and Armstrong found no agreement between the results of theory and experiment. Here it was discovered that the channel boundary layer flow was swept onto the suction surface of the adjacent wall where it rolled up into a concentrated vortex core.

In their investigations with the artificially thickened wall boundary layer, the authors found only moderate agreement between theory and experiment. One difficulty which was encountered in this work, however, was that the "boundary layer" of the approach flow extended all the way to the center of the span, and hence there was no region of

strictly two-dimensional motion; consequently, the authors had no zone of primary flow which could be used as a reference plane for distinguishing between the induced and the undisturbed flow fields.

Hansen, Herzig, and Costello (11) and Kofsky and Allen (12) carried out a series of experiments designed to furnish qualitative information about the behavior of secondary flows. These authors made extensive studies using smoke injection methods to observe the characteristics of boundary layer flows in both compressors and cascades. Many instances of severe primary flow distortion and vortex core roll-up were recorded; the reader is referred to reference (11) for photographs of these phenomena.

1:5 OBJECTIVES OF THE CURRENT STUDY

Although moderate correlation between theoretical and experimental results has been achieved in some instances, attempts to predict the behavior of secondary flows have generally been quite unsatisfactory. In fact, the linearized channel-theory model has often failed to indicate correctly even the qualitative nature of the disturbance flow. The reason for this lack of agreement appears to be that the assumptions inherent in a perfect fluid perturbation analysis are actually often not applicable to the type of experiment which has been carried out to test the validity of the theory. For example, the induced secondary flow velocities are assumed to be perturbation quantities relative to the primary flow; this assumption is not substantiated in the experimental investigations of references (5) and (7), and there is a corresponding invalidation of the hypotheses regarding the distortion of the main flow field and also the self-transport of vortex filaments.

One objective of the current investigation was, therefore, to evaluate experimentally the linearized, perfect fluid, channel-theory model by conducting a series of tests which did not violate any of the fundamental hypotheses upon which the theory itself was based. A second equally important goal of this investigation was to study the nature of the trailing edge vortex sheet and attempt to predict the spanwise variation of cascade loading when the approach flow was non-uniform. As was previously indicated, the secondary flows which have been studied experimentally in the past have been those that were caused by boundary layer distortions in the upstream velocity field. In contrast to this, the secondary flows observed in the current tests were those resulting from upstream velocity gradients which were concentrated approximately midway between the floor and the top of the cascade tunnel and which were, therefore, wholly independent of the natural boundary layer profile, (figure 3). Moreover, both the magnitude and the spanwise extent of the approach velocity non-uniformity were easily varied, thus permitting, in these experiments, an important degree of control which was not previously available to other investigators.

II. THEORETICAL PREDICTION OF SECONDARY FLOWS

Two theoretical methods dealing with the prediction of secondary flows in cascades are discussed in this section. The first procedure to be described is a form of the channel-theory analysis similar to that which was outlined in reference (13); the channel model was used in the current study for quantitatively calculating the induced velocities corresponding to a prescribed upstream flow field and a given cascade geometry.

In contrast to the first approach, which deals with finding the secondary flows resulting from a distributed vortex array in a hypothetical downstream channel, the second method consists of formulating the exact linearized problem and focusing attention on the flow within the turning vane passages. Although no explicit solutions for the induced velocity distributions were obtained by this procedure, the analysis is significant nevertheless in that it gives a system of equations which define the local behavior of the perturbed flow field.

2:1 THE CHANNEL - THEORY MODEL

The channel-theory method for predicting the quantitative behavior of secondary flows was outlined in the Introduction. A modified version of the original Squire and Winter approach is used extensively in this report; however, before examining the details of the method, consider again the general characteristics of the model. Basically, the analysis can be divided into the following three parts:

a. The three dimensional study of secondary flows is first reduced from an airfoil problem to a channel problem by extending the blade surfaces downstream of the trailing

edge plane.

b. The downstream vorticity distribution is then evaluated for a given cascade geometry and a specified inlet flow field.

c. Finally, the secondary velocities are determined in the extended channels for the vorticity distribution which is defined in the preceding steps.

In step one above, a series of channels is substituted for the infinite row of airfoils by supposing that each of the blade surfaces is extended downstream of the actual trailing edge plane; for simplicity in the analysis, it is sufficient to assume that each streamtube of the undisturbed flow field undergoes the same amount of turning and that the hypothetical blade surfaces are continued downstream of the cascade along the main streamlines of the two-dimensional flow.

In the second step, the distortion of the inlet velocity profile is regarded as a prescribed vorticity distribution ahead of the blade row, and a channel-theory analysis is then used to evaluate the downstream vorticity field which is generated as this disturbance flow passes through the turning vanes. The vorticity equations for an inviscid, incompressible fluid are written in linearized form and are integrated along the streamlines of the two-dimensional flow; it is assumed in this procedure that the secondary flows act as perturbations to the undisturbed motion and that the self-transport properties of the secondary velocities may be neglected.

In the final step, the velocity field downstream of the cascade is evaluated from the previously determined vorticity distribution; here the hypothetical channel walls are treated as solid boundaries and the vortex filaments are assumed to be carried directly by the primary

flow without considering the self-transport of the induced velocities.

2.1.1 DETERMINATION OF THE DOWNSTREAM VORTICITY FIELD

The procedure for evaluating the vorticity distribution downstream of the cascade is described in detail below. It is assumed in this analysis that: (a) the flow is steady, incompressible, and inviscid; (b) the secondary flows are perturbations to the two-dimensional motion; (c) the vorticity self-transport effects may be neglected; and (d) the upstream flow field varies in the spanwise direction only. The vorticity equation for the steady flow of an incompressible, inviscid fluid may be written as:

$$(\vec{q}\cdot\nabla)\,\vec{\Omega} - (\vec{\Omega}\cdot\nabla)\,\vec{q} = 0 \qquad (2.1)$$

where $\vec{q}$ and $\vec{\Omega}$ are the velocity and vorticity vectors respectively. Consider the orthonormal coordinate system shown in figure 8; letting $U(s,n)$ be the velocity of the two-dimensional primary flow and u, v, w be the velocity components of the secondary flow, the vector $\vec{q}$ may be expressed as:

$$\vec{q}(s,n,z) = \left[U(s,n) + u(s,n,z)\right]\vec{\imath} + v(s,n,z)\,\vec{j} + w(s,n,z)\,\vec{k} \qquad (2.2)$$

where $\vec{\imath}$, $\vec{j}$, $\vec{k}$ are unit vectors in the s, n, z system. Similarly, the vorticity vector in component form becomes:

$$\vec{\Omega}(s,n,z) = \omega_1(s,n,z)\,\vec{\imath} + \omega_2(s,n,z)\,\vec{j} + \omega_3(s,n,z)\,\vec{k} \qquad (2.3)$$

Substituting equations 2. 2 and 2. 3 into equation 2. 1 gives:

$$\left[(U+u)\frac{\partial}{\partial s}+v\frac{\partial}{\partial n}+w\frac{\partial}{\partial z}\right]\left[\omega_1\vec{\imath}+\omega_2\vec{\jmath}+\omega_3\vec{k}\right]+ \qquad (2.4)$$

$$-\left[\omega_1\frac{\partial}{\partial s}+\omega_2\frac{\partial}{\partial n}+\omega_3\frac{\partial}{\partial z}\right]\left[(U+u)\vec{\imath}+v\vec{\jmath}+w\vec{k}\right]=0$$

The factor $\frac{\partial\vec{\imath}}{\partial n}$ in equation 2. 4 may be evaluated in the following manner. Consider the streamtube element shown in figure 8. From geometry,

$$\frac{\partial\vec{\imath}}{\partial n}\doteq\frac{\frac{\partial(\Delta n)}{\partial s}}{\Delta n}\vec{\jmath} \qquad (2.5)$$

The continuity equation for the element is given by:

$$U\Delta n=\left(U+\frac{\partial U}{\partial s}\Delta s\right)\left(\Delta n+\frac{\partial(\Delta n)}{\partial s}\Delta s\right)\doteq U\Delta n+U\frac{\partial(\Delta n)}{\partial s}\Delta s+\frac{\partial U}{\partial s}\Delta n\Delta s \qquad (2.6)$$

Solving equation 2. 6 for $\frac{\partial(\Delta n)}{\partial s}$ and substituting into equation 2. 5 then gives:

$$\frac{\partial\vec{\imath}}{\partial n}=-\frac{1}{U}\frac{\partial U}{\partial s}\vec{\jmath} \qquad (2.7)$$

The corresponding expression for the term $\frac{\partial\vec{\jmath}}{\partial n}$ in equation 2. 4 is similarly given by:

$$\frac{\partial\vec{\jmath}}{\partial n}=\frac{1}{U}\frac{\partial U}{\partial s}\vec{\imath} \qquad (2.8)$$

The factor $\frac{\partial \vec{\imath}}{\partial s}$ in equation 2.4 can be evaluated as follows. From the geometry of figure 8,

$$\frac{\partial \vec{\imath}}{\partial s} = \frac{(1)(\Delta\theta)(-\vec{\jmath})}{R(\Delta\theta)} = -\frac{1}{R}\vec{\jmath} \qquad (2.9)$$

Assuming no losses, the Bernoulli equation along a streamline may be written:

$$p + \frac{\rho U^2}{2} = \text{constant} \qquad (2.10)$$

Differentiating equation 2.10 with respect to "n" and replacing $\frac{\partial p}{\partial n}$ by $\frac{\rho U^2}{2}$ from the condition for radial equilibrium gives:

$$\frac{1}{R} = -\frac{1}{U}\frac{\partial U}{\partial n} \qquad (2.11)$$

Substituting from equation 2.11 into equation 2.9 then gives:

$$\frac{\partial \vec{\imath}}{\partial s} = \frac{1}{U}\frac{\partial U}{\partial n}\vec{\jmath} \qquad (2.12)$$

In a similar fashion, the factor $\frac{\partial \vec{\jmath}}{\partial s}$ in equation 2.4 becomes:

$$\frac{\partial \vec{\jmath}}{\partial s} = -\frac{1}{U}\frac{\partial U}{\partial n}\vec{\imath} \qquad (2.13)$$

It is interesting to note that the differential equation for the two-dimensional velocity $U(s,n)$ can be derived from equations 2.7 and 2.12; differentiating equation 2.7 with respect to "s" and equation 2.12 with respect to "n" and subtracting gives:

$$\frac{\partial}{\partial s}\left[\frac{1}{U}\frac{\partial U}{\partial s}\right]+\frac{\partial}{\partial n}\left[\frac{1}{U}\frac{\partial U}{\partial n}\right]=0 \qquad (2.14)$$

Expanding equation 2.4 and substituting from equations 2.7, 2.8, 2.12 and 2.13 then gives the following relations corresponding to the three component directions:

$$(U+u)\frac{\partial \omega_3}{\partial s}+v\frac{\partial \omega_3}{\partial n}+w\frac{\partial \omega_3}{\partial z}-\omega_1\frac{\partial w}{\partial s}-\omega_2\frac{\partial w}{\partial n}-\omega_3\frac{\partial w}{\partial z}=0 \qquad (2.15)$$

$$(U+u)\frac{\partial \omega_2}{\partial s}+v\frac{\partial \omega_2}{\partial n}+w\frac{\partial \omega_2}{\partial z}-\frac{v}{U}\omega_1\frac{\partial U}{\partial s}-\omega_1\frac{\partial v}{\partial s}+$$
$$-\omega_2\frac{\partial v}{\partial n}-\omega_3\frac{\partial v}{\partial z}+(U+u)\frac{1}{U}\omega_2\frac{\partial U}{\partial s}=0 \qquad (2.16)$$

$$(U+u)\frac{\partial \omega_1}{\partial s}+v\frac{\partial \omega_1}{\partial n}+w\frac{\partial \omega_1}{\partial z}-(U+u)\frac{1}{U}\omega_2\frac{\partial U}{\partial n}+$$
$$-\omega_1\frac{\partial}{\partial s}(U+u)-\omega_2\frac{\partial}{\partial n}(U+u)-\omega_3\frac{\partial U}{\partial z}+\frac{v}{U}\omega_1\frac{\partial U}{\partial n}=0 \qquad (2.17)$$

The variables s, n, z in the above system of equations may be replaced by the dimensionless coordinates α, β, γ according to the following transformation:

$s = c\alpha$

$n = g\beta$

$z = h\gamma$

where "c" is the blade chord; "g" is the blade gap; and "h" is the spanwise half-width of the upstream screen. The parameters "c", "g", and

"h" have the dimensions of a length; the values of α, β, and τ are of order unity in the region of the flow field where the effects of the secondary flows are concentrated.

Assuming that the secondary flows are small perturbations to the two-dimensional primary motion, the components of velocity may be written as:

$$U(\alpha,\beta) = U_0\left[U^{(0)}(\alpha,\beta)\right]$$

$$u(\alpha,\beta,\tau) = U_0\left[\epsilon u^{(1)}(\alpha,\beta,\tau) + O(\epsilon^2)\right] \qquad (2.19)$$

$$v(\alpha,\beta,\tau) = U_0\left[\epsilon v^{(1)}(\alpha,\beta,\tau) + O(\epsilon^2)\right]$$

$$w(\alpha,\beta,\tau) = U_0\left[\epsilon w^{(1)}(\alpha,\beta,\tau) + O(\epsilon^2)\right]$$

where U_0 is the upstream primary velocity and the dimensionless terms $U^{(0)}$, $u^{(1)}$, $v^{(1)}$, $w^{(1)}$ are of order unity. The factor "ϵ" is used to indicate smallness. The components of vorticity may likewise be written in series form as follows:

$$\omega_1 = \frac{q_0^*}{h}\left[\omega_1^{(0)}(\alpha,\beta,\tau) + \epsilon\omega_1^{(1)}(\alpha,\beta,\tau) + O(\epsilon^2)\right]$$

$$\omega_2 = \frac{q_0^*}{h}\left[\omega_2^{(0)}(\alpha,\beta,\tau) + \epsilon\omega_2^{(1)}(\alpha,\beta,\tau) + O(\epsilon^2)\right] \qquad (2.20)$$

$$\omega_3 = \frac{q_0^*}{h}\left[\omega_3^{(0)}(\alpha,\beta,\tau) + \epsilon\omega_3^{(1)}(\alpha,\beta,\tau) + O(\epsilon^2)\right]$$

where $q_0^* = \sqrt{(u_0^2 + v_0^2)_{max.}}$ is the magnitude of the maximum upstream perturbation velocity vector and "h" is the screen half-width; the parameter $\frac{q_0^*}{h}$ is, therefore, a measure of the vorticity in the approach

flow. The dimensionless terms $\omega_1^{(i)}, \omega_2^{(i)}, \omega_3^{(i)}$ are of order unity and the factor "ϵ" is again used to indicate smallness. Substituting from equations 2. 18, 2. 19, and 2. 20 into equations 2. 15 through 2. 17 then gives the following system of equations:

$$\left[U^{(0)}+\epsilon u^{(1)}\right]\frac{\partial}{\partial\alpha}\left[\omega_3^{(0)}+\epsilon\omega_3^{(1)}\right]+\epsilon v^{(1)}\frac{c}{q}\frac{\partial}{\partial\beta}\left[\omega_3^{(0)}+\epsilon\omega_3^{(1)}\right]+$$

$$+\epsilon w^{(1)}\frac{c}{h}\frac{\partial}{\partial r}\left[\omega_3^{(0)}+\epsilon\omega_3^{(1)}\right]-\left[\omega_1^{(0)}+\epsilon\omega_1^{(1)}\right]\frac{\partial}{\partial\alpha}\left(\epsilon w^{(1)}\right)+$$

$$-\left[\omega_2^{(0)}+\epsilon\omega_2^{(1)}\right]\frac{c}{q}\frac{\partial}{\partial\beta}\left(\epsilon w^{(1)}\right)-\left[\omega_3^{(0)}+\epsilon\omega_3^{(1)}\right]\frac{c}{h}\frac{\partial}{\partial r}\left(\epsilon w^{(1)}\right)+$$

$$+O(\epsilon^2)=0 \qquad \text{(2. 21)}$$

$$\left[U^{(0)}+\epsilon u^{(1)}\right]\frac{\partial}{\partial\alpha}\left[\omega_2^{(0)}+\epsilon\omega_2^{(1)}\right]+\epsilon v^{(1)}\frac{c}{q}\frac{\partial}{\partial\beta}\left[\omega_2^{(0)}+\epsilon\omega_2^{(1)}\right]+$$

$$+\epsilon w^{(1)}\frac{c}{h}\frac{\partial}{\partial r}\left[\omega_2^{(0)}+\epsilon\omega_2^{(1)}\right]-\frac{\epsilon v^{(1)}}{U^{(0)}}\left[\omega_1^{(0)}+\epsilon\omega_1^{(1)}\right]\frac{\partial U^{(0)}}{\partial\alpha}+$$

$$-\left[\omega_1^{(0)}+\epsilon\omega_1^{(1)}\right]\frac{\partial}{\partial\alpha}\left(\epsilon v^{(1)}\right)-\left[\omega_2^{(0)}+\epsilon\omega_2^{(1)}\right]\frac{c}{q}\frac{\partial}{\partial\beta}\left(\epsilon v^{(1)}\right)+$$

$$-\left[\omega_3^{(0)}+\epsilon\omega_3^{(1)}\right]\frac{c}{h}\frac{\partial}{\partial r}\left(\epsilon v^{(1)}\right)+\left[1+\epsilon\frac{u^{(1)}}{U^{(0)}}\right]\left[\omega_2^{(0)}+\epsilon\omega_2^{(1)}\right]\frac{\partial U^{(0)}}{\partial\alpha}+$$

$$+O(\epsilon^2)=0 \qquad \text{(2. 22)}$$

$$\left[U^{(0)}+\epsilon u^{(1)}\right]\frac{\partial}{\partial s}\left[\omega_1^{(0)}+\epsilon\omega_1^{(1)}\right]+\epsilon v^{(1)}\frac{c}{g}\frac{\partial}{\partial\beta}\left[\omega_1^{(0)}+\epsilon\omega_1^{(1)}\right]+$$

$$+\epsilon w^{(1)}\frac{c}{h}\frac{\partial}{\partial\tau}\left[\omega_1^{(0)}+\epsilon\omega_1^{(1)}\right]-\left[1+\epsilon\frac{u^{(1)}}{U^{(0)}}\right]\left[\omega_2^{(0)}+\epsilon\omega_2^{(1)}\right]\frac{c}{g}\frac{\partial U^{(0)}}{\partial\beta}+$$

$$-\left[\omega_1^{(0)}+\epsilon\omega_1^{(1)}\right]\frac{\partial}{\partial\alpha}\left[U^{(0)}+\epsilon u^{(1)}\right]-\left[\omega_2^{(0)}+\epsilon\omega_2^{(1)}\right]\frac{c}{g}\frac{\partial}{\partial\beta}\left[U^{(0)}+\epsilon u^{(1)}\right]+$$

$$+\frac{\epsilon v^{(1)}}{U^{(0)}}\frac{c}{g}\left[\omega_1^{(0)}+\epsilon\omega_1^{(1)}\right]\frac{\partial U^{(0)}}{\partial\beta}+O(\epsilon^2)=0 \qquad (2.23)$$

An additional relation may be derived from the continuity equation; this expression in terms of the above dimensionless parameters becomes:

$$\frac{\partial}{\partial\alpha}\left(\frac{\epsilon u^{(1)}}{U^{(0)}}\right)+\frac{c}{g}\frac{\partial}{\partial\beta}\left(\frac{\epsilon v^{(1)}}{U^{(0)}}\right)+\frac{1}{U^{(0)}}\frac{c}{h}\frac{\partial(\epsilon w^{(1)})}{\partial\tau}=0 \qquad (2.24)$$

Equations 2.21 through 2.24 may be studied systematically for various values of the geometric parameters $\frac{g}{c}$ and $\frac{h}{c}$. For simplicity it is assumed that the cascade solidity $\frac{c}{g}$ is of order unity; the particular cases $\frac{h}{c}=O(1)$ and $\frac{h}{c}=O(\epsilon)$ are discussed below in sections 2:1. 1. 1 and 2:1. 1. 2. For $\frac{h}{c}=O(\frac{1}{\epsilon})$, the restriction that the induced velocities remain perturbation quantities implies that the upstream velocity gradients are very small. This then suggests that the flow may be treated in a two-dimensional manner locally along the span; however, since $\frac{h}{c}$ was not large in the current experimental tests, this procedure is not considered further.

2:1. 1. 1 Case I, $\frac{h}{c} = O(1)$

The restriction that $\frac{h}{c}$ be of order unity is particularly significant in connection with the current investigation because it is this condition which was simulated experimentally in the cascade tunnel. Putting $\frac{h}{c} = \frac{g}{c} = 1$ in equations 2. 21 through 2. 23 and collecting terms of order unity gives:

$$U^{(0)} \frac{\partial \omega_3^{(0)}}{\partial \alpha} = 0 \qquad (2.25)$$

$$\frac{\partial}{\partial \alpha} \left[\omega_2^{(0)} U^{(0)} \right] = 0 \qquad (2.26)$$

$$\frac{\partial}{\partial \alpha} \left(\frac{\omega_1^{(0)}}{U^{(0)}} \right) - \frac{2 \omega_2^{(0)}}{(U^{(0)})^2} \frac{\partial U^{(0)}}{\partial \beta} = 0 \qquad (2.27)$$

Integrating equations 2. 25 and 2. 26 along streamlines and applying boundary conditions from the prescribed upstream flow field gives:

$$\omega_3^{(0)} = \omega_3^{(0)}\Big)_{upstream} = 0 \qquad (2.28)$$

$$\omega_2^{(0)} = \frac{1}{U^{(0)}} \left(\omega_2^{(0)} U^{(0)} \right)_{upstream} \qquad (2.29)$$

It is assumed in equations 2. 28 and 2. 29 that the upstream flow varies in the spanwise direction only. Substituting from equations 2. 28 and 2. 29 into equation 2. 27 and integrating along streamlines then gives

the following integral representation for the streamwise component of vorticity:

$$\omega_1 = 2 U_0 U(s,n) \frac{dU_0}{dz} \int_{-\infty}^{s} \frac{1}{U^3} \frac{\partial U}{\partial n} ds + \frac{U}{U_0} \frac{dV_0}{dz} \qquad (2.30)$$

The variables α, β, τ have been replaced by the more conventional dimensional units s, n, z and the superscripts have been dropped for simplicity. It is noted that equation 2.30 represents the approximation for ω_1 to order ϵ, i.e., $\omega_1^{(0)}$, and that $\frac{dU_0}{dz}$ and $\frac{dV_0}{dz}$ are dependent upon the particular streamline along which the integration is carried out. From equation 2.11, $\frac{\partial U}{\partial n} = -\frac{U}{R}$, where "R" is the local streamline radius of curvature. Changing the variable of integration in equation 2.30 from "s" to "γ", where "γ" is the flow angle measured from the axial direction, the expression for ω_1 becomes:

$$\omega_1 = -2 U_0 U(s,n) \frac{dU_0}{dz} \int_{\gamma_0}^{\gamma} \frac{1}{U^2} d\gamma + \frac{dV_0}{dz} \frac{U}{U_0} \qquad (2.31)$$

Neglecting the streamsurface warpage due to the self-transport effects of the induced flows, the continuity equation is:

$$U = \frac{U_0 \cos \gamma_0}{\cos \gamma} \qquad (2.32)$$

Substituting for U in equation 2.31 and integrating gives the following expression for the streamwise component of vorticity in terms of the prescribed upstream vorticity and the mainstream turning angle:

$$(\omega_1)_2 = -\frac{1}{\cos\gamma_0 \cos\gamma_2}\frac{du_0}{dz}\left[\gamma_2-\gamma_0+\frac{1}{2}\left(\sin 2\gamma_2-\sin 2\gamma_0\right)\right]+ \qquad (2.33)$$

$$-\frac{\cos\gamma_0}{\cos\gamma_2}\frac{dv_0}{dz}$$

The corresponding expressions for $(\omega_2)_2$ and $(\omega_3)_2$ from equations 2.28 and 2.29 are:

$$(\omega_2)_2 = \frac{U_0}{U_2}\frac{du_0}{dz} \qquad (2.34)$$

$$(\omega_3)_2 = 0 \qquad (2.35)$$

where $\omega_1, \omega_2, \omega_3$ are the first order approximations for the components of vorticity in the s, n, z directions respectively;

the subscripts "o" and "2" refer to conditions upstream and downstream of the cascade respectively;

$U(s,n)$ is the magnitude of the primary flow velocity;

" γ " is the angle that the primary flow velocity vector makes with the x-axis; and

u_0 and v_0 are the upstream velocity components of the prescribed disturbance flow in the "s" and "n" directions respectively.

2;1. 1. 2 Case II, $\frac{h}{c} = O(\epsilon)$

Assuming that $\frac{h}{c}$ is of order "ϵ" and that $\frac{g}{c}$ is of order one in equations 2. 21 through 2. 24 and collecting terms of order unity gives:

$$\frac{\partial w^{(1)}}{\partial \tau} = 0 \tag{2.36}$$

$$U^{(0)} \frac{\partial \omega_3^{(0)}}{\partial \alpha} = 0 \tag{2.37}$$

$$\frac{\partial}{\partial \alpha}\left[U^{(0)} \omega_2^{(0)}\right] = 0 \tag{2.38}$$

$$\frac{\partial}{\partial \alpha}\left(\frac{\omega_1^{(0)}}{U^{(0)}}\right) - \frac{2}{(U^{(0)})^2}\,\omega_2^{(0)} \frac{\partial U^{(0)}}{\partial \beta} = 0 \tag{2.39}$$

Applying the boundary condition that $w^{(1)} \longrightarrow 0$ as τ becomes large, equation 2.36 indicates that $w^{(1)} = 0$ throughout the flow field. Equations 2.37 through 2.39 are identical with equations 2.25 through 2.27, and, therefore, the integrated forms of these expressions are given as before by equations 2.33 through 2.35. The restriction that the velocity component "w" remains everywhere equal to zero suggests that the spanwise pressure gradient is negligible and that the secondary flow effects remain concentrated in a thin layer. It is expected that this analysis for $\frac{h}{c} = O(\epsilon)$ should correctly define the flow field in the central regions of the channel for the case of a narrow upstream wake; near the blade surfaces, however, the boundary restrictions that the velocity component "v" goes to zero implies that the spanwise velocity "w" cannot also remain equal to zero since this would mean that fluid must accumulate within the two-dimensional sheet.

The case of a narrow wake was not studied experimentally in the current test program. Earlier investigators, however, have considered the secondary flows emanating from a thin boundary layer upstream of

the blade row; attempts to predict the behavior of these flows by the channel-theory analysis with $\frac{h}{c} = O(1)$, i.e., Case I, have met with no success. The reason for this failure, however, is probably severely influenced both by viscous effects in the boundary layer and by large distortions of the upstream velocity profile; therefore, the applicability of the channel analysis with $\frac{h}{c} = O(\epsilon)$, i.e., Case II, cannot be tested directly from the published data.

2.1.2 DETERMINATION OF THE SECONDARY VELOCITY FIELD

The procedure for finding the secondary velocity field is outlined in Appendix I. It is assumed that the vorticity distribution prescribed in the previous section for the condition $\frac{h}{c} = O(1)$ is carried downstream by the primary flow and that the induced velocities are sufficiently small to permit the streamwise vortex filaments to remain parallel to the original two-dimensional streamlines. The imaginary channel boundaries that were formed by extending the blade surfaces are taken as streamsurfaces for the perturbed motion, and the secondary flow fields in adjacent passages are assumed to be mutually independent. It is further assumed that the velocity distribution just aft of the trailing edge plane is the same as the velocity distribution which is induced far downstream by the two-dimensional vortex array.

The expressions for the horizontal and the vertical components of the induced secondary velocity field are given by equations 9 and 10 respectively of Appendix I. It is noted that these relations are derived for a channel of infinite spanwise extent; therefore, when computing the velocity field for an actual cascade, it is necessary to satisfy additional restrictions at the tunnel boundaries. In the current investigation, the induced velocities were very small at a distance $\geq$ one chord-length from the screen wake, and a correction term accounting for only

the first image effect was found to be adequate for all configurations.

2:2 FORMULATION OF THE EXACT LINEARIZED PROBLEM

Consider again the expressions which were derived in section 2:1. 1. 1 by integrating the linearized vorticity equation from a region far upstream of the blade row to an arbitrary point in the flow field:

$$\omega_1 \equiv \frac{\partial w}{\partial n} - \frac{\partial v}{\partial z} = -U U_0 \frac{dv_0}{dz} \int_{-\infty}^{s} \frac{\partial}{\partial n}\left(\frac{1}{U^2}\right) ds - \frac{U}{U_0}\frac{dv_0}{dz} \qquad (2.40)$$

$$\omega_2 \equiv \frac{\partial u}{\partial z} - \frac{\partial w}{\partial s} = \frac{U_0}{U}\frac{du_0}{dz} \qquad (2.41)$$

$$\omega_3 \equiv U\left[\frac{\partial(v/U)}{\partial n} - \frac{\partial(u/U)}{\partial s}\right] = 0 \qquad (2.42)$$

where $\omega_1, \omega_2, \omega_3 (s,n,z)$ are the components of vorticity in the s, n, z directions;

$u, v, w(s,n,z)$ are the perturbed velocity components in the s, n, z directions;

$U(s,n)$ is the magnitude of the primary velocity vector; and

$u_0, v_0(z)$ are the given perturbation velocities far upstream of the blade row.

The corresponding continuity equation in the (s, n, z) coordinate system may be written as:

$$\frac{\partial}{\partial s}\left(\frac{u}{U}\right) + \frac{\partial}{\partial n}\left(\frac{v}{U}\right) + \frac{1}{U}\frac{\partial w}{\partial z} = 0 \qquad (2.43)$$

Differentiating equation 2.43 with respect to "z" and substituting for $\frac{\partial u}{\partial z}$ and $\frac{\partial v}{\partial z}$ from equations 2.40 and 2.41 gives the following expression for the spanwise component of velocity "w":

$$\frac{\partial}{\partial s}\left[\frac{1}{U}\frac{\partial w}{\partial s}\right] + \frac{\partial}{\partial n}\left[\frac{1}{U}\frac{\partial w}{\partial n}\right] + \frac{1}{U}\frac{\partial^2 w}{\partial z^2} = -U_0\frac{dU_0}{dz}\left[\frac{\partial^2}{\partial s^2} + \frac{\partial^2}{\partial n^2}\right]\int_{-\infty}^{s}\frac{1}{U^2}ds \qquad (2.44)$$

A second differential equation for "w" can be derived by taking the partial derivative of equation 2.40 with respect to "s" and the partial of equation 2.41 with respect to "n" and adding; using equation 2.42 to simplify then gives:

$$\frac{\partial U}{\partial n}\frac{\partial w}{\partial s} - \frac{\partial U}{\partial s}\frac{\partial w}{\partial n} = 0 \qquad (2.45)$$

This expression may be regarded as a condition on "w" which the solution to equation 2.44 must satisfy.

The corresponding relations for the remaining perturbation velocity components can be derived from equations 2.40, 2.41, and 2.42. Differentiating equation 2.40 with respect to "s" and equation 2.41 with respect to "n" and adding gives:

$$\frac{\partial}{\partial z}\left[\frac{\partial}{\partial n}\left(\frac{u}{U}\right) - \frac{\partial}{\partial s}\left(\frac{v}{U}\right)\right] + \frac{\partial U}{\partial n}\frac{\partial}{\partial z}\left(\frac{u}{U}\right) - \frac{\partial U}{\partial s}\frac{\partial}{\partial z}\left(\frac{v}{U}\right) = -\Lambda(s,n,z) \qquad (2.46)$$

where $\Lambda(s,n,z) = U_o \frac{dw_o}{dz}\left[-\frac{1}{U^2}\frac{\partial U}{\partial n} + \frac{\partial U}{\partial s}\int_{-\infty}^{s}\frac{\partial}{\partial n}\left(\frac{1}{U^2}\right)ds\right] + \frac{1}{U_o}\frac{\partial U}{\partial s}\frac{dw_o}{dz}$

Taking the partial derivative of equation 2. 42 with respect to "z" and substituting from equation 2. 46 then gives the following differential expressions for "u" and "v":

$$\frac{\partial}{\partial z}\left\{\frac{1}{U}\frac{\partial U}{\partial n} - \frac{\alpha}{U}\frac{\partial U}{\partial s} + w\left[\frac{\partial}{\partial n}\left(\frac{1}{U}\right) - \frac{\partial}{\partial s}\left(\frac{\alpha}{U}\right)\right]\right\} = \frac{\partial}{\partial s}\left[\frac{1}{\frac{\partial U}{\partial s}}\Lambda\right] \qquad (2.47)$$

$$\frac{\partial}{\partial z}\left\{\frac{1}{\alpha U}\frac{\partial v}{\partial n} - \frac{1}{U}\frac{\partial v}{\partial s} + w\left[\frac{\partial}{\partial n}\left(\frac{1}{\alpha U}\right) - \frac{\partial}{\partial s}\left(\frac{1}{U}\right)\right]\right\} = \frac{\partial}{\partial n}\left[\frac{1}{\frac{\partial U}{\partial n}}\Lambda\right] \qquad (2.48)$$

where $\alpha(s,n) = \frac{\frac{\partial U}{\partial n}}{\frac{\partial U}{\partial s}}$ and "Λ" is given in equation 2. 46. The boundary conditions for the above system of equations are as follows: (a) the flow field far upstream of the blade row is a given function of spanwise position only; (b) the static pressure is continuous both upstream and downstream of the turning vanes; this condition, in conjunction with the assumption that the total pressure is constant along a streamline, implies that the induced secondary velocities may be discontinuous only across the solid blade elements; and (c) the blades are themselves streamsurfaces of both the perturbed and the unperturbed flows. The cascade geometry is prescribed and the two-dimensional flow is assumed to be known.

As was indicated earlier, no explicit solutions for the secondary velocity distributions were obtained from the previous set of differen-

tial equations. Some simplification can be made, however, by assuming that the solutions for "u", "v", and "ω" are of the following form:

$$u(s,n,z) = \sum_{\lambda=0}^{\infty} u_1(s,n;\lambda)\, e^{i\lambda z}$$

$$v(s,n,z) = \sum_{\lambda=0}^{\infty} v_1(s,n;\lambda)\, e^{i\lambda z} \qquad (2.49)$$

$$\omega(s,n,z) = \sum_{\lambda=0}^{\infty} \omega_1(s,n;\lambda)\, e^{i\lambda z}$$

Substituting from equation 2.49 into equations 2.44, 2.47, and 2.48 then gives:

$$\frac{\partial}{\partial s}\left[\frac{1}{U}\frac{\partial \omega_1}{\partial s}\right] + \frac{\partial}{\partial n}\left[\frac{1}{U}\frac{\partial \omega_1}{\partial n}\right] - \frac{\lambda^2}{U}\omega_1 = -U_0(u_1)_0 i\lambda\left[\frac{\partial^2}{\partial s^2} + \frac{\partial^2}{\partial n^2}\right]\int_{-\infty}^{s} \frac{1}{U^2}\, ds \qquad (2.50)$$

$$\frac{1}{U}\frac{\partial u_1}{\partial n} - \frac{\alpha}{U}\frac{\partial u_1}{\partial s} + u_1\left[\frac{\partial}{\partial n}\left(\frac{1}{U}\right) - \frac{\partial}{\partial s}\left(\frac{\alpha}{U}\right)\right] = \frac{\partial}{\partial s}\left[\frac{1}{\frac{\partial U}{\partial s}}\,\beta\right] \qquad (2.51)$$

$$\frac{1}{\alpha U}\frac{\partial v_1}{\partial n} - \frac{1}{U}\frac{\partial v_1}{\partial s} + v_1\left[\frac{\partial}{\partial n}\left(\frac{1}{\alpha U}\right) - \frac{\partial}{\partial s}\left(\frac{1}{U}\right)\right] = \frac{\partial}{\partial n}\left[\frac{1}{\frac{\partial U}{\partial n}}\,\beta\right] \qquad (2.52)$$

where $\alpha(s,n) = \dfrac{\dfrac{\partial U}{\partial n}}{\dfrac{\partial U}{\partial s}}$ and

$$\beta(s,n) = U_0(u_1)_0\left[\frac{1}{U^2}\frac{\partial U}{\partial n} + \frac{\partial U}{\partial s}\int_{-\infty}^{s}\frac{\partial}{\partial n}\left(\frac{1}{U^2}\right) ds\right] + \frac{(v_1)_0}{U_0}\frac{\partial U}{\partial s}$$

It is noted that if $\omega_1(s,n;\lambda)$ can be found from equation 2. 50, then "u" and "v" can be determined directly from equations 2. 40, 2. 41, and 2. 49.

2:2. 1 ALTERNATE FORMULATION OF THE EXACT LINEARIZED PROBLEM

If a local coordinate change is made wherein the variables (s, n, z) are replaced by (ϕ, ψ, z) according to the transformation $d\phi = U\,ds$, $d\psi = U\,dn$, the expressions for the components of vorticity become:

$$\omega_1(\phi,\psi,z) \equiv U\frac{\partial w}{\partial \psi} - \frac{\partial v}{\partial z} = 2U_0 U \frac{dU_0}{dz}\int_{-\infty}^{\phi} \frac{1}{U^3}\frac{\partial U}{\partial \psi}\,d\phi - \frac{U}{U_0}\frac{dv_0}{dz} \qquad (2.53)$$

$$\omega_2(\phi,\psi,z) \equiv \frac{\partial U}{\partial z} - U\frac{\partial w}{\partial \phi} = \frac{U_0}{U}\frac{dU_0}{dz} \qquad (2.54)$$

$$\omega_3(\phi,\psi,z) \equiv U^2\left[\frac{\partial}{\partial \phi}\left(\frac{v}{U}\right) - \frac{\partial}{\partial \psi}\left(\frac{U}{U}\right)\right] = 0 \qquad (2.55)$$

In these relations, the variables are regarded as functions of (ϕ, ψ, z). The transformed continuity equation becomes:

$$\frac{\partial}{\partial \phi}\left(\frac{U}{U}\right) + \frac{\partial}{\partial \psi}\left(\frac{v}{U}\right) + \frac{1}{U^2}\frac{\partial w}{\partial z} = 0 \qquad (2.56)$$

Following the procedure which was used earlier in connection with the (s, n, z) coordinate system, it can be shown that the differential equations for the secondary velocity components are given by:

$$\frac{\partial^2 w}{\partial \phi^2} + \frac{\partial^2 w}{\partial \psi^2} + \frac{1}{U^2}\frac{\partial^2 w}{\partial z^2} = -U_0 \frac{dU_0}{dz}\left[\frac{\partial^2}{\partial \phi^2} + \frac{\partial^2}{\partial \psi^2}\right]\int_{-\infty}^{\phi} \frac{1}{U^2}\, d\phi \qquad (2.57)$$

$$\frac{\partial}{\partial z}\left[\frac{\partial u}{\partial \psi} - \alpha^* \frac{\partial u}{\partial \phi} - u\frac{\partial \alpha^*}{\partial \phi}\right] = u - \frac{\partial}{\partial \psi}\left(\frac{uU}{\frac{\partial U}{\partial \psi}}\right) \qquad (2.58)$$

$$\frac{\partial}{\partial z}\left[\frac{\partial v}{\partial \phi} - \frac{1}{\alpha^*}\frac{\partial v}{\partial \psi} - v\frac{\partial (1/\alpha^*)}{\partial \psi}\right] = u - \frac{\partial}{\partial \phi}\left(\frac{uU}{\frac{\partial U}{\partial \psi}}\right) = 0 \qquad (2.59)$$

where $\alpha^*(\phi, \psi) = \dfrac{\frac{\partial U}{\partial \psi}}{\frac{\partial U}{\partial \phi}}$ and

$$u(\phi, \psi, z) = -\frac{1}{U_0}\frac{dU_0}{dz}\frac{\partial U}{\partial \phi}$$

Some simplification of the above equations can be made by assuming that the solutions for "u", "v", and "w" are of the following form:

$$u(\phi, \psi, z) = \sum_{\lambda=0}^{\infty} u_2(\phi, \psi; \lambda)\, e^{i\lambda z}$$

$$v(\phi, \psi, z) = \sum_{\lambda=0}^{\infty} v_2(\phi, \psi; \lambda)\, e^{i\lambda z} \qquad (2.60)$$

$$w(\phi, \psi, z) = \sum_{\lambda=0}^{\infty} w_2(\phi, \psi; \lambda)\, e^{i\lambda z}$$

Substituting from equation 2.60 into equations 2.57, 2.58, and 2.59 then gives:

$$\frac{\partial^2 w_2}{\partial \phi^2}+\frac{\partial^2 w_2}{\partial \psi^2}-\frac{\lambda^2}{U^2} w_2 = i\lambda U_0 (u_2)_0 \left[\frac{\partial^2}{\partial \phi^2}+\frac{\partial^2}{\partial \psi^2}\right] \int_{-\infty}^{\phi} \frac{1}{U^2}\, d\phi \qquad (2.61)$$

$$\frac{\partial u_2}{\partial \psi}-\alpha^*\frac{\partial u_2}{\partial \phi}-u_2\frac{\partial \alpha^*}{\partial \phi} = -i\lambda \frac{(v_2)_0}{U_0}\left[\frac{\partial U}{\partial \phi}-\frac{\partial}{\partial \psi}\left(\frac{U}{\alpha^*}\right)\right] \qquad (2.62)$$

$$\frac{\partial v_2}{\partial \phi}-\frac{1}{\alpha^*}\frac{\partial v_2}{\partial \psi}-v_2\frac{\partial}{\partial \psi}\left(\frac{1}{\alpha^*}\right)=0 \qquad (2.63)$$

It is noted that if the solution for $w_2(\phi,\psi;\lambda)$ can be found from equation 2.61, then the functional relations for u_2 and v_2 can be determined directly from equations 2.53, 2.54, and 2.60.

As was the case in dealing with the equations for the induced velocities in the (s, n, z) system, no explicit solutions were obtained for "u", "v", and "ω" from the analogous differential equations in terms of (ϕ, ψ, z). These equivalent systems of equations are significant, however, because they do give a correct representation of the velocity perturbations which the solutions to the exact linearized problem must satisfy.

III. EXPERIMENTAL APPARATUS

The cascade wind tunnel which was used in this test program is fully described in reference (13), and the reader is referred to this publication for a detailed description of the apparatus. For completeness in this report, however, the important features of the equipment are outlined below.

3:1 TUNNEL GEOMETRY

The general appearance of the cascade tunnel is shown in figures 9, 10, 11 and 12, and the geometry of the turning vanes is shown in figure 13. Five equally spaced diffusing blades having 8.5 inch chord, 0.920 solidity, and aspect ratio = 2.82 were mounted in the 2' by 3' test section at a stagger angle of $46^{\circ}13'$. The design turning of the vanes was $21^{\circ}59'$ at an angle of attack of $14^{\circ}59'$: however, to reduce separation on the suction surfaces of the blades, the actual angle of attack was maintained at 13.5° and the resultant average turning was approximately 19.5°. The flexible side walls of the tunnel were adjusted so that the static pressure was the same at corresponding points in the four center passages. A fan speed was selected so that the velocity ahead of the cascade was approximately 36 f. p. s.; the corresponding Reynolds number based on chord was 159,000.

The approach flow into the cascade was varied by installing the strips of screening shown in figure 14; these obstruction elements were mounted ahead of the blades at the mid-span position to give a controlled distortion of the upstream velocity profile.

3:2 PRESSURE AND VELOCITY MEASUREMENTS

Total pressure surveys were made with the Kiel and the pitot-

static probes shown in figures 15-a and 15-b. The Kiel probe was relatively insensitive to flow direction and was used primarily for collecting preliminary data. The pitot-static probe was used for those tests run in which both static and total pressure data were desired; this tube was found to be insensitive to flow direction for approach angles of approximately only $\pm$ 5 degrees from the probe axis; and it was necessary, therefore, to carry out lateral and vertical angle surveys preparatory to using this apparatus. The magnitudes of all pressure readings were determined by using the transducer-bridge circuit which is described in reference 14; this equipment was statically calibrated by comparing indicated scale readings with direct water manometer readings.

The distribution of static pressure on the surface of the center cascade blade was measured using the specially tapped vane shown in figure 16. A complete description of this apparatus is given in reference 13.

3.3 FLOW ANGLE MEASUREMENTS

The claw, the wedge, and the hot-wire probes shown in figures 15-c, 15-d and 15-e were used to measure the direction of flow in the tunnel; additional surveys were also made using tuft instrumentation, but this procedure was generally employed only for obtaining preliminary qualitative data. The transducer-bridge circuit was used as a null-sensing device when the flow angles were being measured with the claw and the wedge probes; here the output from each pair of pressure sensitive tubes was fed into opposite sides of the transducer, and the probe was then rotated until the bridge circuit was balanced.

The hot-wire angle measuring apparatus is shown schematically in figure 17. The current for the heater element was supplied by a Variac rheostat; the sensing wire was connected to a constant temperature hot-wire set. The voltage potential across the sensing wire was kept very small so that this element would not respond to velocity fluctuations. The current in the sensing wire was metered and the probe head was rotated until the null point was reached, thus indicating the angle setting at which the wire was in the wake of the hot heater element.

The angle measuring probes were calibrated upstream of the cascade. The directional steadiness of the flow was tested locally by making a series of tuft observations; the zero point for each of the devices was then determined by carrying out angle surveys with the probe first in a normal operating position and then in an inverted position. As an additional check on the accuracy of the calibration procedure, the angle data from the different probes were compared at corresponding points in the flow field.

3:4 STREAMLINE TRACING

The corresponding upstream and downstream points on the same streamline were found by placing a small heater coil ahead of the cascade and then using hot wire instrumentation aft of the blade row to determine the downstream location of the warmed filament of air. The heater coil is shown in figure 15-f; the current for this element was supplied by the Variac rheostat. The hot-wire probe is shown in figure 15-g; this probe was connected to the constant temperature hot-wire set and the voltage potential was again kept very small so that

the element would not respond to local velocity fluctuations. The current in the sensing wire was monitored and the probe location was varied until the minimum reading was obtained, thereby indicating the downstream position of the heated streamtube.

3:5 EXPERIMENTAL ACCURACY

The accuracy of the total pressure data was tested by comparing the results of Kiel probe surveys with the corresponding results of surveys made using the pitot-static tube. It was found that excellent correlation was achieved between the two sets of readings and that maximum deviations were of the order of one percent. The accuracy of the static pressure data was tested by mounting the pitot-static tube far upstream of the blade row and comparing the readings from this probe with the readings from a reference static pressure tap in the tunnel wall. The maximum deviation between the data from these methods was again approximately one percent. The transducer-bridge system which was used in making pressure measurements was checked periodically, and no significant variations were detected during the test program.

The calibration of the angle sensing probes was discussed in section 3:3. The data from these devices was generally found to be accurate to within ± 0.25 degrees in regions of steady flow; in those regions of the flow field where angle gradients were large and where appreciable turbulent fluctuations existed, the measured data are believed to be correct to within ± 0.75 degrees.

IV. EXPERIMENTAL INVESTIGATIONS

A primary objective of the current investigation was to test the usefulness of the channel-theory model of secondary flows by carrying out a series of experiments which were compatible with the fundamental assumptions upon which the analysis itself was based. To accomplish this goal, a family of screens, each of which extended over approximately ten percent of the blade height, were installed ahead of the cascade to produce various desired amounts of distortion in the upstream velocity profile. These screen segments were positioned at the center of the span so that the secondary flows induced by them would be readily distinguishable from the effects of all other disturbances, e.g., viscous losses, boundary layer effects, etc.

The general nature of the experimental test program is described in section 4:1; the detailed results of the flow measurement surveys are presented in section 4:2 for each of the four tunnel configurations which was studied.

4:1 SCOPE OF THE EXPERIMENTAL INVESTIGATION

The experimental testing which was done in the cascade tunnel was designed to furnish quantitative information about the secondary flows which resulted when various obstructions were installed upstream of the blade row. In the following paragraphs, a brief discussion is given regarding the different tunnel arrangements which were studied; also included is a resume of the type of experimental data which were measured for each particular configuration.

4:1.1 CONFIGURATION I.

The tunnel was run in normal operating condition, i.e., without any external sources of disturbances located upstream of the blade row. For this and for all subsequent test runs, the blading angle of attack was set at 13.5° and the Reynolds number based on chord was maintained at approximately 159,000. The distributions of total pressure, velocity head, and flow direction were measured both upstream and downstream of the cascade to determine the fluid motion in these regions. In addition, the distribution of static pressure was measured on the surface of the center vane to determine the spanwise variation in blade loading.

4:1.2 CONFIGURATION II.

A three-ply screen segment covering approximately 10 percent of the floor-to-roof tunnel height was installed at mid-span some 2.5 chordlengths upstream of the turning vanes. This obstruction, which was mounted parallel to the leading edge plane, extended completely across the cascade and produced a disturbance region in which the minimum wake velocity was 47 percent of the freestream velocity. As in configuration I, the distributions of total pressure, velocity head, and flow direction were measured at the upstream and downstream reference stations, and the variation of static pressure was measured on the surface of the center blade. In addition, data was taken to determine the amount of streamsurface displacement which resulted from the self-transport effects of the induced secondary velocities; this information was desired in order to test the validity of the assumption that streamline distortion is actually negligible in the linearized analysis.

4:1.3 CONFIGURATION III.

The tunnel arrangement for this configuration was the same as in the foregoing case except that a single ply, rather than a three-ply, strip of screen was installed upstream of the cascade; the corresponding minimum wake velocity for this obstruction was 69 percent of the freestream velocity. The variations of total pressure, velocity head, and flow direction were measured fore and aft of the cascade, and the static pressure distribution was evaluated as usual on the surface of the center blade.

4:1.4 CONFIGURATION IV.

In this configuration, a single ply screen was installed at midspan height approximately four chordlengths upstream of the leading edge position; however, in contrast with the previous two cases, this obstruction was placed perpendicular to the oncoming flow rather than parallel to the cascade axis. This procedure was followed in an effort to eliminate completely the slight cross-flow effects which were noted in configurations II and III. The distributions of total pressure, velocity head, and flow direction were again measured upstream and downstream of the cascade. The blade static pressure loading was recorded but was subsequently found to be incorrect due to equipment malfunction.

4:2 EXPERIMENTAL RESULTS

4:2.1 CONFIGURATION I.

In accordance with the definition given on page 1, the notation "primary flow" refers to the flow field which exists when no external

blockage obstruction, i.e., screen segment, is placed upstream of the blade row; consequently, it is this reference flow which is defined by the "no screen" arrangement of configuration I.

Upstream Flow

The reference station at which the upstream flow field was determined was approximately two chord lengths ahead of the cascade. The spanwise variations of the velocity head, the horizontal and vertical flow angles, and the total and static pressures were measured at this position and are shown in figure 18. It is seen from this plot that the undisturbed upstream flow was very nearly two dimensional outside the lower wall boundary-layer region.

Downstream Flow

The reference plane which was used for the determination of the downstream flow field was 1.5 inches aft of the cascade trailing edge station; velocity, pressure and angle surveys were made at this position, and the results of these measurements are shown in figures 19 through 21. It is seen from the total pressure graphs of figures 19 and 20 that the thickness of the blade wake is approximately one inch; in addition, comparison of these plots with figure 18-a indicates that viscous losses through the blade row are negligible in the central regions of the channel. The variations in the downstream flow angles are shown in figures 19-b, 20-b, and 21; the contour map method of presentation is used in figure 21 in order to permit easy comparison with the corresponding data of later tunnel configurations.

The variation in static pressure on the surface of the center cascade blade was measured using the specially tapped vane which

was described earlier. The blade loading was found to be almost wholly independent of spanwise position over the entire vertical traverse range of the equipment; the recorded pressure distribution for z = 3" is shown in figure 22 and is fully representative of the analogous curves for $|z| \leq 9$ inches. The component of blade load parallel to the cascade axis at each vertical station was computed by integrating the corresponding measured vane pressure distribution. The general two-dimensional character of the flow is particularly evident from the resultant curve of figure 23.

It was noted early in the experimental program that there was some tendency for the flow to separate from the suction surfaces of the blades. Subsequent testing showed that this condition could be substantially alleviated by reducing the blade angle of attack; this form of corrective action was not practical in the present case, however, because the adjustability of the tunnel side walls was not sufficient to permit simulation of flow through an infinite cascade when the vane angle of attack was appreciably different from the design value. Therefore, as an alternative, a 0.020 inch diameter turbulence wire was permanently mounted on the suction surface of each blade just aft of the leading edge position; it was found that the installation of these "turbulators" caused the separation point to shift downstream, thereby giving a blade wake of acceptable thickness.

4:2.2 CONFIGURATION II.

In this configuration, a 2.4 inch strip of three-ply screening was mounted at midspan approximately 2.5 chord lengths upstream of the cascade; a description of the obstruction element was given earlier in section 3:1.

Upstream Flow

To determine the nature of the flow field ahead of the cascade, pressure, velocity, and angle surveys were carried out at the upstream reference plane. The results of these measurements are described briefly below.

The spanwise variation in flow velocity at the upstream station is shown in figure 24; it is seen from this plot that the minimum wake velocity is approximately 47 percent of the free stream velocity and that the influence of the screen is concentrated in the center ten percent of the span height ($-2 \leq z \leq 2$).

The spanwise variation in total and static pressure is shown in figures 25 and 26. The total pressure data is reduced to dimensionless form by introducing the fictitious velocity head $\frac{\rho}{2}\left(q_o^2 - q_{wake_{max.}}^2\right)$; this particular parameter was used in order to normalize the pressure data in a consistent manner for all screen configurations.

The measured variation in the lateral flow angle is shown in figure 27. It is seen that a component of velocity normal to the free-stream direction was induced by the oblique orientation of the screen and that high local angles of attack existed in the mid-span portion of the cascade. The magnitude of this distortion was sufficiently large to cause some concern regarding the possibility of serious flow separation from the blades; however, the anticipated adverse effects did not occur, probably because of the relatively strong overturning tendencies of the fluid in this region.

Downstream Flow

The nature of the flow field downstream of the cascade was determined by making a series of velocity, pressure and angle surveys

in the trailing edge reference plane. The variation in the downstream total pressure parameter is presented in the form of a contour map in figure 28. The characteristic distortion of the flow field in accordance with the qualitative secondary flow model is at once apparent from this plot. It is seen that the low energy fluid from the screen wake is swept toward the suction side of the blade and that the "void" thus created near the pressure surface is filled with high energy air. It is also noted that although there was some accumulation of low energy flow near the suction side of the vanes, there was no evidence of the existence of a high loss vortex-core such as has been frequently observed in studies of boundary layer overturning.

The distribution of lateral flow angle in the downstream reference plane is shown as a contour map in figure 29. These data were measured using the hot wire instrumentation and were verified with both tuft and claw probe surveys. The regions of overturning and underturning are clearly outlined and are in agreement with the qualitative channel-theory model which was described previously.

The variation of the vertical flow angle in the downstream reference plane is shown for various "z" in figure 30; comparison of these results with the data of figures 19 and 20 shows the distinct circulatory motion which is produced by the secondary flows.

The variation in the spanwise component of velocity at specific values of "z" is shown in figure 31; the variable "w" is of particular significance in this investigation because it is used directly as a correlation parameter in comparing the experimental and the theoretical results. It is interesting to note that the magnitude of $\frac{w}{U_o}$ is everywhere less than 0. 20, this being substantially in agreement with the

assumption that the induced velocities are indeed perturbation quantities.

The amount of streamsurface warpage produced by the secondary flows is shown in figure 32. To obtain these data, a small heater coil was placed at numerous positions along lines of constant "z" in the upstream reference plane and the locations of the corresponding streamtubes in the trailing edge reference plane were then determined by using hot wire instrumentation to detect temperature variations.

Blade Loading

The static pressure distribution on the surface of the center blade was measured using the tapped vane and is shown plotted in dimensionless form for various values of "z" in figure 33. The spanwise variation in the component of blade loading parallel to the cascade was calculated from this data and is presented in figure 34. It is noted from this graph that the magnitude of the blade force is strongly dependent upon vertical position, this being in marked contrast with the two-dimensional form of loading which was observed for the "no screen" case of configuration I (figure 23).

4:2.3 CONFIGURATION III.

In this portion of the investigation, the relatively dense screen of the previous configuration was replaced by a lighter single-ply obstruction element which is shown in figure 14-b: no further changes were made in the tunnel geometry.

Upstream Flow Field

A series of test surveys were again carried out in the upstream

reference plane to determine the distributions of pressure, velocity, and flow direction. The results of these measurements are briefly described below.

The spanwise variation in flow velocity at the upstream station is shown in figure 35; it is observed that the minimum wake velocity was approximately 69 percent of the free stream velocity and that the influence of the screen is once again concentrated in the center ten percent of the span height.

The upstream total and static pressure distributions are presented in dimensionless form in figures 36 and 37; the parameter $\frac{\rho}{2}\left[q_0^2 - q^2_{wake_{max.}}\right]$ has again been used in the normalization process to give results which are consistent in form with the data from configuration II.

The measured variation in the lateral flow angle is shown in figure 38. As was the case with the heavier three-ply obstruction, a component of velocity normal to the two-dimensional flow was induced locally by the oblique orientation of the screen.

Downstream Flow

For this configuration, no attempt was made to describe the flow field in the entire downstream reference plane. Instead, the only test surveys that were made were those which were required for evaluating the strength of the trailing edge vortex sheet, i.e., velocity and angle measurements in the neighborhood of the blade wake region. This particular data was needed for comparing the results of theory and experiment; the qualitative nature of the downstream flow field was satisfactorily established in configuration II, and it was felt that further extensive testing would not add materially to the general

description of the induced secondary flows.

Blade Loading

The static pressure distribution was measured on the surface of the center vane and is shown for various values of "z" in figure 39. These data were used to determine the variation in cascade loading which is plotted in figure 40. It is seen from this graph that the magnitude of the blade force is once again functionally dependent on spanwise position and is substantially different from the characteristically two-dimensional plot of configuration I.

4:2.4 CONFIGURATION IV.

In configuration IV, a single ply strip of screening was mounted near the end of the convergent section of the upstream "bellmouth"; this obstruction element was mounted perpendicular to the tunnel side walls rather than parallel to the axis of the cascade. A series of test surveys were made ahead of the turning vanes to determine the nature of the approach flow; the results of these measurements are shown in figures 41 through 44. It is seen from figure 44 that the distinct cross-flows which existed in configurations II and III were completely eliminated by the reorientation of the screen.

As in configuration II, the only downstream flow data which were recorded were those velocity and angle measurements that were needed for calculating the strength of the trailing edge vortex sheet. The pressure distributinn on the surface of the center vane was recorded but was found to be incorrect due to a manometer line break; the spanwise variation in blade loading, therefore, was not calculated for this configuration.

V. DISCUSSION

Two methods dealing with the theoretical prediction of secondary flows were discussed in section II. The details of the channel-theory analysis were presented in connection with the first method, and the exact linearized problem was formulated in the second approach. It is noted that whereas the second procedure gives a system of differential equations which are a true representation of the three-dimensional perturbed flow field, the method is at present not quantitatively useful since no explicit solutions have been obtained for the derived set of equations.

In contrast to the exact formulation of the problem, the channel-theory method does not consider the details of the flow in the turning vane passages and does not satisfy the correct boundary conditions downstream of the cascade. This procedure, therefore, is admittedly not completely satisfactory; it is, however, the only approach which is now available for predicting the behavior of secondary flows, and it has been found in the current study that the channel model does give results which are in surprisingly good agreement with the measured data. The applicability of the channel-theory analysis to the study of secondary flows is considered in section 5:1 below: this is followed in section 5:2 by a comparison of theoretical and experimental results.

5:1 APPLICABILITY OF THE LINEARIZED CHANNEL-THEORY MODEL TO THE EXPERIMENTAL INVESTIGATION

In previous attempts to test the validity of linearized secondary flow theories, investigators have often carried out experimental programs which were distinctly large disturbance in character and

which, therefore, were not readily amenable to study by a perturbation type of analysis; it is believed that this factor has been a primary cause for the overall lack of quantitative agreement between experimental and theoretical results. With this in mind, an important goal of the present study was to conduct a series of tests which were basically consistent with the fundamental hypotheses that were built into the theory.

The applicability of the channel-theory model in the current experimental investigation can be examined by testing to see that the nature of the measured flow actually is compatible with that which is prescribed in the theoretical analysis. Consider, for example, the flow field of configuration II, this being the least linear, and hence the most restrictive, case studied. Here the maximum ratio of the measured secondary velocity to the local primary flow velocity was found to be approximately 0.50 in the downstream reference plane. It is noted immediately that the assumption of perturbation velocity distortion is, therefore, only approximately true; however, since no vortex core roll-up was observed, and since the qualitative nature of the flow field was everywhere compatible with that of the channel-theory model, it is plausible to expect the linearized analysis to give a good first order solution, even in this limiting case.

A second basic assumption which is inherent in the linearized theory is that fluid surfaces which are originally horizontal upstream of the cascade tend to remain level planes as they pass through the blade row. The validity of this hypothesis was tested by following the motion of fluid particles through the vanes. The measured amount of level plane distortion is shown in figure 32, and it is seen that the experimental results again show only approximate agreement with the

non-warpage assumption of the theory; this, of course, is due to the fact that the induced spanwise velocities were somewhat larger than perturbation quantities. It was found, however, that a satisfactory estimate of the level plane warpage could be easily determined by considering the self-transport effects of the induced spanwise velocities which were predicted by the theory; this, therefore, implies that a very simple iterative type of correction is probably adequate for computing the streamsurface distortion when the non-linearity of the experiment is not too severe.

A third assumption of the theory is that viscous losses in the blade row are negligible. This hypothesis was verified by measuring the total pressure fore and aft of the cascade and then observing that, outside of the blade wake regions, no significant differences were noted at corresponding points upstream and downstream of the turning vanes on the same streamline. It is important to point out that the assumption of negligible viscosity was often, if not always, violated in those studies of secondary flows which resulted from boundary-layer type distortions in the upstream velocity profile; here it was found that the high energy air which moved in to replace the overturned boundary flow was subsequently reduced to low energy fluid by viscous shear losses at the solid boundary.

The final basic assumption of the linearized theory is that the components of vorticity may be treated as perturbation quantities in the analysis. The validity of this hypothesis can not be verified directly for a particular case because no exact reference level of vorticity is available. However, it is sufficient to specify that the magnitude of the vorticity must be such that the secondary flow velocities

induced by it remain small; this then is equivalent to saying that the product of the upstream vorticity times the amount of turning acts effectively, as in the present case, as a perturbation quantity.

5:2 COMPARISON OF EXPERIMENTAL AND THEORETICAL RESULTS

The brief discussion of the preceding paragraphs indicates that the linearized channel-theory analysis should, even with the existence of a relatively large upstream disturbance, give a satisfactory description of the secondary flows induced by the cascade turning. In the remainder of this section, various quantitative comparisons of theoretical and experimental results are given; for simplicity, these comparisons are initially limited primarily to a consideration of the measured data from configuration II. The corresponding results for configurations III and IV are discussed later.

5:2.1 STREAMSURFACE DISTORTION

The concept of streamsurface distortion was introduced in the preceding section; there it was pointed out that an important assumption of the linearized channel-theory model is that fluid surfaces which are horizontal upstream of the cascade tend to remain level planes as they pass through the blade row. This, of course, is equivalent to specifying that the self-transport effects of the induced secondary velocities are sufficiently small to be negligible in the analysis.

To test the above assumption, the actual amount of level plane warpage was determined experimentally for the "heavy screening" case of configuration II. Here a small heater coil was moved along lines of constant "z" in the upstream reference plane, and the locations

of the warmed stream filaments were determined downstream of the blade row by hot wire measurements. A number of horizontal traverses were made at various spanwise positions; the results of these surveys are shown in figure 45. It is noted that because of the turbulence level at the lower boundary of the screen wake, the data points for the $z = 1.0''$ test run were extremely difficult to obtain and should, therefore, be regarded as only qualitatively correct.

Also presented in figure 45 are curves which show the theoretically calculated variations in streamsurface distortion for the above values of "z". These plots were obtained as follows (the particular case $z = 3''$ is considered without loss of generality): the variation in the spanwise component of velocity was first calculated, on the basis of no level plane distortion, for $z = 3$ in the downstream reference plane; this was done using the linearized channel-theory analysis in conjunction with the known upstream flow conditions. These results were then used in an iterative fashion in the following equation to determine the amount of streamsurface warpage.

$$\frac{\Delta h(\eta; z=3)}{\Delta L} \doteq \frac{\overline{w}(\eta; z=3)}{\overline{q_s}(z=3)} \qquad (5.1)$$

where Δh is the spanwise distance that a particle is shifted by the self-transport effects of the induced secondary flows;

ΔL is the streamwise distance that a particle travels in going through the blade row;

$\overline{w}$ is the average spanwise component of velocity which exists along the particle path (calculated from theory), and

$\overline{q_s}$ is the average streamwise component of velocity which exists along the particle path.

Now ΔL is known from blade geometry;

$$\overline{w}(\eta; z=3) \doteq \frac{1}{2} w(\eta; z=3)_{downstream}$$ (known from theoretical calculations);

and

$$q_{bs}(z=3) \doteq \frac{1}{2}\left[q_{bs}(z=3)_{upstm.} + q_{bs}(z=3)_{downstm} \right]$$ (known from the upstream flow and the blade geometry)

Therefore, a rough estimate of the amount of streamsurface distortion can be calculated from the above equation.

Comparison of the theoretical and the experimental curves of figure 45 shows that the extremely simple approach of the previous paragraph is probably satisfactory when the induced velocities are small.

5:2.2 DISTRIBUTION OF SPANWISE COMPONENT OF VELOCITY

The most direct method of comparing the analytic results of the channel-theory approach with the measured results of the experimental investigation is to test the agreement between the predicted and actual distributions of the spanwise component of velocity. This method of comparison was made for the "heavy screening" case of configuration II, and the results thereof are discussed in the remainder of this section.

The variation of the secondary velocity component "w" was computed from the analytic channel-theory model by the method which was outlined earlier. However, before attempting an immediate comparison with the corresponding flow data, the following very important adjustment was made: the calculated velocity vector at each particular

point in the flow field was locally displaced, in the spanwise direction, a distance equal in value to the amount of streamsurface distortion which was predicted from the theory to exist at that same respective point. In other words, the magnitude of the distributed spanwise component of velocity was computed directly from the theory; but the position at which each vector of this field was assumed to act was physically displaced, the amount of displacement at each point being set equal to the amount of streamsurface distortion which was theoretically predicted at that point.

The measured and the calculated variations in the downstream vertical component of velocity are shown for various values of "z" in figure 46. It is seen that there is consistently good agreement between experimental and theoretical results only when suitable correction is made for the self-transport properties of the secondary flow. This fact is particularly significant when it is noted that the maximum value of $\frac{w}{U}$ in the entire trailing edge reference plane was approximately only 0.20, thereby implying relatively small amounts of streamsurface distortion. It is not at all surprising, therefore, that the agreement between theory and experiment is poor for those cases where $\frac{w}{U}$ is of the order of 0.50 to 0.60 and where no adjustment is made for level plane warpage. The data shown in figure 5 of reference (5) is a case in point; here it is seen that the shape of the measured spanwise velocity distribution is distinctly unsymmetric and tends, at least qualitatively, toward that form which would be expected from theory if self-transport effects were included in the analysis.

5:2.3 DISTRIBUTION OF TRAILING EDGE CIRCULATION

The applicability of the channel-theory model as a method for predicting secondary flows was studied in the preceding section by comparing, in the entire downstream reference plane, the experimental and the analytically calculated distributions of induced spanwise velocity. In an effort to simplify this procedure, it was decided to focus attention on the trailing edge vortex sheet and to test the agreement between the measured and the theoretical distributions of shed circulation; the purpose of this analysis was to study the advisability of using the magnitude of the shed vorticity as a second meaningful parameter for testing the predicted results of the channel-theory model. This approach appeared to be especially attractive for two reasons: first, the nature of the analytic calculations was such that the strength of the theoretical vortex sheet was particularly easy to evaluate; and secondly, experimental measurements were required only in the vicinity of the trailing edge sheet and not over the entire downstream channel area, thus substantially reducing the amount of flow distribution data which were needed. Furthermore, there was considerable interest at the onset of this investigation as to the exact composition of the trailing edge vortex sheet, and it was accordingly felt that extensive experimental data should be collected in this particular region of the flow field.

In experimentally finding the distribution of vorticity downstream of the blade trailing edge, it was necessary to compute the circulation around a series of elemental paths of the type shown in figure 47; this procedure was dictated because the lateral variation of the spanwise velocity "w" was known to be relatively smooth across

the blade wake rather than sharply discontinuous, (see figure 48). The variation of the parameter $\frac{\partial \Gamma}{\partial z}$ was computed in the following manner: consider the circulation around the incremental path ABCD in figure 47.

$$\Delta \Gamma_{ABCD} = \oint_{ABCD} \vec{q} \cdot d\vec{\ell} = (w_{AB} - w_{CD})\,\Delta z + \int_{D}^{A} v_n\, dn - \int_{C}^{B} v_n\, dn \qquad (5.2)$$

or

$$\Delta \Gamma_{ABCD} \doteq (w_{AB} - w_{CD})\,\Delta z \qquad (5.3)$$

since the net contribution from the two integral terms in equation 5.2 was generally found to be negligible for small values of Δz. Rewriting equation 5.3 in differential form then gives

$$\left.\frac{\partial \Gamma}{\partial z}\right)_{Exp.} \doteq w_{s^*} - w_{p^*} \quad ; \qquad (5.4)$$

here the subscripts s* and p* have been used to indicate that the quantity "w" is evaluated at points on the pressure and suction sides of the finite blade wake rather than at points which are spaced an infinitesimal distance apart.

The variation of the parameter $\left.\frac{\partial \Gamma}{\partial z}\right)_{Theory}$ can similarly be expressed as

$$\left.\frac{\partial \Gamma}{\partial z}\right)_{Theory} = w_s - w_p \quad ; \qquad (5.5)$$

here it is not necessary to consider a finite blade wake, and the subscripts "s" and "p" refer to infinitesimally separated points on opposite sides of the extended channel wall. The spanwise distributions

of " ω_s " and " ω_p " can be calculated directly from the channel-theory model; however, because of the marked improvement that was noted earlier when the self-transport effects of the induced velocity field were included in the analysis, it was deemed advisable to again make the same simplified correction before comparing the experimental and the theoretical results.

5:2.3.1 Comparison of Experimental and Theoretical Distributions of Trailing Edge Circulation

The experimental variation of $\frac{\partial \Gamma}{\partial z}$ downstream of the trailing edge was evaluated from the test data and is shown for configurations II, III, and IV in figure 49; also presented in these plots is the theoretical variation of $\frac{\partial \Gamma}{\partial z}$ (for case II the results are shown both with and without compensation for the self-transport effects of the induced secondary flow field). It is seen from figure 49-a that satisfactory agreement for configuration II was obtained between the measured and the calculated results only when the simplified correction for stream-surface warpage was included in the analysis. Here it is once again emphasized that even in those cases where the relative magnitude of the spanwise velocity field appears to be numerically quite small, the level plane distortion which corresponds to the induced secondary flows must not be arbitrarily neglected when comparing the experimental and the theoretical results.

The curves from figure 49 show that the measured and the calculated distributions of $\frac{\partial \Gamma}{\partial z}$ in the trailing edge vortex sheet were in good agreement; this then implies that the channel-theory model is indeed expected to give a satisfactory description of the downstream secondary flows for those cases in which acceptable correlation exists

between the theoretical and the experimental variations of shed circulation.

5:2.4 BLADE LOADING

An important goal of the current study was to attempt to predict the distribution of blade loading when the approach velocity into the cascade was non-uniform along the span. In the remainder of this section, two new analytic methods for accomplishing the above objective are outlined. In the first approach, the variation of bound vorticity is evaluated along the blade, and the cascade loading is then determined from a sort of localized two-dimensional flow analysis; in the second approach, the blade loading is evaluated directly from computation of momentum changes across the cascade. It will be seen that the results of the previously discussed channel-theory study play an important role in each of these two analyses.

5:2.4.1 Method I

In the first method, the cascade lift is functionally expressed in terms of the known upstream velocity and the unknown bound circulation; a procedure is then given for estimating the spanwise variation in bound vorticity, thereby permitting a direct computation of blade loading.

Consider the cascade shown in figure 50. Assuming that the streamsurface warpage may be neglected, the component of blade load parallel to the cascade can be written from momentum principles as:

$$F_y = \Delta(\dot{m} v_y) = \rho g v_x(z)\left[\overline{v_{y_1}}(z) - \overline{v_{y_2}}(z)\right] \qquad (5.6)$$

where F_y is the component of blade load parallel to the cascade;

g is the blade gap;

v_x is the axial velocity;

$\overline{v_{y_2}}$ is the value of v_y at station 2 averaged over a blade gap, and

$\overline{v_{y_1}}$ is the value of v_y at station 1 averaged over a blade gap.

Computing the circulation around path ABCD of figure 50 gives

$$\oint \vec{q}\cdot d\vec{\ell} = \Gamma_v(z) + \iint_{ABCD} \omega_3 \, dA = \int_A^B \vec{q}\cdot d\vec{\ell} + \int_B^C v_y \, dy + \int_C^D \vec{q}\cdot d\vec{\ell} + \int_D^A v_y \, dy =$$

$$= \int_B^C v_y \, dy + \int_D^A v_y \, dy = g\left[\overline{v_{y_1}} - \overline{v_{y_2}}\right] \; ; \text{ thus}$$

$$\Gamma_v(z) = g\left[\overline{v_{y_1}}(z) - \overline{v_{y_2}}(z)\right] \qquad (5.7)$$

Substituting from equation 5.7 into equation 5.6 then gives the standard cascade relation

$$F_y(z) = \rho \, v_x(z) \, \Gamma_v(z) \qquad (5.8)$$

An expression for $\Gamma_v(z)$ can be determined as follows: the circulation around path A'B'CD is given by

$$\oint_{A'B'CD} \vec{q}\cdot d\vec{\ell} = \Gamma_v + \iint_{A'B'CD} \omega_3 \, dA = \int_{A'}^{A} \vec{q}\cdot d\vec{\ell} + \int_A^B \vec{q}\cdot d\vec{\ell} - \int_B^{B'} \vec{q}\cdot d\vec{\ell} +$$

$$+ \int_{B'}^{C} \vec{q}\cdot d\vec{\ell} + \int_C^D \vec{q}\cdot d\vec{\ell} + \int_D^{A'} \vec{q}\cdot d\vec{\ell} \qquad (5.9)$$

Using the standard (s, n, z) coordinate system, equation 5.9 can be expanded as

$$\Gamma_v = v_{s_1} g \sin\alpha_1 + \int_A^B \vec{q}\cdot d\vec{\ell} - v_{s_2} g \sin\alpha_2 + \overline{v_{n_2}} g \cos\alpha_2 + \int_C^D \vec{q}\cdot d\vec{\ell} - \overline{v_{n_1}} g \cos\alpha_1 \qquad (5.10)$$

where α_1 and α_2 are the angles between the axial direction and the mean velocity vectors of the primary flow at stations 1 and 2 respectively; and

U_s and U_n are the components of velocity parallel and perpendicular respectively to the mean primary flow direction. Noting that $\int_C^D \vec{q}\cdot d\vec{\ell} = -\int_A^B \vec{q}\cdot d\vec{\ell}$ in equation 5.10 and simplifying gives

$$\Gamma_v(z) = g\left[U_{s_1}(z)\sin\alpha_1 - U_{n_1}(z)\cos\alpha_1 - U_{s_2}(z)\sin\alpha_2 + U_{n_2}(z)\cos\alpha_2\right] \qquad (5.11)$$

Replacing z by z+Δz in equation 5.11 then gives

$$\Gamma_v(z+\Delta z) = g\left[U_{s_1}(z+\Delta z)\sin\alpha_1 - U_{n_1}(z+\Delta z)\cos\alpha_1 + - U_{s_2}(z+\Delta z)\sin\alpha_2 + U_{n_2}(z+\Delta z)\cos\alpha_2\right] \qquad (5.12)$$

Subtracting equation 5.11 from equation 5.12 and expressing the result in differential form gives

$$\frac{d\Gamma_v}{dz} = g\left[\left(\frac{dU_s}{dz}\right)_1\sin\alpha_1 - \left(\frac{dU_s}{dz}\right)_2\sin\alpha_2 - \left(\frac{d\bar{U}_n}{dz}\right)_1\cos\alpha_1 + \left(\frac{d\bar{U}_n}{dz}\right)_2\cos\alpha_2\right] \qquad (5.13)$$

Assuming that the axial velocity is a function of spanwise position only, the continuity equation can be written as $U_{x_1}(z) = U_{x_2}(z)$; expressing U_x in terms of U_s and U_n at the upstream and downstream stations and then solving for U_{s_2} , the following equivalent form of the continuity equation can be derived:

$$U_{s_2}(z) = \frac{\cos\alpha_1}{\cos\alpha_2}\left[U_{s_1} + U_{n_1}\tan\alpha_1\right] - \bar{U}_{n_2}\tan\alpha_2 \qquad (5.14)$$

It is noted that $\overline{v_{n_2}}$ rather than v_{n_2} can be used in the last term of equation 5. 14 without loss of generality by considering v_{s_2} to be evaluated at the particular normal position at which $v_{n_2} = \overline{v_{n_2}}$. Differentiating equation 5. 14 with respect to "z" gives:

$$\left(\frac{dv_s}{dz}\right)_2 = \frac{\cos\alpha_1}{\cos\alpha_2}\left[\left(\frac{dv_s}{dz}\right)_1 + \tan\alpha_1\left(\frac{dv_n}{dz}\right)_1\right] - \tan\alpha_2\left(\frac{d\overline{v_n}}{dz}\right)_2 \qquad (5.15)$$

substituting equation 5. 15 into equation 5. 14 gives:

$$\frac{d\Gamma_v}{dz} = q\left\{\left(\frac{dv_s}{dz}\right)_1\left[\sin\alpha_1 - \sin\alpha_2\frac{\cos\alpha_1}{\cos\alpha_2}\right] - \left(\frac{dv_n}{dz}\right)_1\left[\sin\alpha_1\tan\alpha_2 + \cos\alpha_1\right] + \right. \qquad (5.16)$$

$$\left. + \frac{1}{\cos\alpha_2}\left(\frac{d\overline{v_n}}{dz}\right)_2\right\}$$

All of the terms in equation 5. 16 are known except the final factor $\left(\frac{d\overline{v_n}}{dz}\right)_2$; a method is described below for evaluating this parameter in terms of quantities which are known from the results of the channel-theory analysis. Consider the flow cross-section in the (n, z) plane at station 2 which is defined by the normal line B'C and is of height Δs (see figure 51). The circulation around this elemental area is given by the following

$$\oint_{B'CC''B''} \vec{q}\cdot d\vec{\ell} = q\cos\alpha_2\left[\overline{v_{n_2}}(z) - \overline{v_{n_2}}(z+\Delta z)\right] \doteq -q\cos\alpha_2\left(\frac{d\overline{v_n}}{dz}\right)_2\Delta z \qquad (5.17)$$

here it is noted that the contributions of the two vertical legs cancel. The circulation in this section B'CC"B" can also be expressed as

$$\oint_{B'CC''B''} \vec{q}\cdot d\vec{\ell} = \iint_{B'CC''B''} (\omega_1)_2\, dA + \Delta\Gamma_{concentrated} =$$

$$= (\omega_1)_2\, q \cos\alpha_2\, \Delta z + (w_P - w_S)\,\Delta z \qquad (5.18)$$

where both $(\omega_1)_2$, the distributed passage vorticity at station 2, and $(w_P - w_S)$, the jump in the spanwise component of velocity across the extended trailing edge wall, are assumed to be known from channel-theory calculations. Equating equations 5.17 and 5.18 and solving for $\left(\frac{d\bar{v}_n}{dz}\right)_2$ then gives

$$\left(\frac{d\bar{v}_n}{dz}\right)_2 = \frac{1}{q\cos\alpha_2}\,(w_S - w_P) - (\omega_1)_2 \qquad (5.19)$$

An expression for $(\omega_1)_2$ was derived in Section II, (2.33):

$$(\omega_1)_2 = -\frac{1}{\cos\alpha_1 \cos\alpha_2}\left(\frac{dv_S}{dz}\right)_1\left[\alpha_2 - \alpha_1 + \frac{1}{2}\left(\sin 2\alpha_2 - \sin 2\alpha_1\right)\right] - \frac{\cos\alpha_1}{\cos\alpha_2}\left(\frac{dv_n}{dz}\right)_1 \qquad (5.20)$$

Substituting equations 5.19 and 5.20 into equation 5.16 gives the following expression for $\frac{d\Gamma_v}{dz}$ in terms of known quantities.

$$\frac{d\Gamma_v}{dz} = q\left\{\left(\frac{dv_S}{dz}\right)_1\left[\sin\alpha_1 \tan\alpha_2\left(\tan\alpha_1 - \tan\alpha_2\right) + \frac{\alpha_2 - \alpha_1}{\cos\alpha_1 \cos^2\alpha_2}\right] + \right.$$

$$\left. -\left(\frac{dv_n}{dz}\right)_1\left[\cos\alpha_1 \tan\alpha_2\left(\tan\alpha_1 - \tan\alpha_2\right)\right]\right\} + \frac{w_S - w_P}{\cos^2\alpha_2} \qquad (5.21)$$

Equation 5. 21 is the desired expression showing the spanwise variation in the bound circulation; the usual assumption has been made that v_{s_1} and v_{n_1} are functions only of "z". The distribution of blade loading for a particular case can be calculated by integrating equation 5. 21 to find $\Gamma_v(z)$ and then substituting the result into equation 5. 8.

An interesting feature of the foregoing analysis is that the so-called component of "stretching circulation", which is discussed at length in references (4), (5), (9), and (10), can be directly evaluated from equation 5. 21. The total strength per unit span of the circulation in the concentrated trailing edge vortex sheet is equal to $-(w_p - w_s)$, the minus sign being used to indicate clockwise rotation when looking upstream. The contribution per unit span to this sheet due to the shedding of bound vorticity is equal to $\left(\frac{d\Gamma_v}{dz}\right)_{shed} = -\frac{d\Gamma_v}{dz}$ and is known from equation 5. 21. The remaining circulation per unit span in the concentrated vortex sheet is called the stretching circulation and is equal to $\left[-(w_p - w_s) + \frac{d\Gamma_v}{dz}\right]$. Substituting for $\frac{d\Gamma_v}{dz}$ from equation 5. 21 gives the following expression for $\frac{d\Gamma_2}{dz}$, the stretching circulation per unit span:

$$\frac{d\Gamma_2}{dz} = \left[-(w_p - w_s) + \frac{d\Gamma_v}{dz}\right] = q\left\{\left(\frac{dv_s}{dz}\right)_1\left[\sin\alpha_1 \tan\alpha_2(\tan\alpha_1 - \tan\alpha_2) + \right.\right.$$

$$\left. + \frac{\alpha_2 - \alpha_1}{\cos\alpha_1 \cos^2\alpha_2}\right] - \left(\frac{dv_n}{dz}\right)_1\left[\cos\alpha_1 \tan\alpha_2(\tan\alpha_1 - \tan\alpha_2)\right] + \qquad (5.22)$$

$$\left. + \tan^2\alpha_2(w_s - w_p)\right.$$

Hawthorne (5) used the kinematical method which was suggested by Preston (4) to derive an expression for $\frac{\partial\Gamma_2}{\partial z}$ for the restricted case of $\alpha_2 = -\alpha_1$ and $\left(\frac{dv_n}{dz}\right)_1 = 0$. One important assumption which

was made in this work was that the portions of the vortex filaments which do not come in contact with the blade surfaces are only slightly deformed as they are carried through the cascade. It is shown below that, for the case of very small turning, the results of the current analysis are identical with the results of reference (5); this, therefore, implies, as perhaps might be expected, that the assumptions which were made in the kinematical approach concerning the shape of the distorted vortex filament are in reality equivalent to specifying small changes in flow angle across the blade row. Consider for example equation 5. 14 and suppose that $\overline{v_{\eta_2}} \tan\alpha_2 << v_{s_1} \frac{\cos\alpha_1}{\cos\alpha_2}$; ($\tan\alpha_2 \neq << 1$ necessarily); imposing the condition that $v_{\eta_1} = 0$ then gives:

$$v_{s_2}(z) \doteq v_{s_1}(z) \frac{\cos\alpha_1}{\cos\alpha_2} \qquad (5.14')$$

Replacing equation 5. 14 by equation 5. 14' in the analysis and solving for $\frac{d\Gamma_2}{dz}$ gives:

$$\frac{d\Gamma_2}{dz} = \frac{g}{\cos\alpha_1}\left(\frac{dv_s}{dz}\right)_1 \left[-\tan\alpha_2 \cos^2\alpha_1 + \frac{1}{2}\sin 2\alpha_2 + \alpha_2 - \alpha_1\right] \qquad (5.22')$$

It is noted that this expression reduces to the following form when $\alpha_2 = -\alpha_1$:

$$\frac{d\Gamma_2}{dz} = \frac{g}{\cos\alpha_1}\left(\frac{dv_s}{dz}\right)_1 (\alpha_2 - \alpha_1) \qquad (5.22'')$$

Equation 5. 22'' is identical with the corresponding relation of reference (5), provided that equation 5. 20, rather than the result of Squire and Winter, is used throughout for expressing the streamwise com-

ponent of vorticity. It is also noted that equation 5. 22 reduces directly to equation 5. 22" if $\alpha_2 = 0$; this particular restriction, however, was not built into the kinematical analysis and appears to be merely a specific cascade configuration for which the two analyses give the same expression for the "stretching circulation". In the present study, equation 5. 22" is of no value since $\alpha_2 \neq -\alpha_1$; the more general expression 5. 22 is, however, valid within the limits of the linearized perturbation analysis.

5:2. 4. 2 Method II

The second method which is presented for computing the distribution of blade loading is conceptually a simple application of the momentum principle applied to the results of the channel-theory analysis.

Consider once again the cascade geometry shown in figure 5l and recall the expression for the blade loading per unit span given by equation 5. 6:

$$F_{y_{blade}}(z) = \Delta(\dot{m} v_y)_{blade} = \rho g v_x(z)\left[\overline{v_{y_1}}(z) - \overline{v_{y_2}}(z)\right] \qquad (5.\ 23)$$

where F_y is the component of blade load parallel to the cascade;

g is the blade gap;

v_x is the axial velocity;

ρ is the fluid density;

$\overline{v_{y_2}}$ is the value of v_y at station 2 averaged over a blade gap;

$\overline{v_{y_1}}$ is the value of v_y at station 1 averaged over a blade gap.

It is noted here that streamsurface warpage due to secondary flow self-transport effects has been neglected and also that v_x is assumed to be a function of spanwise position alone. The only unknown in equa-

tion 5. 23 is the term $\overline{v_{y_2}}$; the magnitude of this factor can be determined as follows:

$$\overline{v_{y_2}}(z) \equiv \frac{1}{g}\int_{-g/2}^{g/2} v_{y_2}(y,z)\,dy = \frac{1}{g}\int_{-g/2}^{g/2}\left[v_{x_1}(z)\tan\alpha_2 - \frac{v_{n_2}(y,z)}{\cos\alpha_2}\right]dy = \tag{5. 24}$$

$$= v_{x_1}(z)\tan\alpha_2 - \frac{\overline{v_{n_2}}(z)}{\cos\alpha_2}$$

Substituting $\overline{v_{y_2}}$ from equation 5. 24 into equation 5. 23 and simplifying then gives the desired expression for the distribution of blade loading per unit span:

$$F_{y_{blade}}(z) = \rho g v_{x_1}(z)\left[v_{y_1}(z) - v_{x_1}(z)\tan\alpha_2 + \frac{\overline{v_{n_2}}(z)}{\cos\alpha_2}\right] \tag{5. 25}$$

The quantities $v_{x_1}(z)$ and $v_{y_1}(z)$ are known from the given upstream velocity field. The spanwise variation of $\overline{v_{n_2}}$ can be evaluated using the channel-theory analysis; this was done earlier and the appropriate relation is given by equation 11 of Appendix I.

5:2. 5 COMPARISON OF THEORETICAL AND EXPERIMENTAL DISTRIBUTIONS OF BLADE LOADING

5:2. 5. 1 Experimental Blade Loading

The experimental spanwise variation in blade loading was evaluated from the measured distribution of static pressure on the surface of the center cascade vane. The results of these calculations for configurations I, II, and III are shown in figure 52: it is seen that the loading was approximately constant for case I (no screen), but was distinctly non-uniform for cases II and III.

5:2. 5. 2 Theoretical Blade Loading for Configuration II

The predicted spanwise variation in blade loading was evaluated for configuration II by the two theoretical methods which were described in section 5:2. 4; the results of these computations are shown in figure 53. It is seen from this plot that the agreement between analysis and experiment was generally quite good. Of special interest here is the fact that the results of method I (section 5:2. 4. 1) are considerably better than was originally anticipated; it was thought that this particular approach would be extremely sensitive to the warpage effects of the induced secondary flows, thus making it quantitatively less accurate than the analytic procedure of method II (section 5:2. 4. 2). The final curve which is shown in figure 53 is the variation of loading that was calculated by assuming that the flow was locally two dimensional along the span and left the cascade at a constant exit angle; this curve is presented to show the serious error which is incurred if the downstream overturning is neglected when computing the distribution of blade force.

5:2. 5. 3 Theoretical Blade Loading for Configuration III

The theoretical distribution of cascade loading was computed for configuration III by each of the two analytic methods of section 5:2. 4 and is shown plotted in dimensionless form in figure 54. It is seen from this graph that excellent agreement was achieved between the measured and the calculated spanwise variations in blade force. As in the previous case, the loading was also determined on the basis of zero overturning; it is seen from figure 54 that this method is once again completely unsatisfactory.

VI. CONCLUDING REMARKS

The channel-theory analysis was found to be extremely useful in theoretically predicting the behavior of small disturbance secondary flows. Because the extended blade surfaces do not actually exist and because the true downstream boundary conditions should impose restrictions on the pressure field rather than on the normal component of velocity, it would appear that the channel model might not give an accurate representation of cascade flows. However, it has been demonstrated in the current investigation that the predicted results from the channel-theory analysis are in good agreement with the measured results from experimental testing; this then suggests that the important features of the assumed flow are actually simulated downstream of the cascade and that the detailed nature of the fluid motion within the turning vane passages is not a dominant factor in the generation of the induced flows.

A simple iterative method is proposed for incorporating the self-transport effects of the secondary flows into the theoretical analysis. It was shown that these self-transport effects must not arbitrarily be neglected when using the channel-theory model to calculate induced velocities. It was also shown that streamsurface warpage resulting from small disturbance secondary flows can be satisfactorily predicted.

Two methods are presented for determining the spanwise distribution in blade loading which results when the velocity profile far upstream of the cascade is non-uniform. These methods were tested experimentally and were found to give good agreement with measured

data when the secondary flows were perturbation quantities.

The exact linearized problem was formulated by deriving the differential equations for the three-dimensional perturbed flow field. Although not solved explicitly, this system of equations, in conjunction with a set of prescribed boundary conditions, is a correct representation for the secondary flow in a given cascade.

APPENDIX I

Let ϕ be the velocity potential for a concentrated two-dimensional vortex in the infinite channel shown in figure 56. From the Laplace equation in rectangular coordinates,

$$\frac{\partial^2 \Phi}{\partial \eta^2} + \frac{\partial^2 \Phi}{\partial z^2} = 0 \qquad \begin{matrix} 0 \leq \eta \leq b \\ -\infty \leq z \leq \infty \end{matrix} \tag{1}$$

The restriction that the "n" component of velocity vanishes at the channel walls gives:

$$\left.\frac{\partial \Phi}{\partial \eta}\right)_{\eta=0} = \left.\frac{\partial \Phi}{\partial \eta}\right)_{\eta=b} = 0 \tag{2}$$

The restriction that the "z" component of velocity vanishes far from the vortex gives:

$$\left.\frac{\partial \Phi}{\partial z}\right)_{|z| \to \infty} \longrightarrow 0 \tag{3}$$

Separating variables in equation 1 and applying the boundary conditions from equations 2 and 3 gives the following solution for ϕ :

$$\Phi(\eta, z) = \sum_{\lambda=0}^{\infty} A_\lambda \cos \frac{\lambda \pi}{b} \eta \; e^{\mp \frac{\lambda \pi}{b} z} \qquad (z \gtrless 0) \tag{4}$$

From symmetry considerations, the line z = o is a potential line; putting

$$\phi(\gamma \leq \eta \leq b, \; z = 0+) = 0 \tag{5-a}$$

and solving for the corresponding values of the velocity potential on the remainder of the line z = o gives:

$$\phi\left(0 \le n < \eta,\ z=0\right) = \frac{\Gamma}{2} \qquad (5\text{-b})$$

$$\phi\left(\eta < n \le b,\ z=0-\right) = \Gamma \qquad (5\text{-c})$$

Substituting from equation 5 into equation 4 and solving for the unknown constants gives the following expressions for ϕ :

$$z>0 : \ \phi(n,z) = \frac{\Gamma}{2b}\eta + \sum_{\lambda=1}^{\infty} \frac{\Gamma}{\lambda\pi} \sin\frac{\lambda\pi}{b}\eta \cos\frac{\lambda\pi}{b}n \ e^{-\frac{\lambda\pi}{b}z} \qquad (6\text{-a})$$

$$z<0 : \ \phi(n,z) = \frac{\Gamma}{2}(2b-\eta) - \sum_{\lambda=1}^{\infty} \frac{\Gamma}{\lambda\pi} \sin\frac{\lambda\pi}{b}\eta \cos\frac{\lambda\pi}{b}n \ e^{\frac{\lambda\pi}{b}z} \qquad (6\text{-b})$$

Replacing "z" in equation 6 by "z -ζ" to account for a concentrated vortex at (η, ζ) rather than at (η, 0) and then differentiating with respect to "z" to find the spanwise velocity distribution gives:

$$z \gtrless \zeta : \ w = -\sum_{\lambda=1}^{\infty} \frac{\Gamma}{b} \sin\frac{\lambda\pi}{b}\eta \cos\frac{\lambda\pi}{b}n \ e^{\mp\frac{\lambda\pi}{b}(z-\zeta)} \qquad (7)$$

Replacing Γ by a distributed vortex of strength ω_1 at (η,ζ) gives an expression for the incremental contribution to $w(n,z)$ due to the element of area $d\eta\, d\zeta$:

$$z \gtrless \zeta : \ dw = -\sum_{\lambda=1}^{\infty} \frac{\omega_1(\eta,\zeta)}{b} d\eta\, d\zeta \sin\frac{\lambda\pi}{b}\eta \cos\frac{\lambda\pi}{b}n \ e^{\mp\frac{\lambda\pi}{b}(z-\zeta)} \qquad (8)$$

Assume for simplicity that the strength of the distributed vorticity is an odd function of ζ alone and is not dependent on η ; substituting

into equation 8 and integrating over the entire flow field gives the following expression for w on $z \geq 0$, the region of primary interest in the current investigation:

$$w(\eta,z) = -\frac{2}{\pi}\sum_{\lambda=1,3,5,\ldots}^{\infty}\frac{1}{\lambda}\cos\frac{\lambda\pi}{b}\eta\left\{e^{-\frac{\lambda\pi}{b}z}\left[\int_0^z \omega_1(\rho)\left[e^{\frac{\lambda\pi}{b}\rho}-e^{-\frac{\lambda\pi}{b}\rho}\right]d\rho\right]+\right.$$
$$\left.+\left[e^{\frac{\lambda\pi}{b}z}-e^{-\frac{\lambda\pi}{b}z}\right]\int_z^{\infty}\omega_1(\rho)e^{-\frac{\lambda\pi}{b}\rho}d\rho\right\} \qquad (9)$$

A similar relation may be derived for "v", the lateral component of velocity, by differentiating the expression for "ϕ" with respect to "n"; the resulting expression for the restriction that the distributed vorticity is again an odd function of "ρ" alone is:

$$v(\eta,z)\Big|_{z\geq 0} = \frac{2}{\pi}\sum_{\lambda=1,3,5,\ldots}^{\infty}\sin\frac{\lambda\pi}{b}\eta\left\{-e^{-\frac{\lambda\pi}{b}z}\int_0^z \omega_1(\rho)\left[e^{\frac{\lambda\pi}{b}\rho}-e^{-\frac{\lambda\pi}{b}\rho}\right]d\rho+\right. \qquad (10)$$
$$\left.+\left[e^{\frac{\lambda\pi}{b}z}-e^{-\frac{\lambda\pi}{b}z}\right]\int_z^{\infty}\omega_1(\rho)e^{-\frac{\lambda\pi}{b}\rho}d\rho\right\}$$

The mean value of v(n, z) is used in this report for finding the average momentum change of the fluid as it passes through the blade row; the quantity $\bar{v}(z)$ can be calculated directly from equation 10 and is given by the following relation:

$$\bar{v}(z)\Big|_{z\geq 0} \equiv \frac{1}{b}\int_{\eta=0}^{b} v(\eta,z)\,d\eta = \left(\frac{2}{\pi}\right)^2\sum_{\lambda=1,3,5,\ldots}^{\infty}\frac{1}{\lambda^2}\left\{\right. \qquad (11)$$
$$\left.\cdot\left\{-e^{-\frac{\lambda\pi}{b}z}\int_0^z \omega_1(\rho)\left[e^{\frac{\lambda\pi}{b}\rho}-e^{-\frac{\lambda\pi}{b}\rho}\right]d\rho+\left[e^{\frac{\lambda\pi}{b}z}-e^{-\frac{\lambda\pi}{b}z}\right]\int_z^{\infty}\omega_1(\rho)e^{-\frac{\lambda\pi}{b}\rho}d\rho\right\}\right.$$

REFERENCES

(1) Herzig, H. E. and Hansen, A. G.: "Experimental and Analytic Investigations of Secondary Flows in Ducts," Journal of the Aeronautical Sciences, (1957), March, pp. 217-231.

(2) Mager, Artur: "Three-Dimensional Laminar Boundary Layer with Small Cross Flow," Journal of the Aeronautical Sciences, (1954), Volume 21, pp. 835-845.

(3) Squire, H. B. and Winter, K. G.: "The Secondary Flow in a Cascade of Airfoils in a Non-Uniform Stream," Journal of the Aeronautical Sciences (1951), Volume 18, pp. 271-277.

(4) Preston, J. H.: "A Simple Approach to the Theory of Secondary Flows," Aeronautical Quarterly, Volume 5, Part 3 (1954).

(5) Hawthorne, W. R. and Armstrong, W. D.: "Rotational Flow Through Cascades, Parts I and II", Quarterly Journal of Mechanics and Applied Mathematics, (1955), Volume 8, pp. 266-292.

(6) Loos, Henk G.: "Analysis of Secondary Flow in the Stator of an Axial Turbomachine", California Institute of Technology Jet Propulsion Center, Technical Report No. 3, (1953).

(7) Armstrong, W. D.: "The Secondary Flow in a Cascade of Turbine Blades," Aeronautical Research Council R. and M. No. 2979, (1957).

(8) Hawthorne, W. R.: "Secondary Circulation in Fluid Flow," Proceedings of the Royal Society, (1951), Volume 206, p. 374

(9) Soundranayagan: "The Secondary Flow Behind a Cascade," Journal of the Aeronautical Sciences,(1957), Volume 24, p. 707

(10) Smith, L. H.: "Three-Dimensional Flow in Axial-Flow Turbomachinery," Parts I and II, Johns Hopkins University, (1953).

(11) Hansen, A. G.; Herzig, H. E.; and Costello, G. R.: "A Visualization Study of Secondary Flows in Cascades," NACA TN 2947, (1953).

(12) Kofskey, M. G. and Allen, H. W.: "Smoke Study of Nozzle Secondary Flows in a Low Speed Turbine," NACA TN 3260, (1954).

(13) Lindley, Charles A.: "Secondary Flow in Compressor Cascades," Doctoral Thesis, California Institute of Technology, (1956).

(14) Alsworth, C. C. and Iura, T.: "Theoretical and Experimental Investigations of Axial Flow Compressors, Part 3," Mechanical Engineering Laboratory, California Institute of Technology, (1951).

(15) Hansen, A. G.; Herzig, H. Z.; and Costello, G. R.: "Smoke Studies of Secondary Flows in Bends, Tandem Cascades, and High Turning Configurations," NACA RM E52L24a, (1953).

(16) Herzig, H. Z. and Hansen, A. G.: "A Survey of Unclassified Axial Flow Compressor Literature," NACA RM E55L24a, (1953).

(17) Hansen, A. G.; Costello, G. R.; and Herzig, H. Z.: "Effect of Geometry on Secondary Flows in Blade Rows," NACA RM - E52H26, (1952).

(18) Kofskey, M. G.; Rohlik, H. E.; and Monroe, D. E.: "Experimental Investigation of Flow in an Annular Cascade of Turbine Nozzle Blades of Constant Discharge Angle," NACA RM - E 52A09, (1952).

(19) Lieblein, S. and Ackley, R. H.: "Secondary Flows in Annular Cascades and Effects on Flow in Inlet Guide Vanes," NACA RM E51G27, (1951).

(20) Wilbur, S. W.: "An Investigation of Flow in Circular and Annular 90 Degree Bends with a Transition in Cross Section," NACA TN 3995, (1957).

(21) Stanitz, J. D.; Osborn, W. M.; and Mizisin, J.: "An Experimental Investigation of Secondary Flow in an Accelerating Rectangular Elbow with 90 Degrees of Turning," NACA TN 3015, (1953).

(22) Dean, Robert C. Jr.: "Secondary Flow in Axial Compressors," Gas Turbine Laboratory, Massachusetts Institute of Technology, (1954).

(23) Hawthorne, W. R.: "Some Aerodynamic Problems of Aircraft Engines," Journal of the Aeronautical Sciences, (1957), Volume 24, pp. 713-731.

(24) Hawthorne, W. R.: "The Secondary Flow About Struts and Airfoils," Journal of the Aeronautical Sciences, (1954), Volume 21, pp. 588-608.

(25) Armstrong, W. D.: "The Secondary Flow in Compressor Blades at High Negative Incidences," Current Paper No. 297, (1956).

(26) Carter, A. D. S. and Cohen, E. M.: "Preliminary Investigation into the Three-Dimensional Flow Through a Cascade of Aerofoils," Aeronautical Research Council R. and M. No. 2339, (1949).

(27) Ehrich, F. F.: "Secondary Flows in Cascades with Twisted Blades," Journal of the Aeronautical Sciences, (1955), Vol. 22, pp. 51-60.

(28) Conrad, W. E.; Hanson, M. P.; and McAulay, J. E.: "Effects of Inlet-Air-Flow Distortion on Steady-State Altitude Performance of an Axial-Flow Turbojet Engine," NACA RM E55A04, (1955).

(29) Whitney, W. J.; Buckner, H. A.; and Monroe, D. E.; "Effect of Nozzle Secondary Flows on Turbine Performance as Indicated by Exit Surveys of a Rotor," NACA RM E54B03, (1954).

(30) Mair, W. A.: "The Distribution of Pressure on an Airfoil in a Stream with a Spanwise Velocity Gradient," Aeronautical Quarterly, (1955), Volume 4, pp. 2-12.

(31) Hausmann, G. F.; "Theoretical Induced Deflection Angle in Cascades with Wall Boundary Layers," Journal of the Aeronautical Sciences, (1948), Volume 15, p. 686.

(32) Ehrich, F. F. and Detra, R. W.: "Transport of the Boundary Layer in Secondary Flow," Journal of the Aeronautical Sciences, (1954), pp. 136-138

(33) Moore, R. W. and Richardson, D. L.: "Skewed Boundary-Layer Flow Near the End Walls of a Compressor Cascade," Transactions of A. S. M. E., (1957), Volume 79, pp. 1789-1800.

(34) Turner, J. R.: "An Investigation of the End-Wall Boundary Layer of a Turbine-Nozzle Cascade," Transactions of A. S. M. E., (1957), Volume 79, pp. 1801-18-6.

(35) Mager, Artur and Hansen, Arthur G.: "Laminar Boundary Layer Over Flat Plate in a Flow Having Circular Streamlines," NACA TN 2658, (1952).

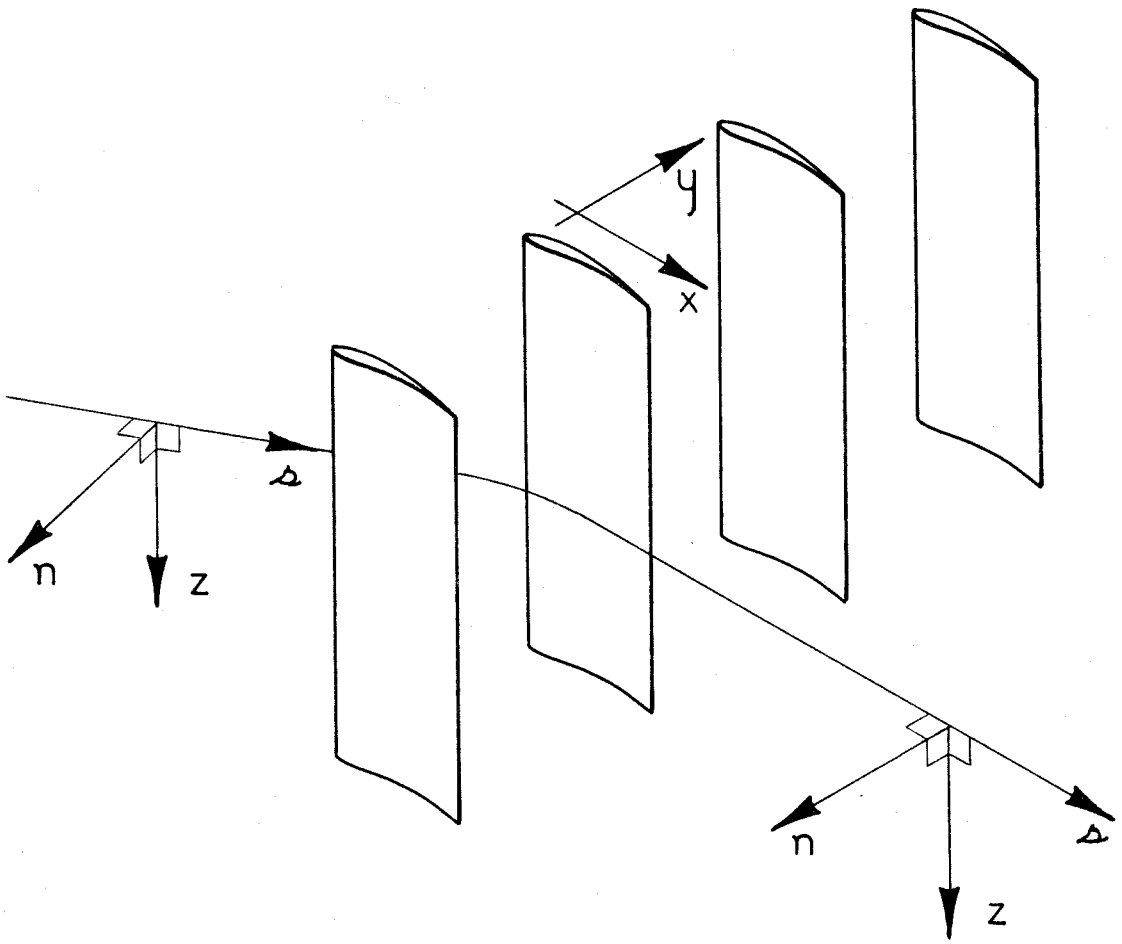

FIG. 1 COORDINATE SYSTEM

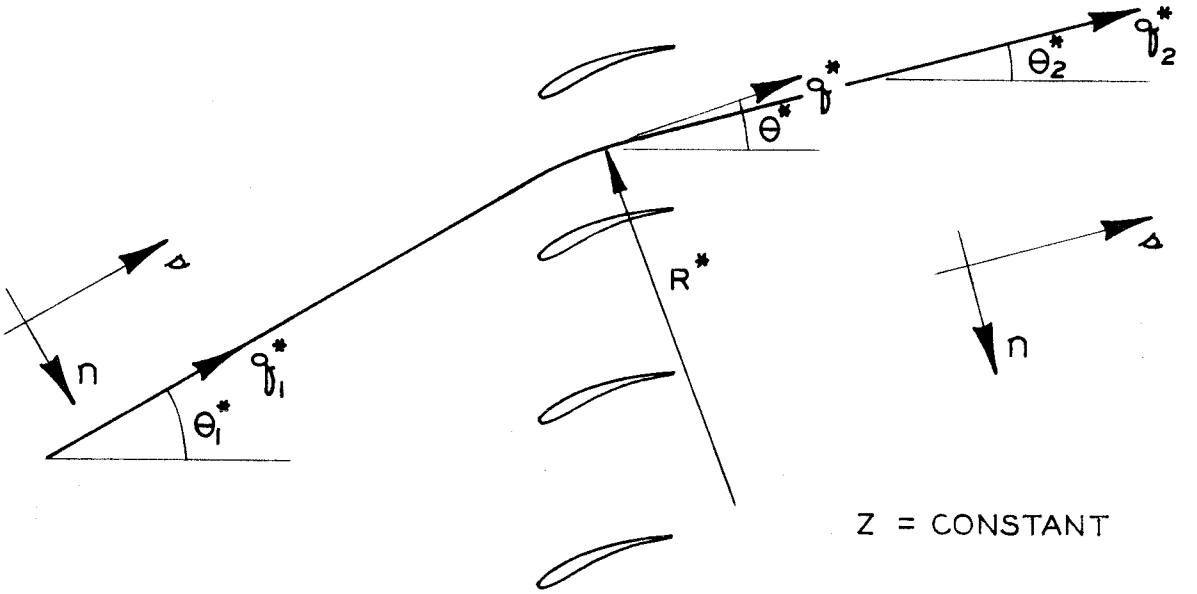

FIG. 2 MEAN STREAMLINE, PRIMARY FLOW

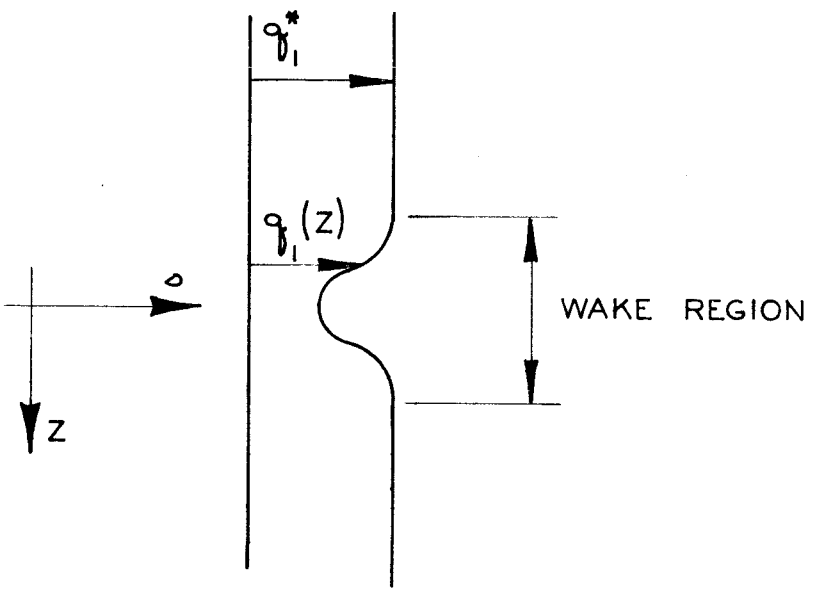

FIG. 3 UPSTREAM VELOCITY PROFILE

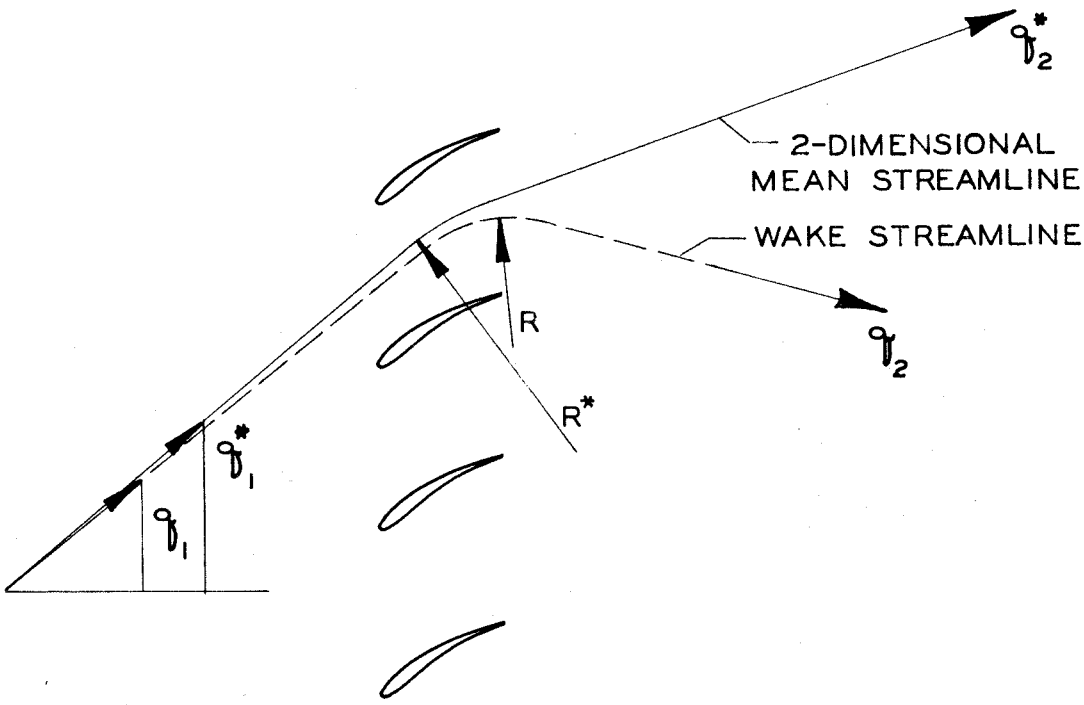

FIG. 4 STREAMLINE OVERTURNING

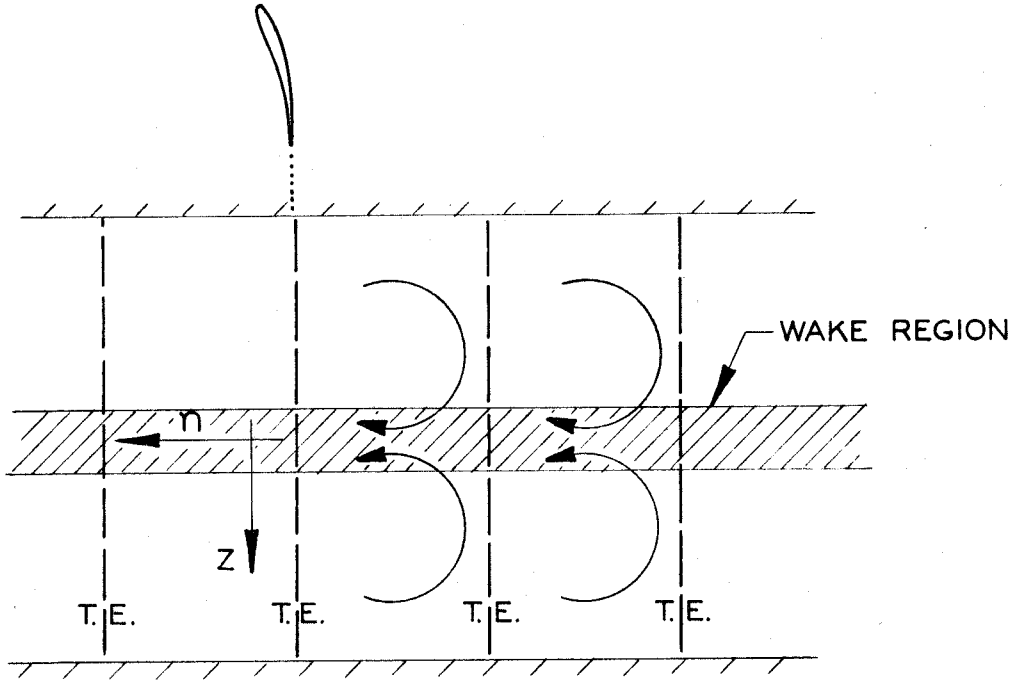

FIG. 5 SECONDARY CIRCULATION, LOOKING UPSTREAM AT TRAILING EDGE PLANE

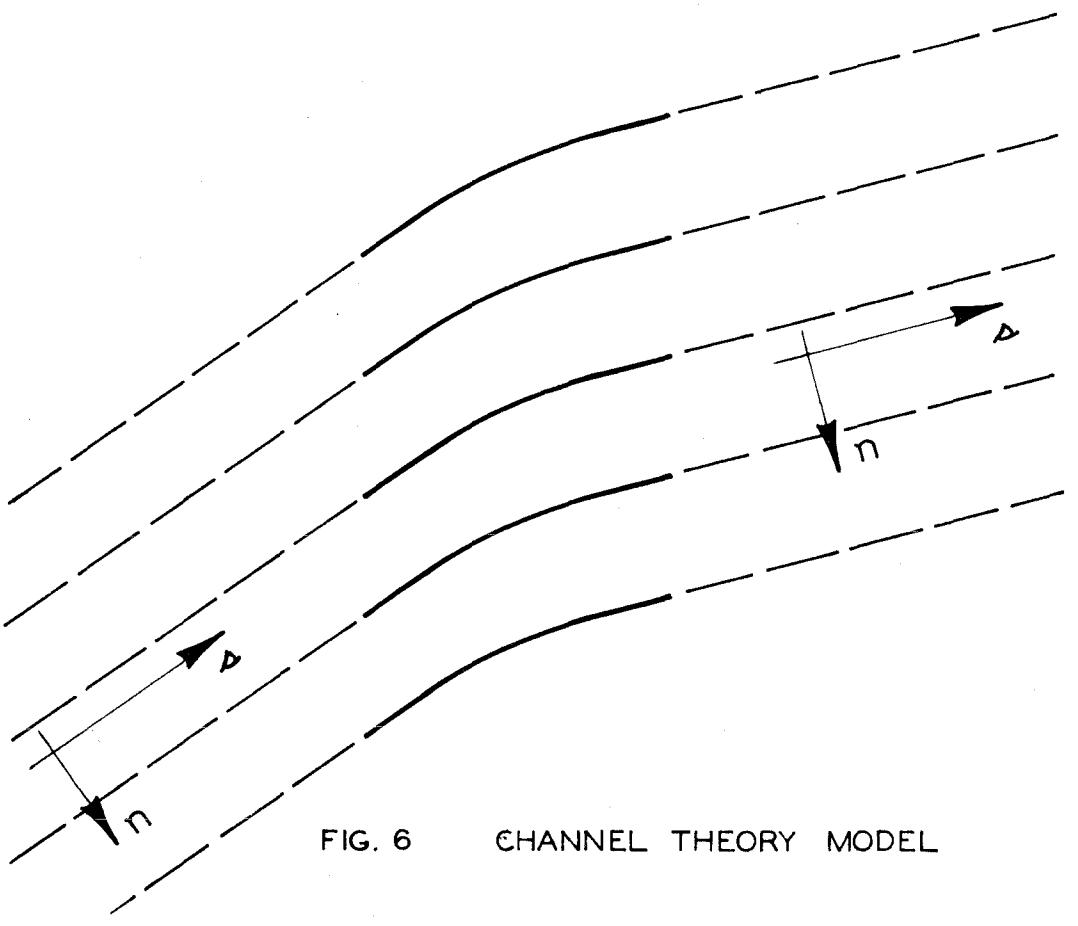

FIG. 6 CHANNEL THEORY MODEL

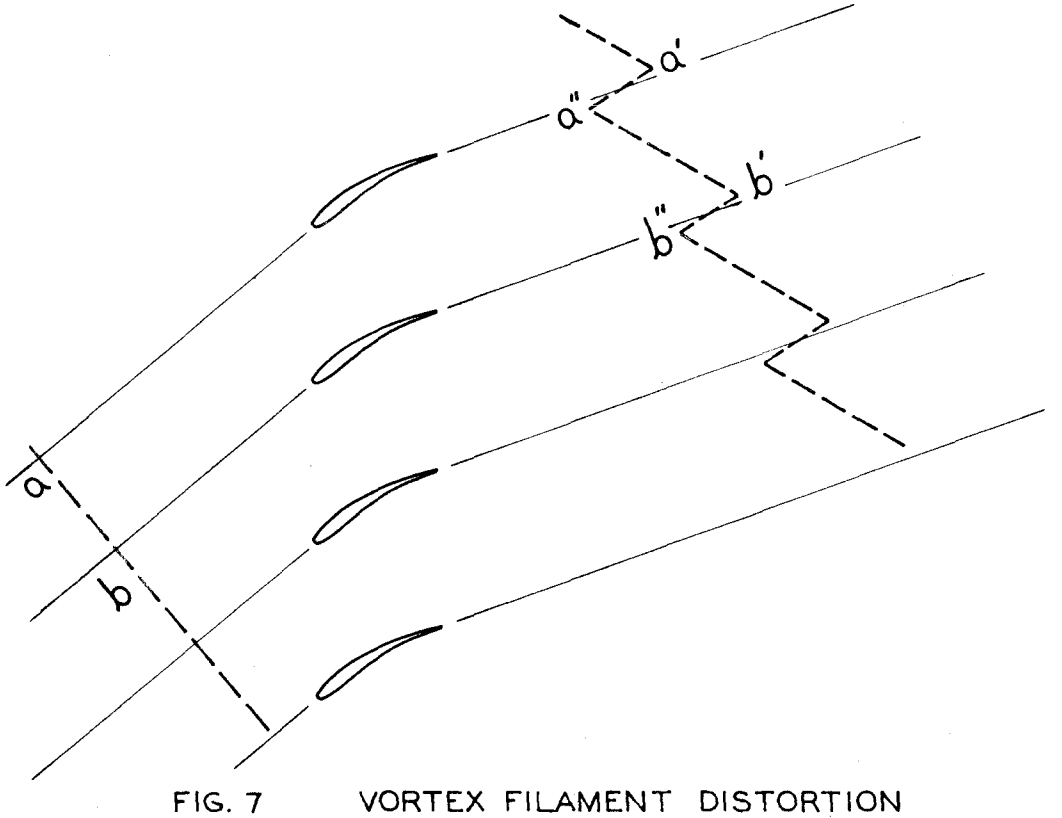

FIG. 7 VORTEX FILAMENT DISTORTION

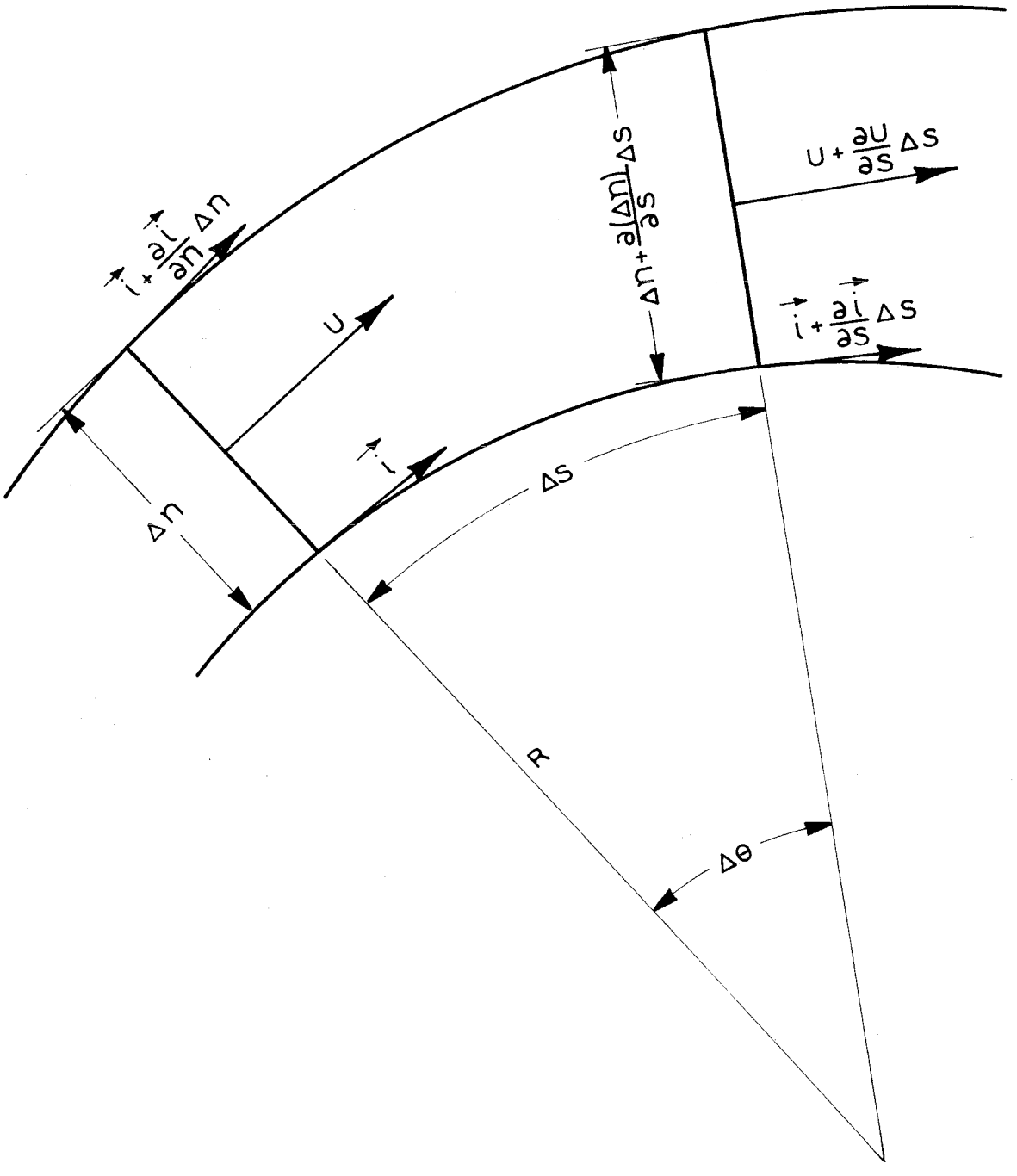

FIG. 8 STREAMTUBE ELEMENT

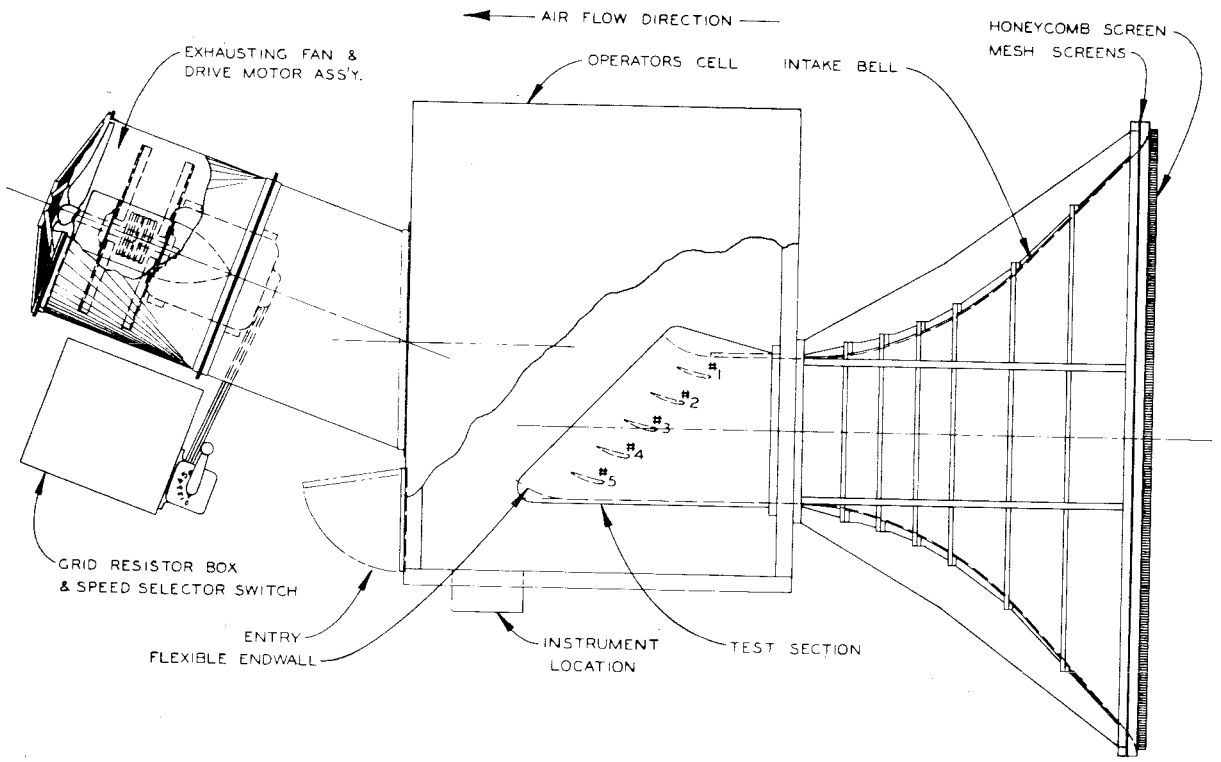

FIG. 9 CASCADE TUNNEL

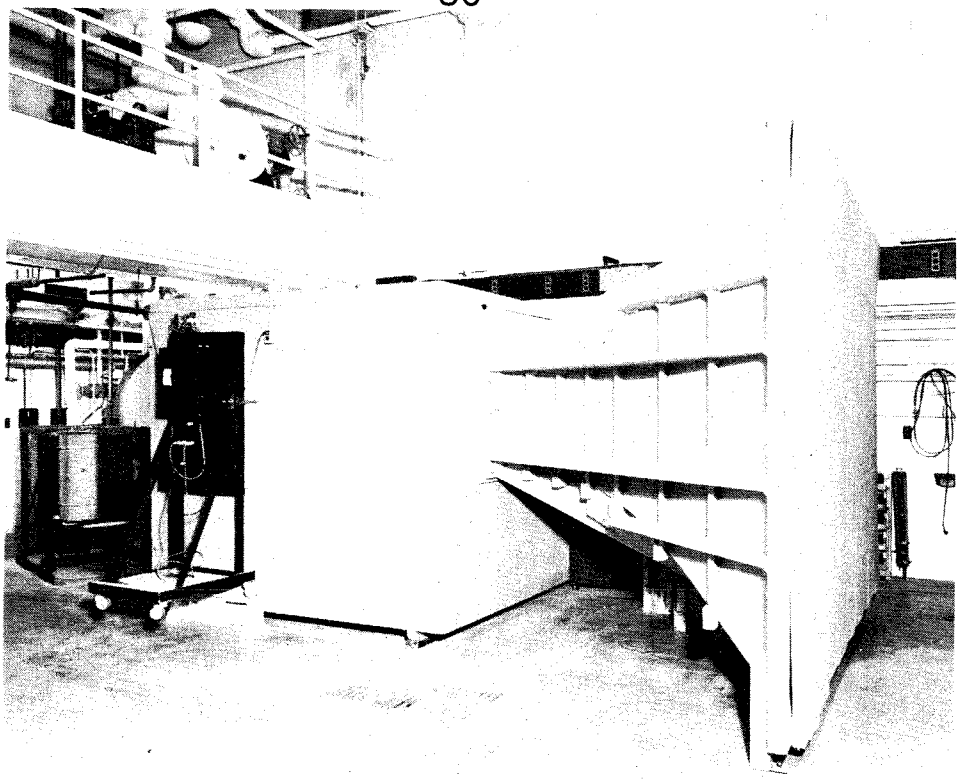

FIG. 10 VIEW OF CASCADE TUNNEL FROM INLET

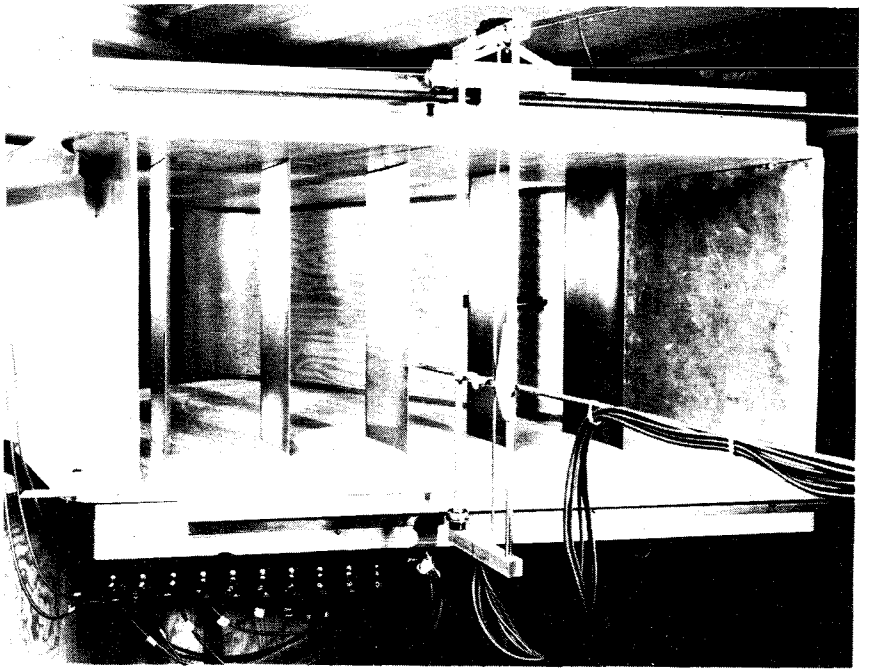

FIG. 11 TEST SECTION VIEWED FROM DOWNSTREAM

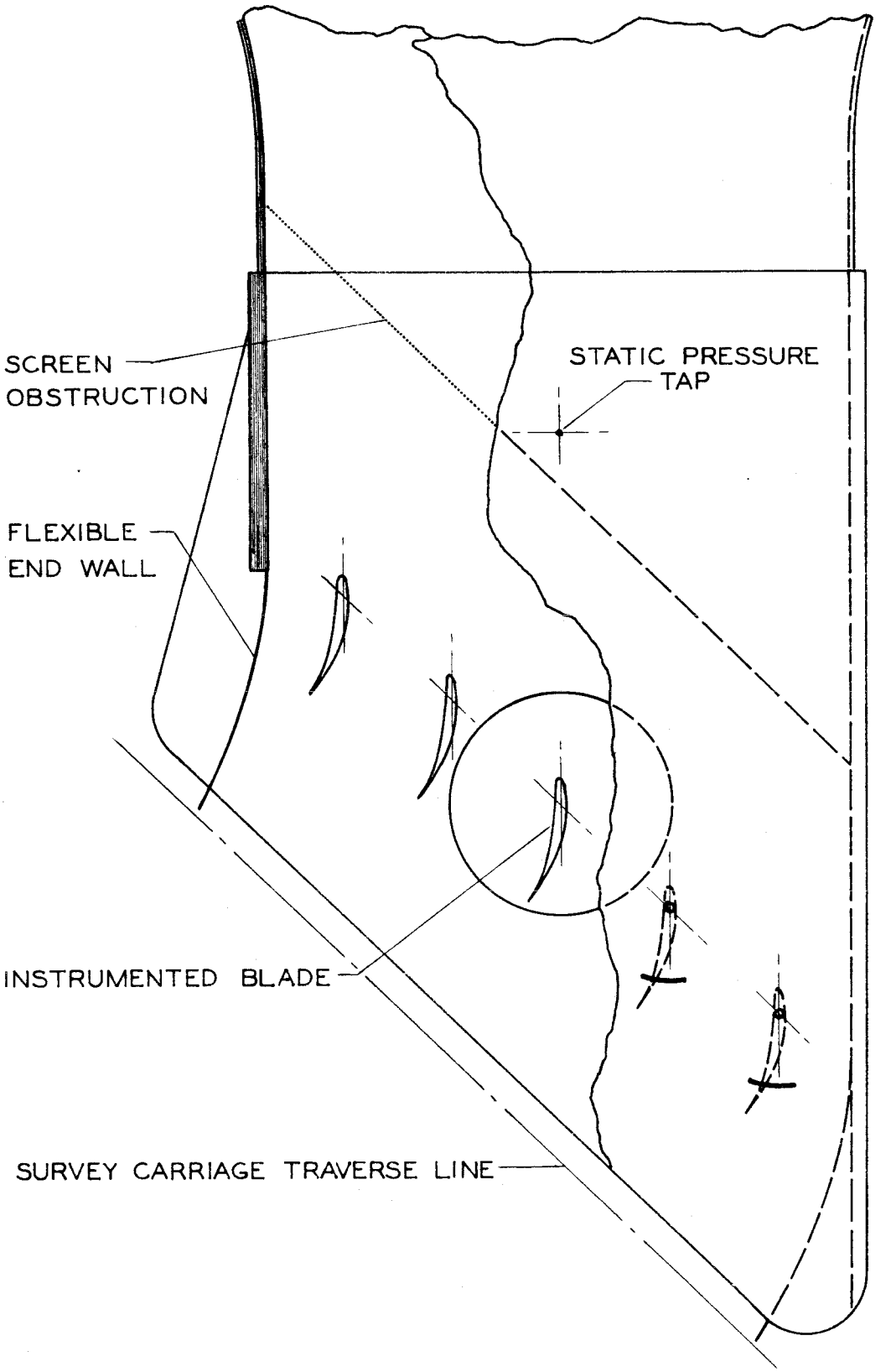

FIG. 12 TEST SECTION ARRANGEMENT

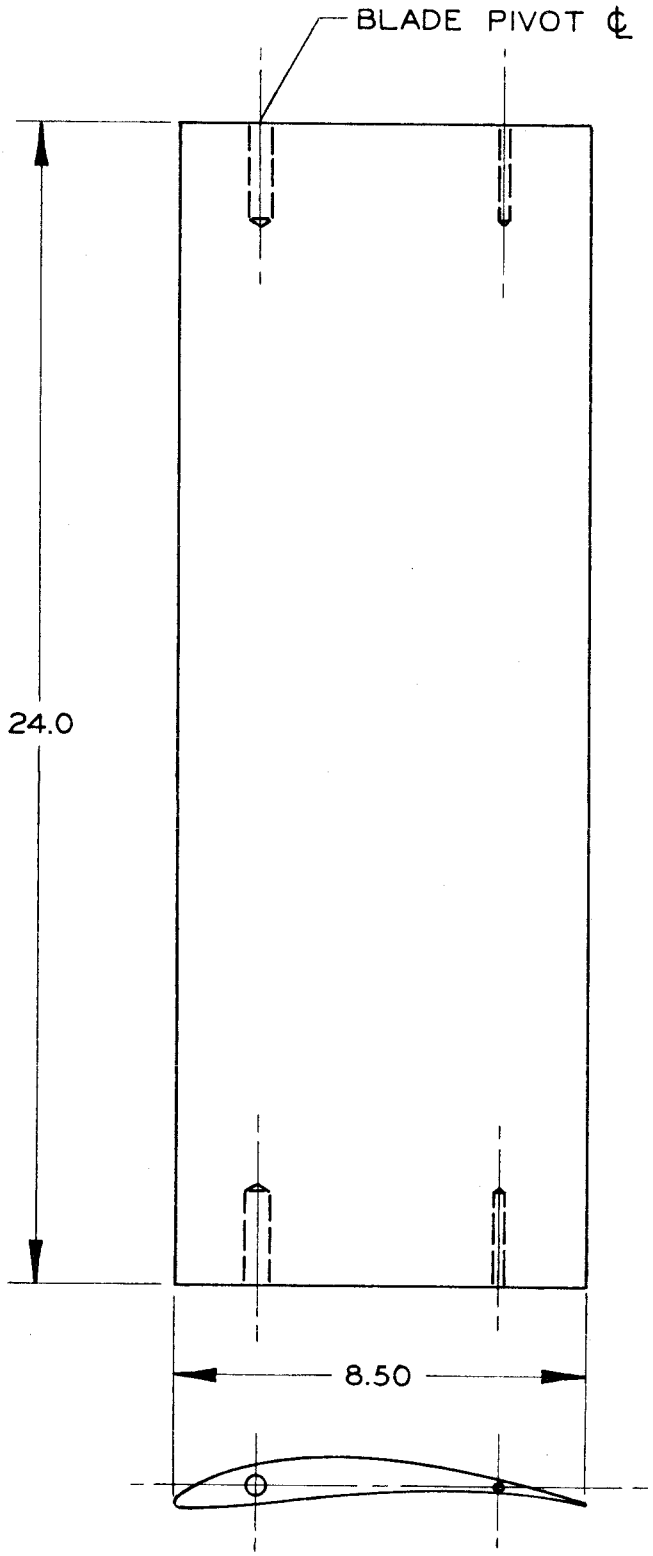

FIG. 13 CASCADE BLADE

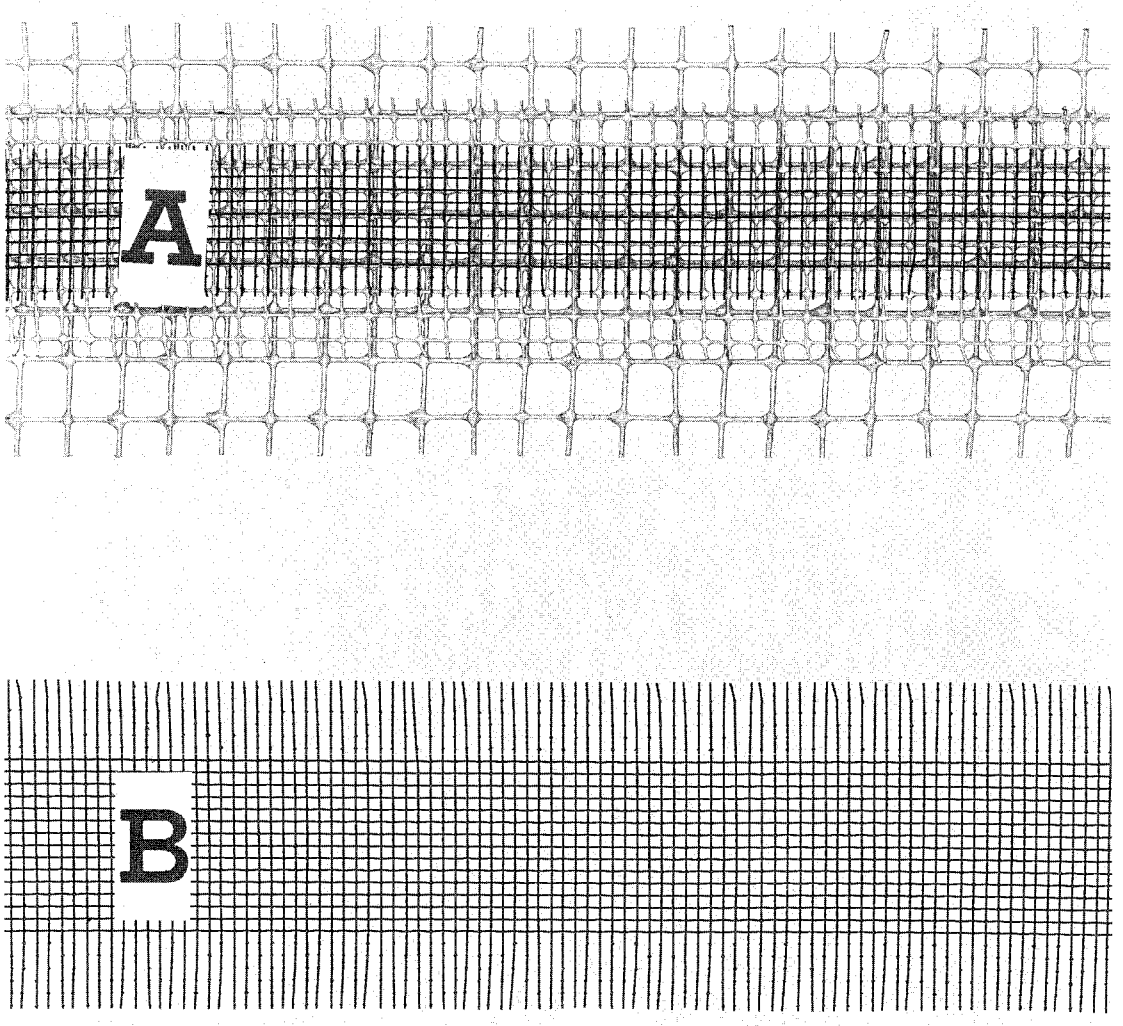

FIG. 14 SCREEN OBSTRUCTIONS

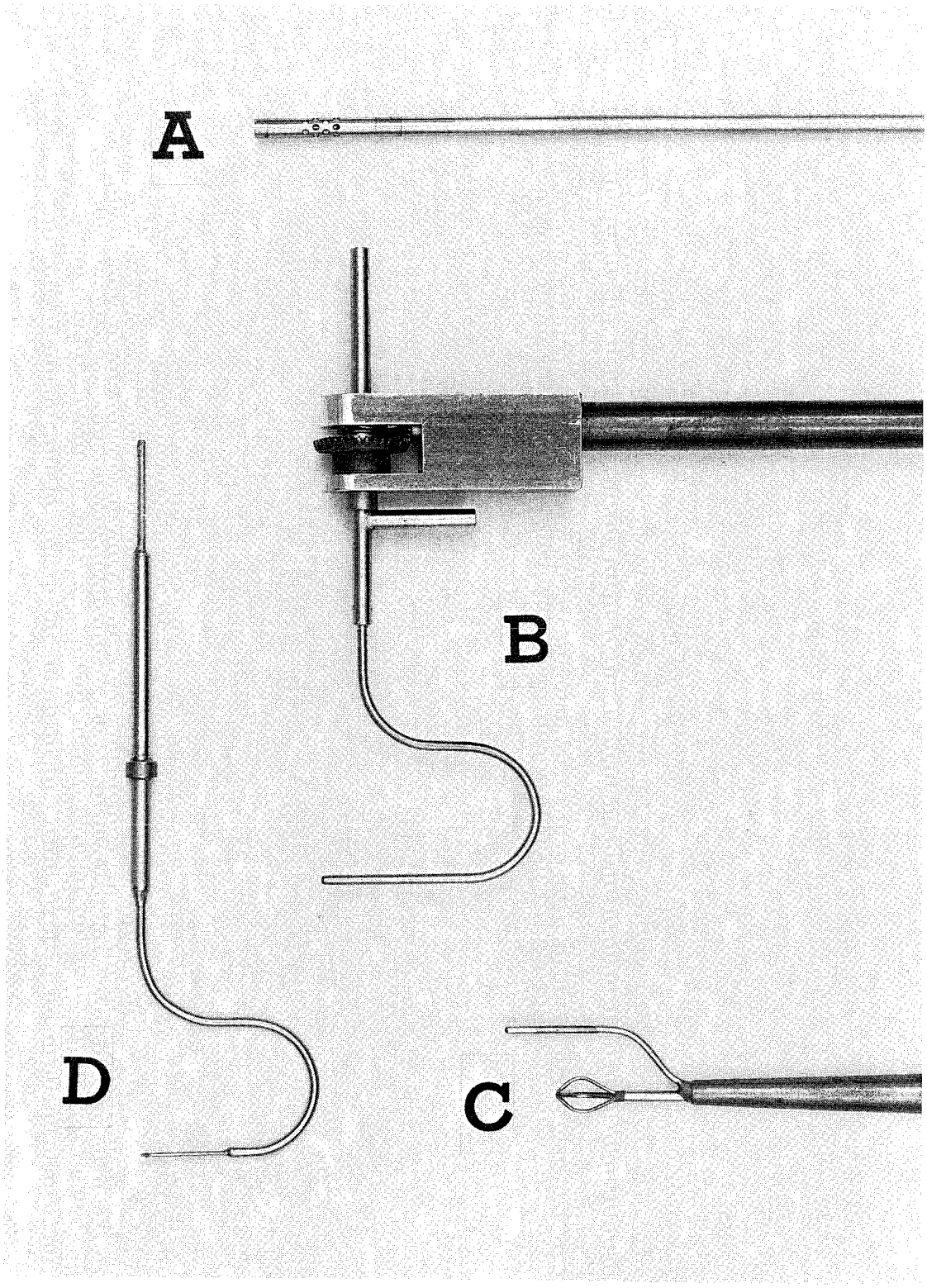

FIG. 15 SURVEY PROBES

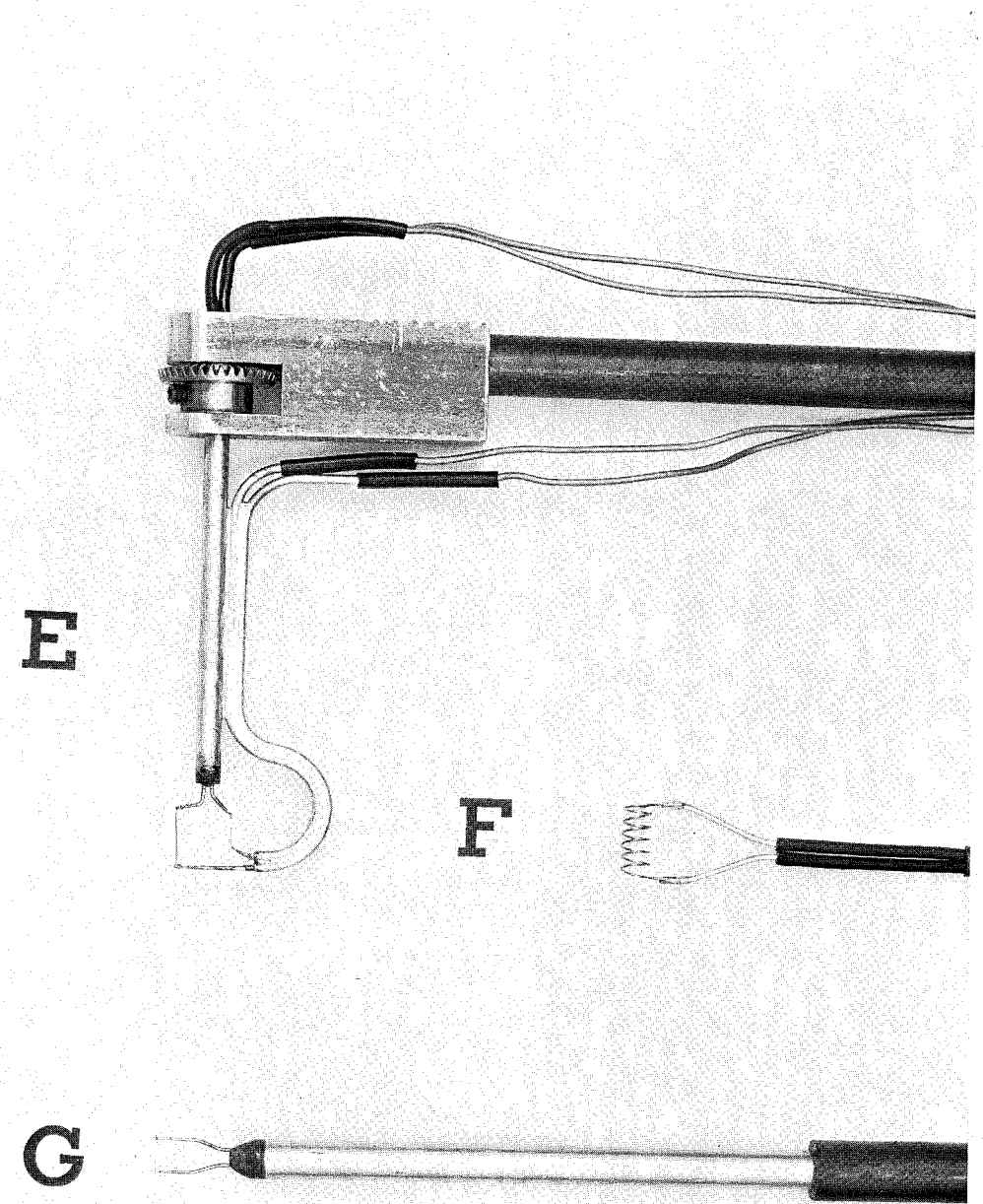

FIG. 15 CONCLUDED SURVEY PROBES

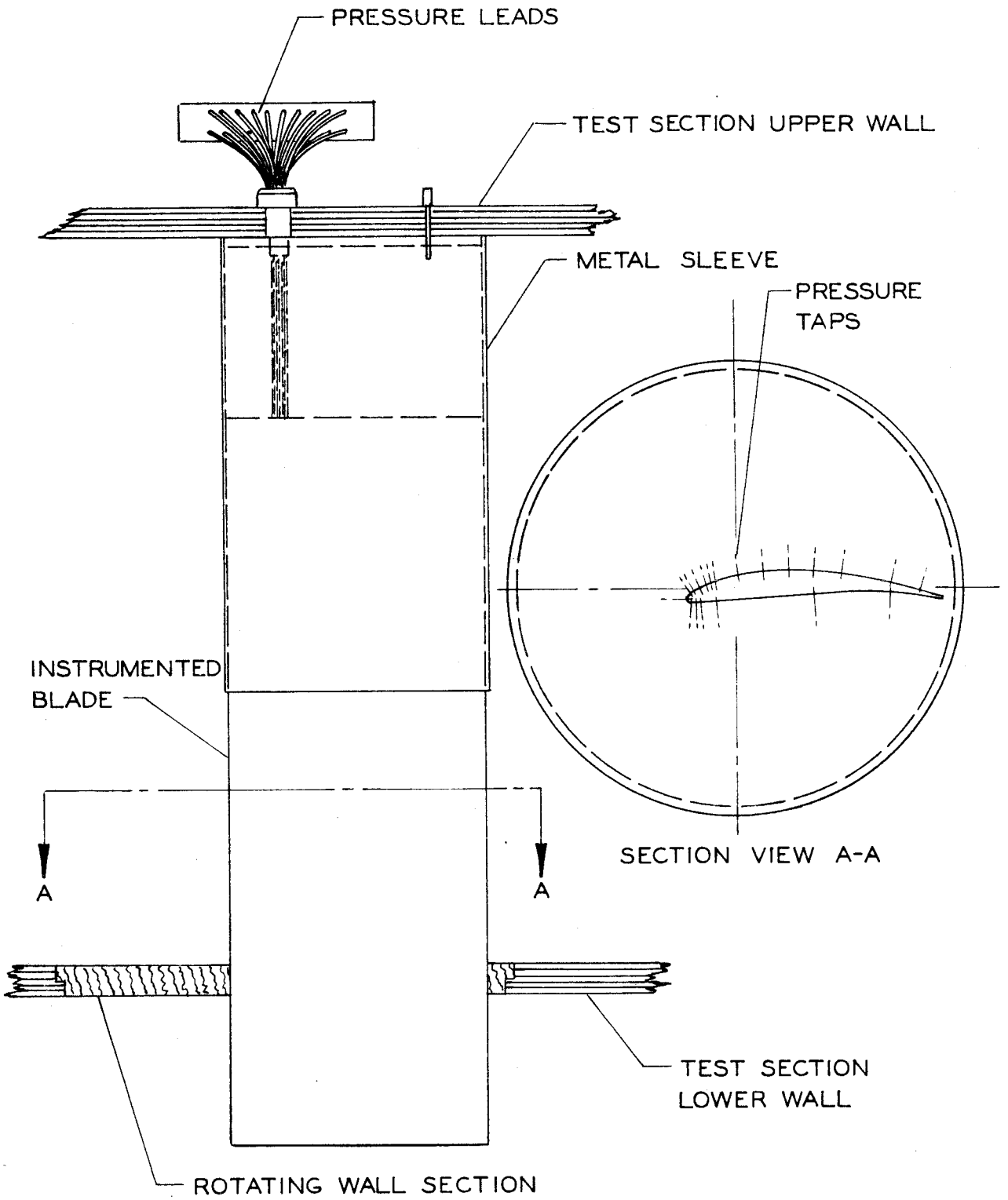

FIG. 16 INSTRUMENTED BLADE & SLEEVE ARRANGEMENT

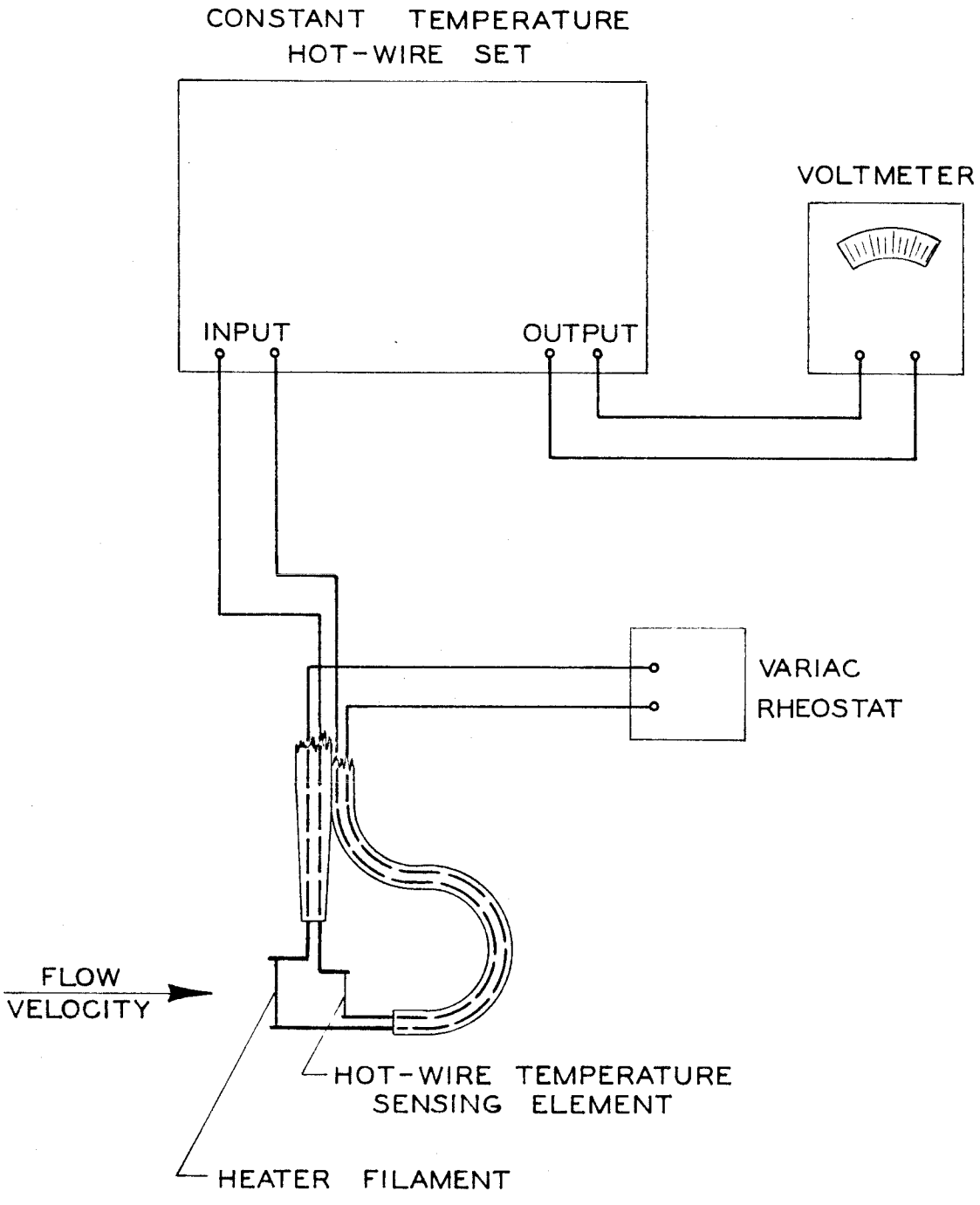

FIG. 17 HOT-WIRE ANGLE MEASURING APPARATUS

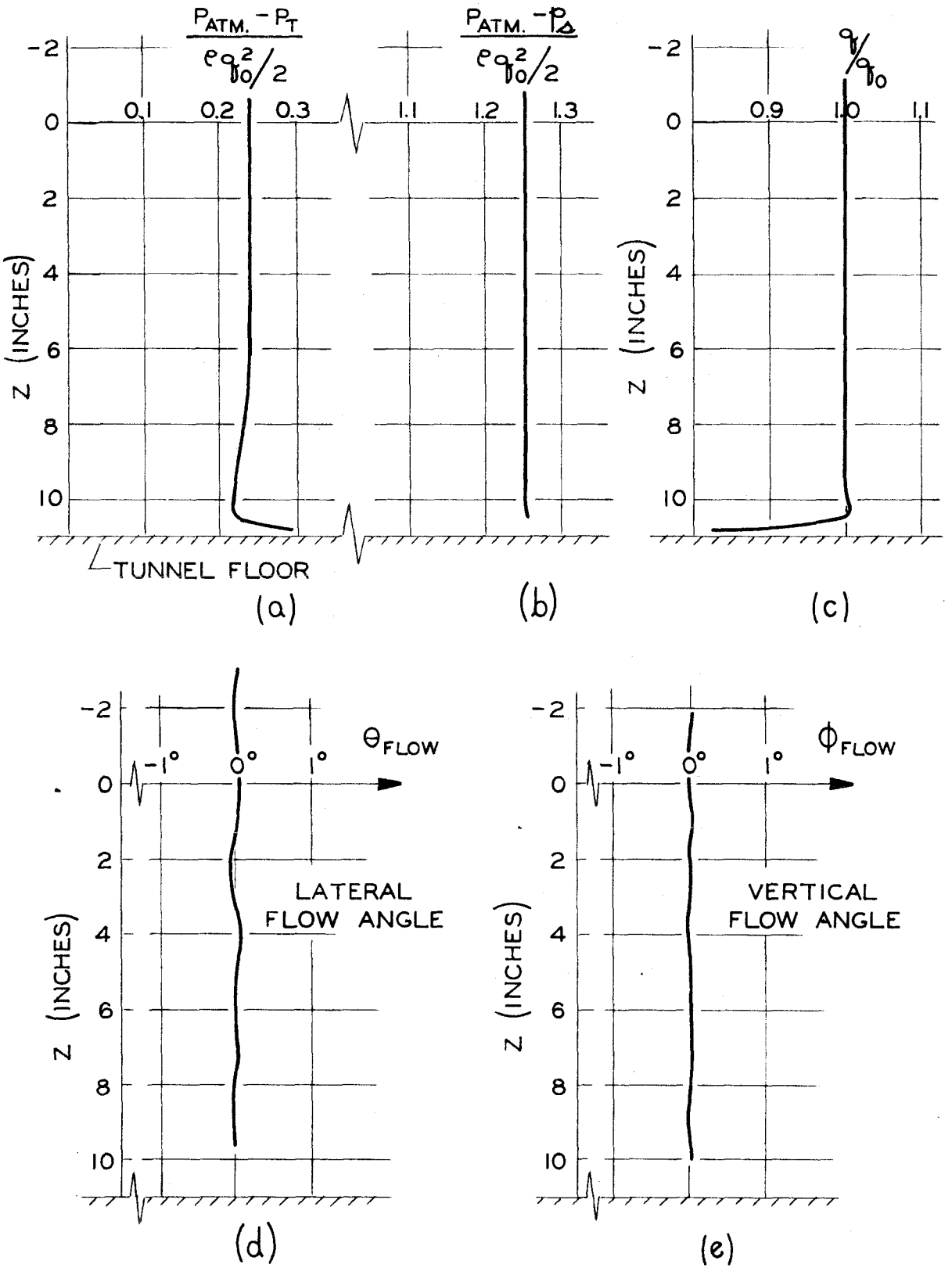

FIG. 18 UPSTREAM FLOW, CONFIGURATION I

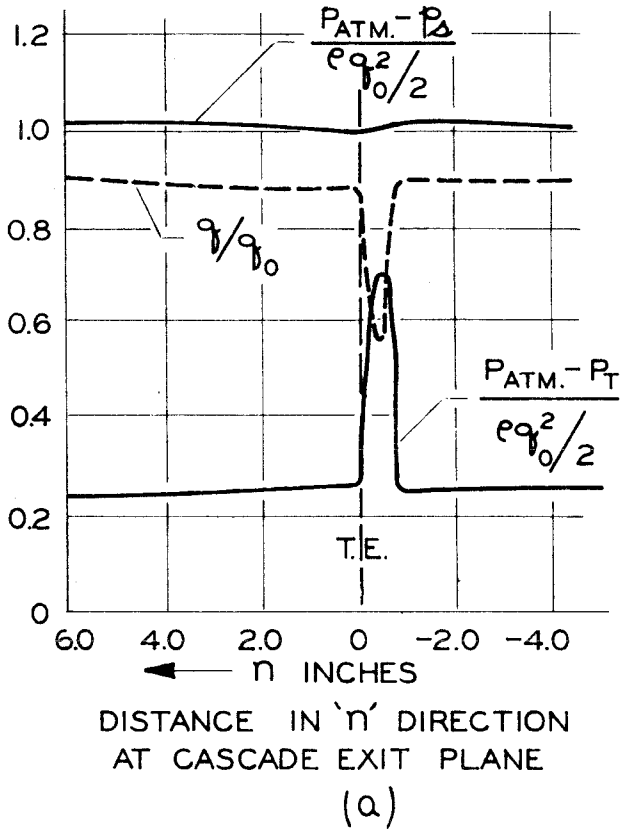

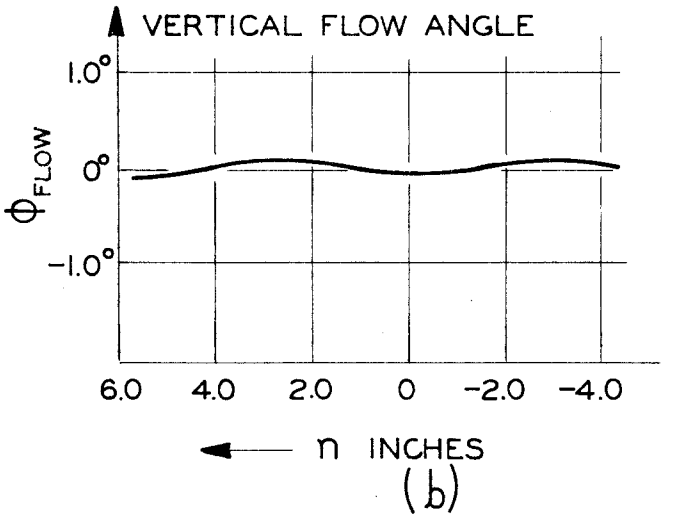

FIG. 19 FLOW IN DOWNSTREAM REFERENCE PLANE CONFIGURATION I, Z = 1 IN.

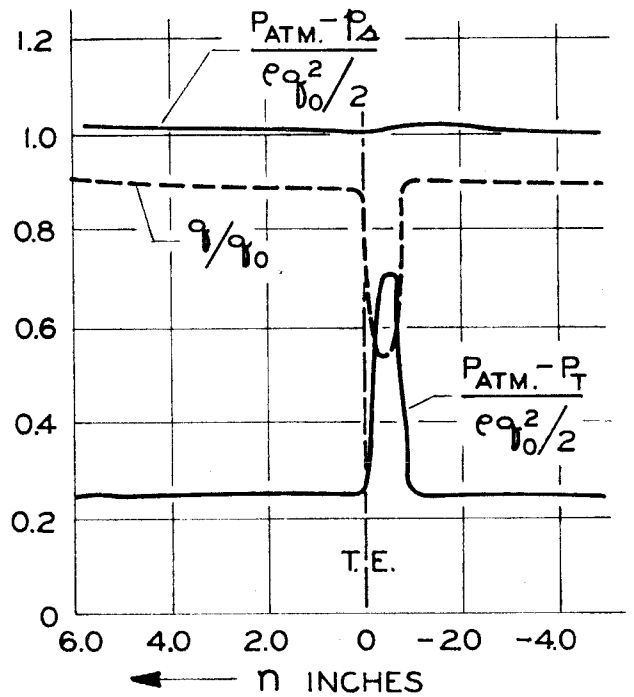

DISTANCE IN 'n' DIRECTION
AT CASCADE EXIT PLANE

(a)

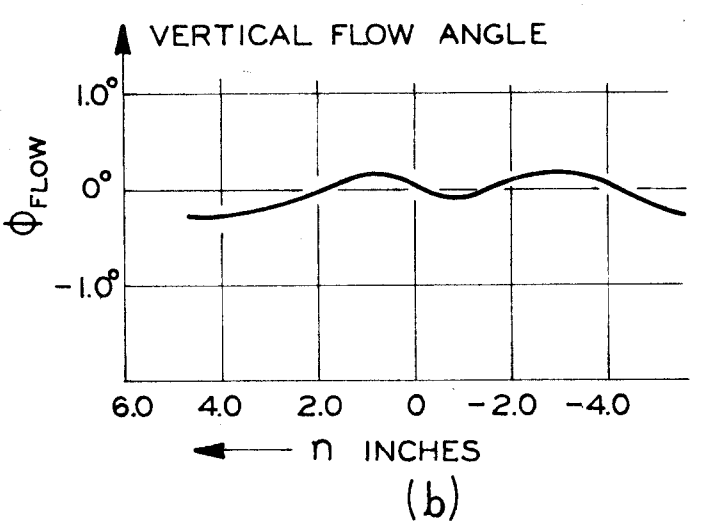

(b)

FIG. 20 FLOW IN DOWNSTREAM REFERENCE PLANE
CONFIGURATION I, Z = 5 IN.

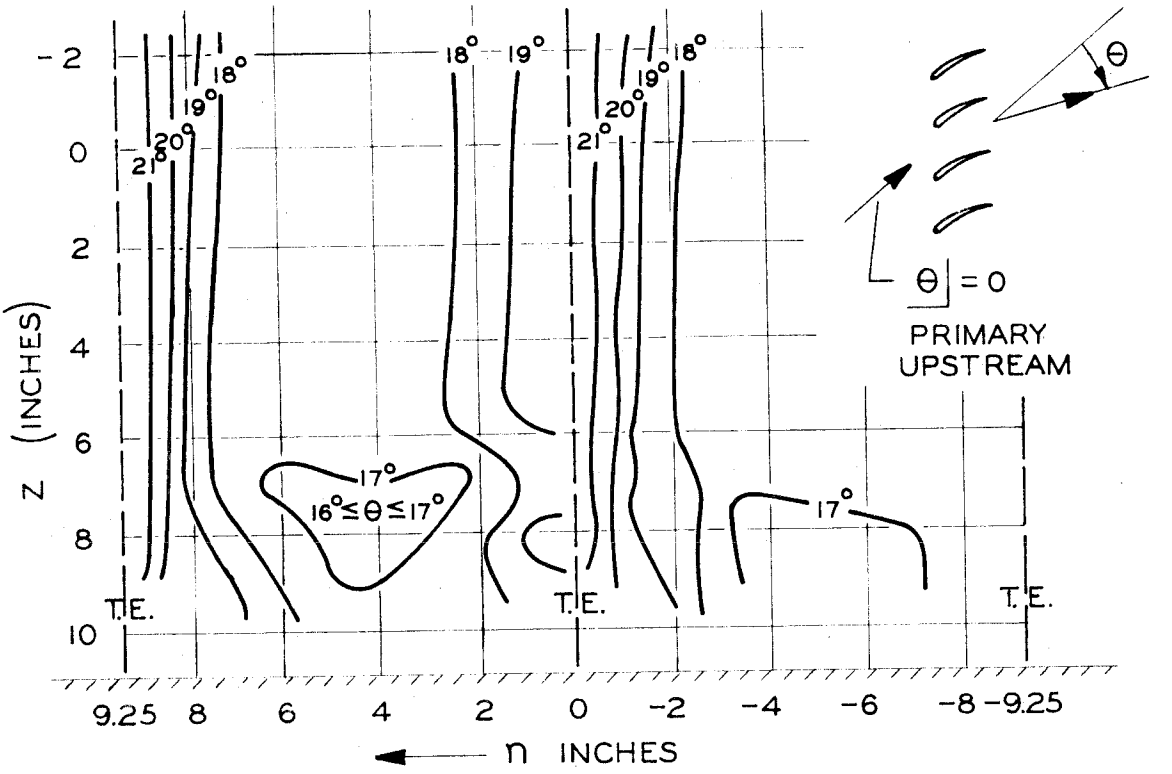

FIG. 21 DOWNSTREAM CONTOURS OF LATERAL FLOW ANGLE Θ_{FLOW}, CONFIGURATION I

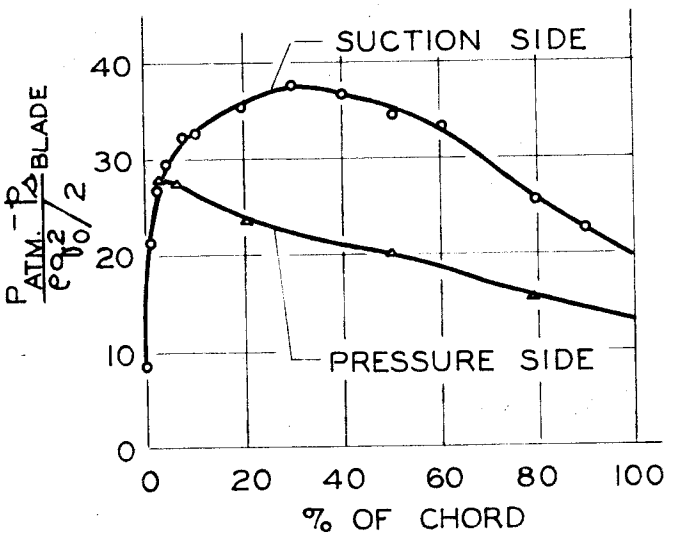

FIG. 22 BLADE PRESSURES CONFIGURATION I Z = 3 IN.

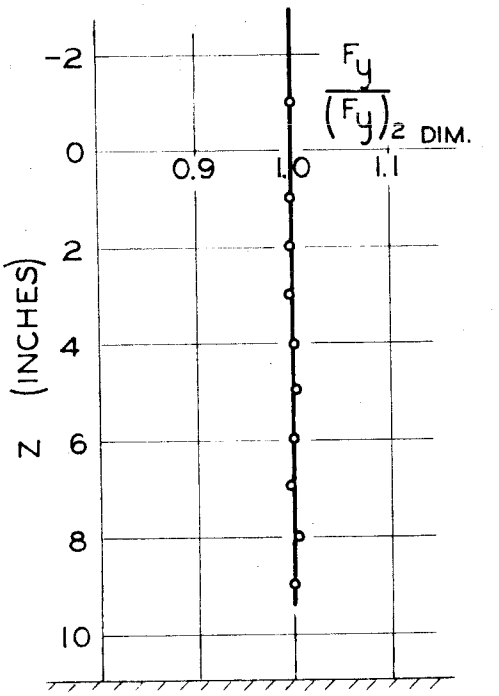

FIG. 23 BLADE LOADING CONFIGURATION I

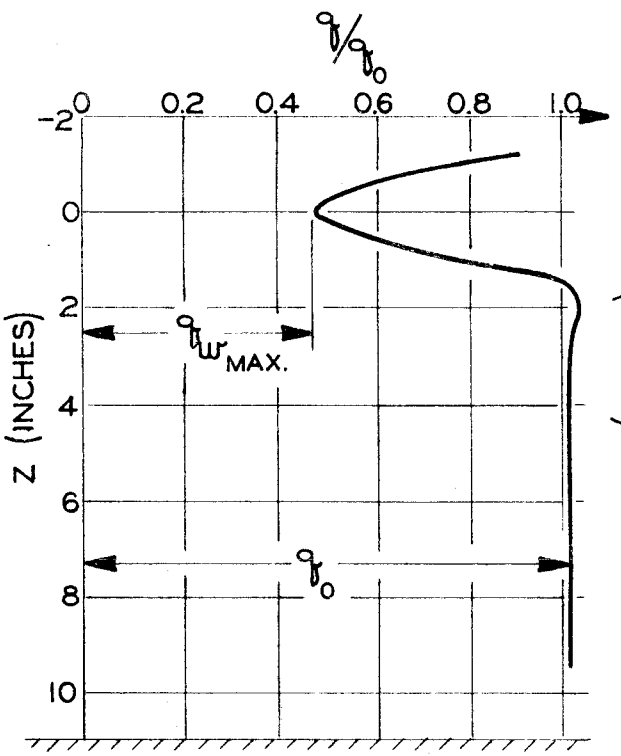

FIG. 24 UPSTREAM VELOCITY DISTRIBUTION, CONFIG. II

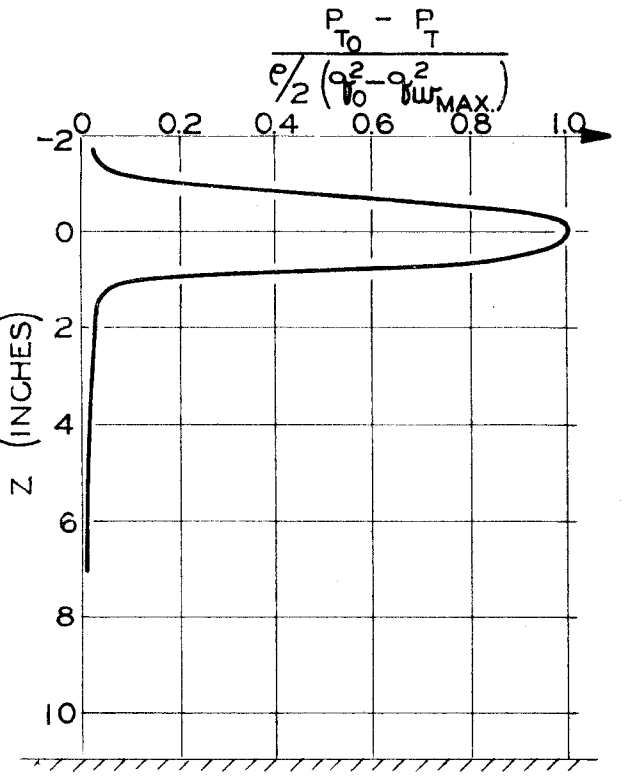

FIG. 25 UPSTREAM TOTAL PRESSURE DISTRIBUTION CONFIGURATION II

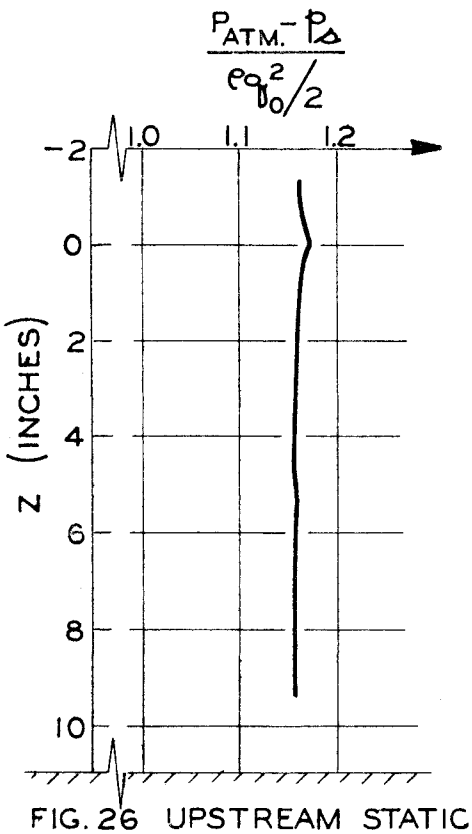

FIG. 26 UPSTREAM STATIC PRESS. DISTRB., CONFIG. II

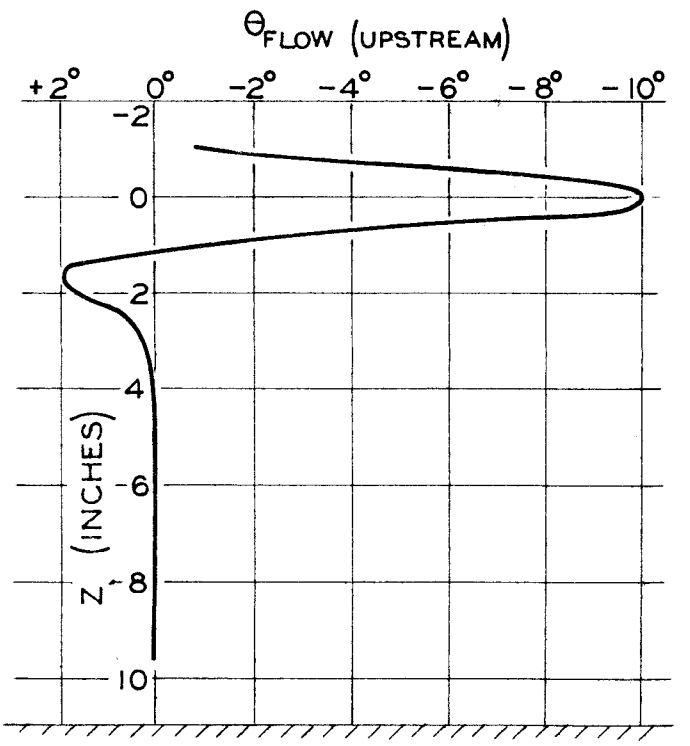

FIG. 27 UPSTREAM LATERAL FLOW ANGLE, CONFIG. II

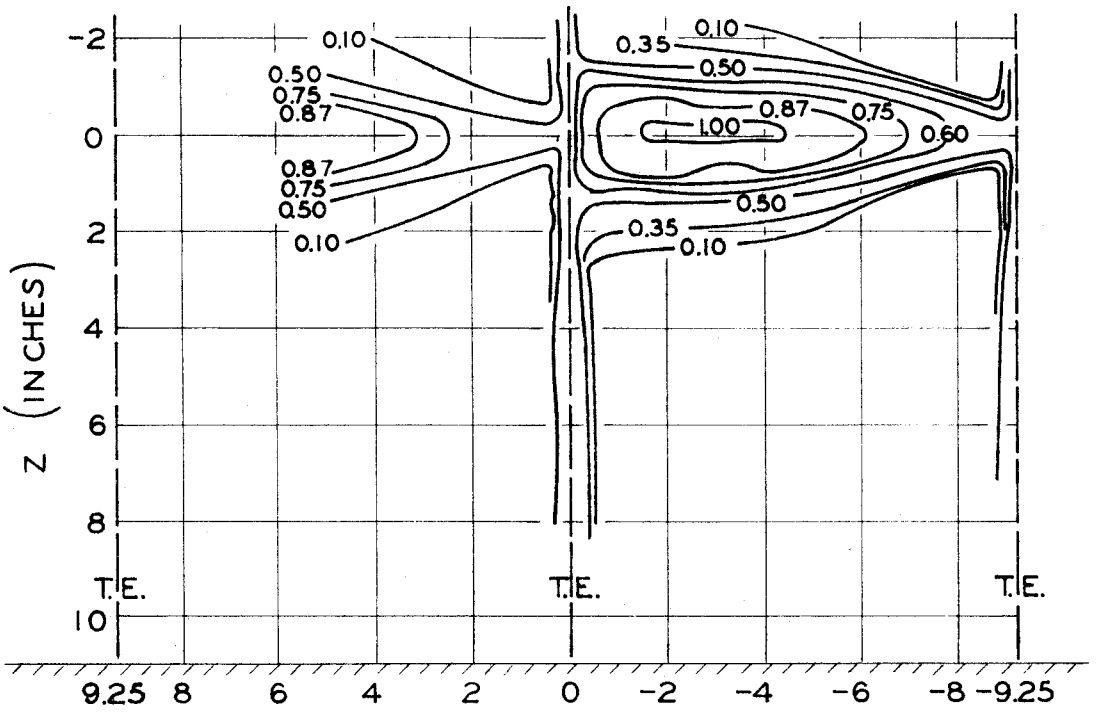

FIG. 28 DOWNSTREAM CONTOURS OF $\frac{P_{T_0} - P_T}{\rho/2\left(q_0^2 - q_{w_{MAX.}}^2\right)}$ CONFIGURATION II

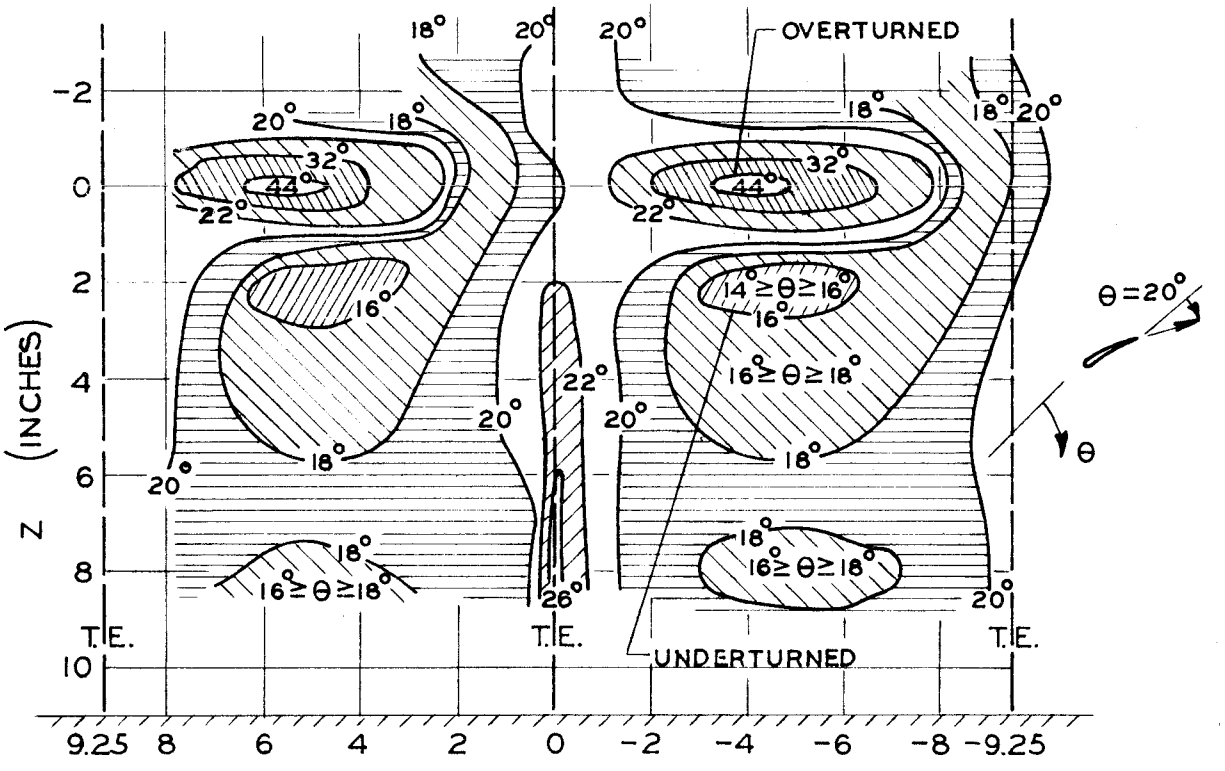

FIG. 29 DOWNSTREAM CONTOURS OF LATERAL FLOW ANGLE, Θ_F CONFIGURATION III

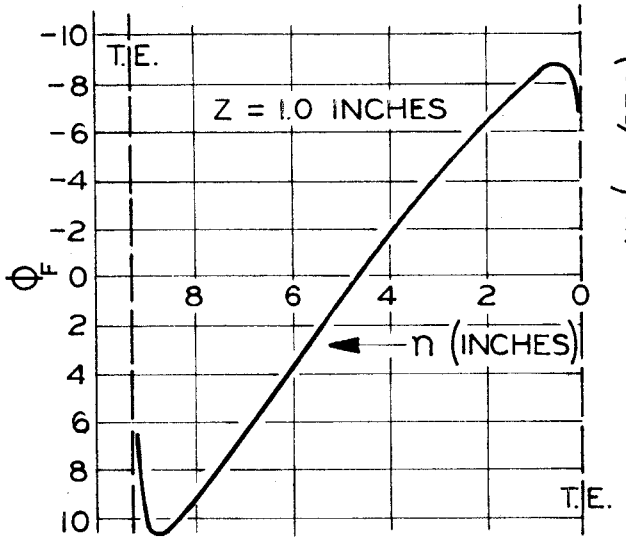

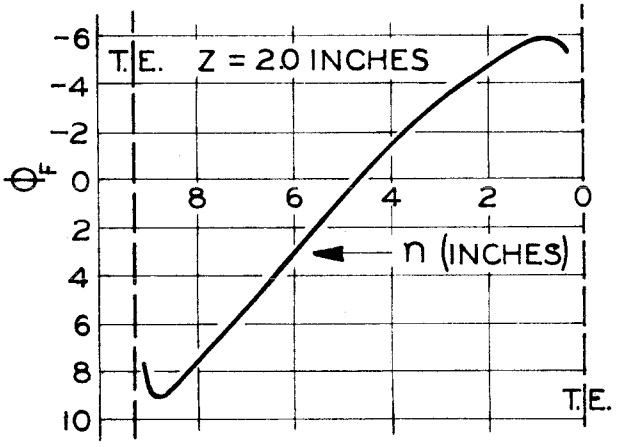

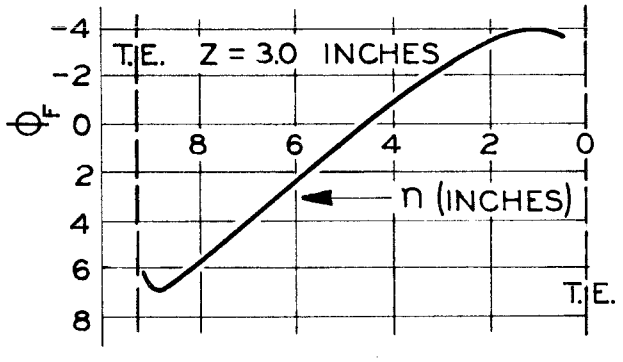

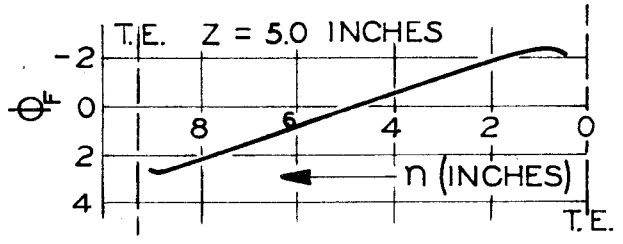

FIG. 30
VERTICAL FLOW ANGLE Φ_F,
CONFIGURATION II

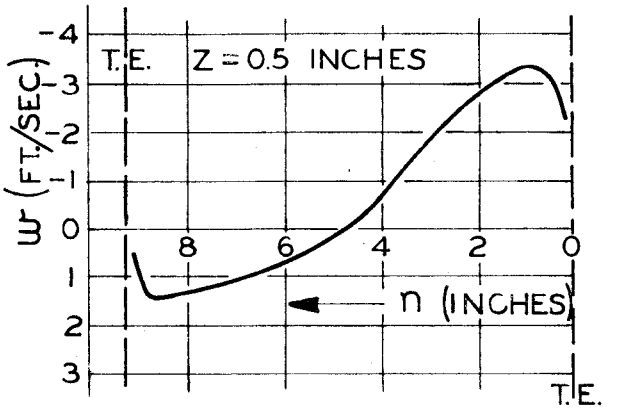

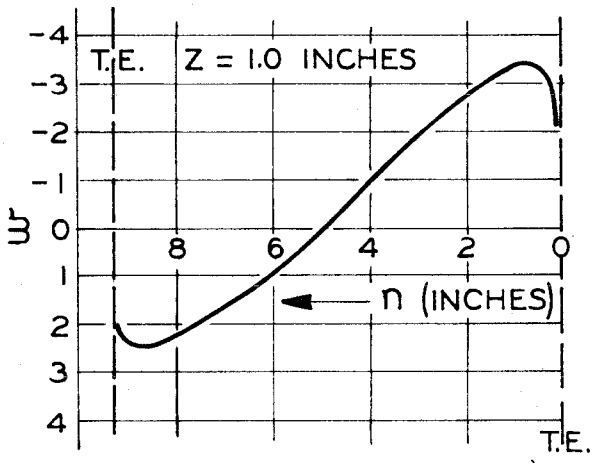

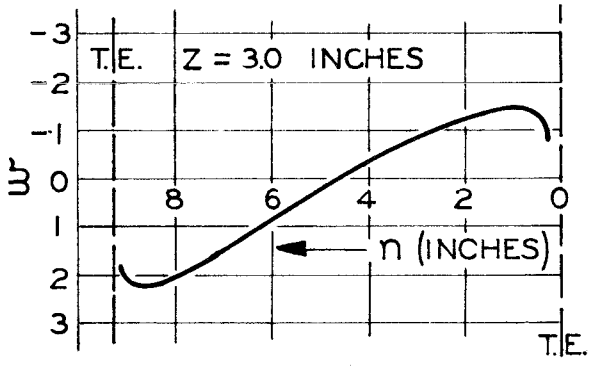

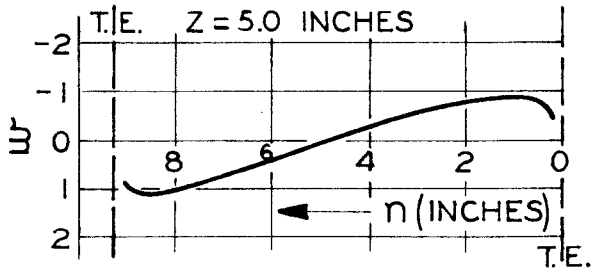

FIG. 31
SPANWISE COMPONENT OF
VELOCITY, CONFIG. II

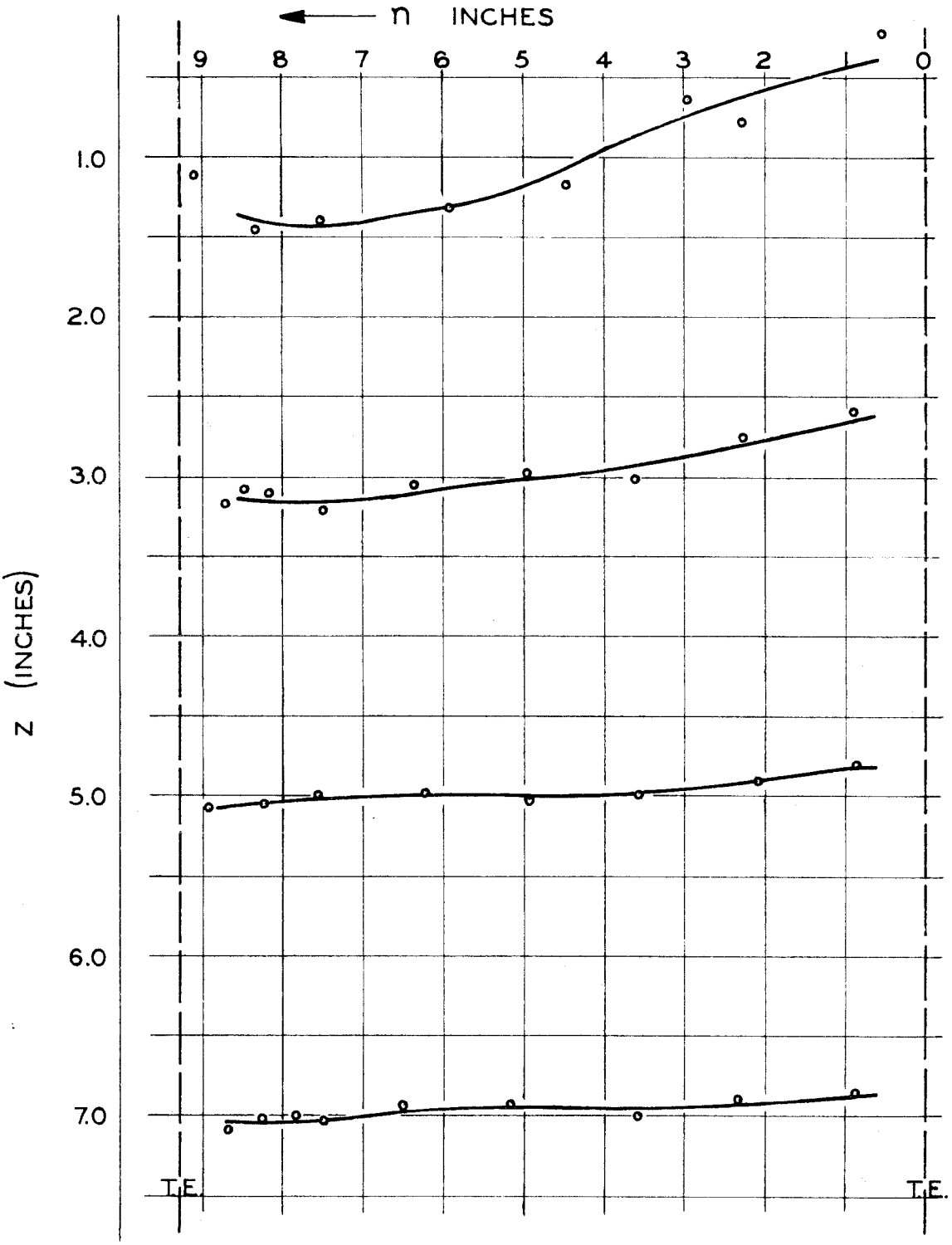

FIG. 32

MEASURED STREAMSURFACE DISTORTION AT TRAILING EDGE

CONFIGURATION II

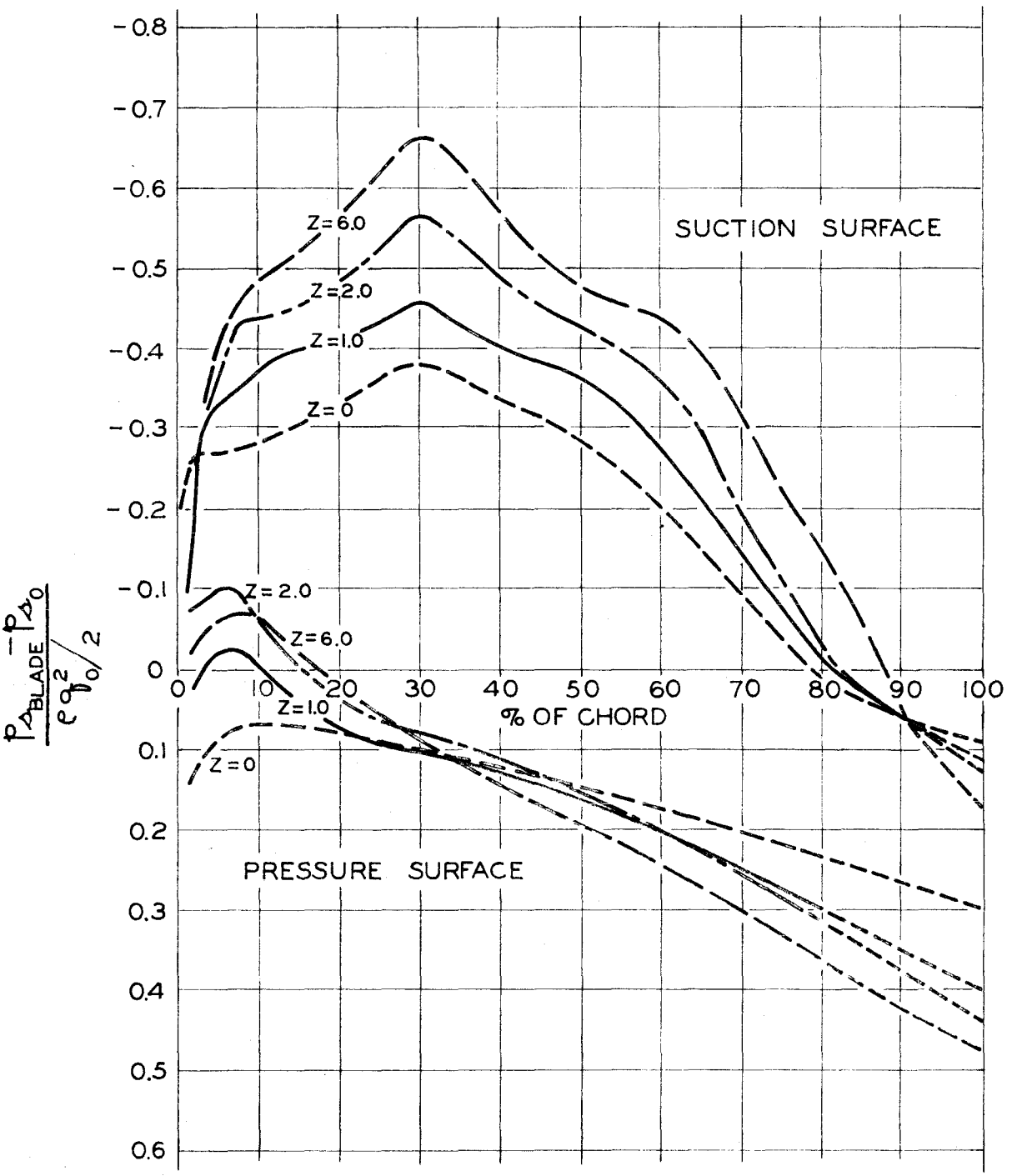

FIG. 33
BLADE PRESSURES
CONFIGURATION II

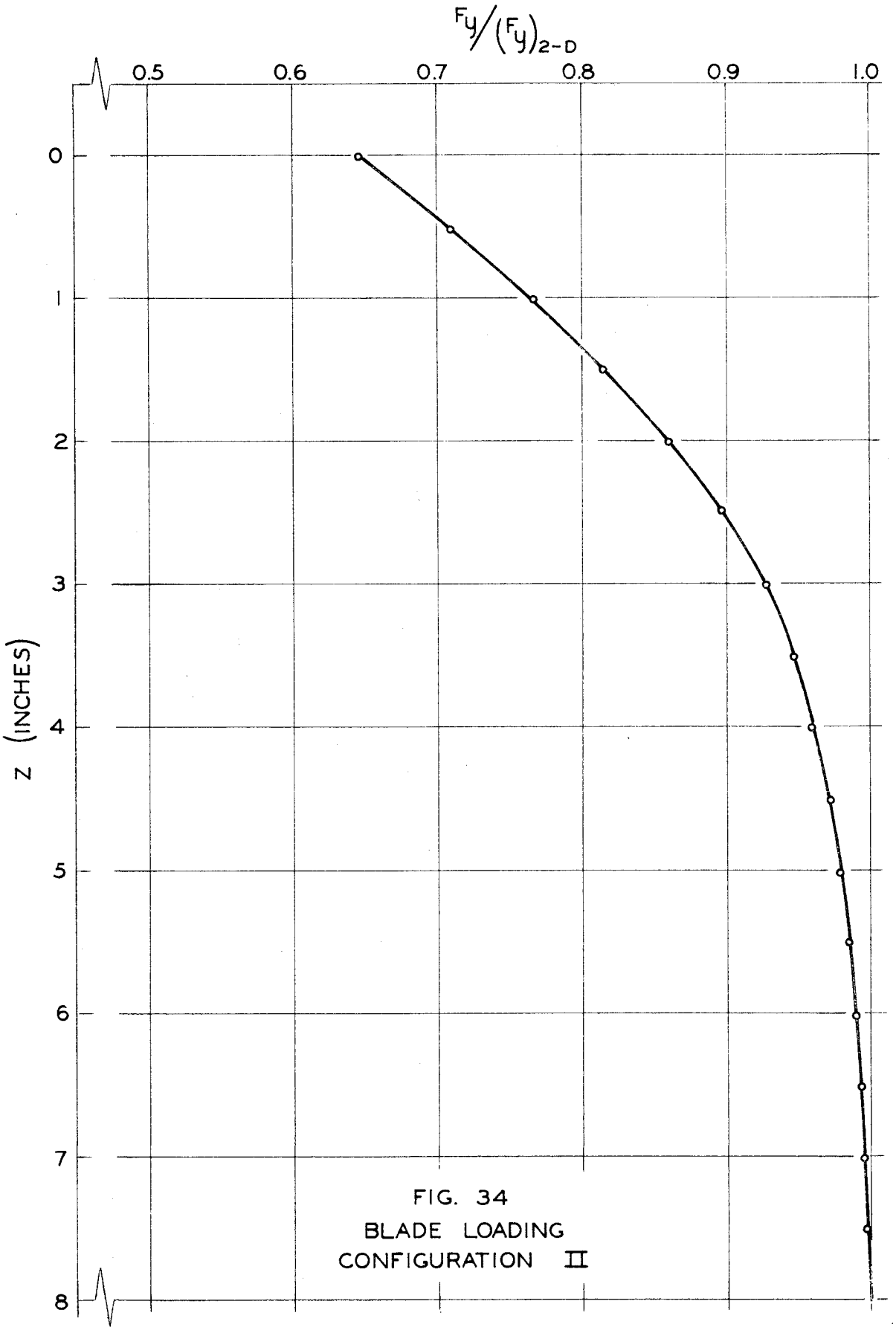

FIG. 34
BLADE LOADING
CONFIGURATION II

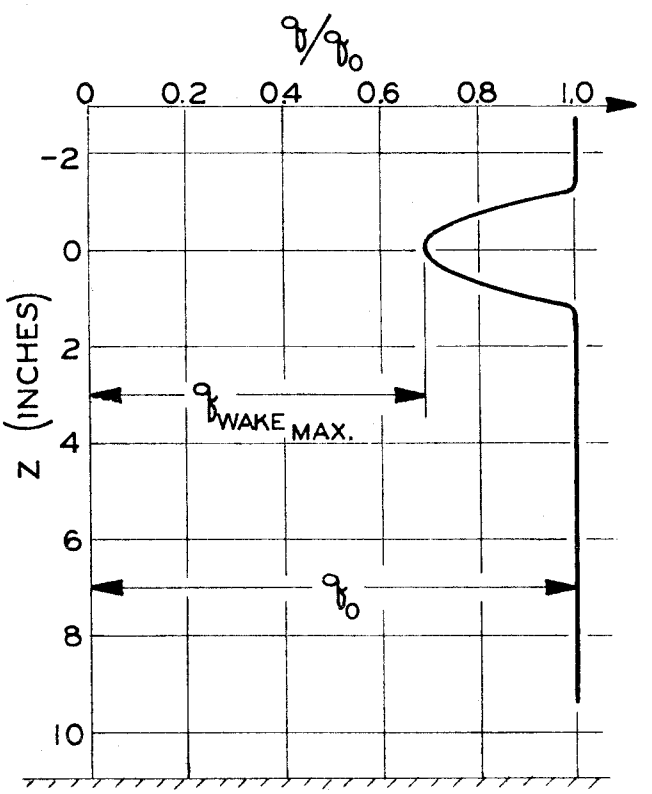

FIG. 35 UPSTREAM VELOCITY DISTRIBUTION, CONFIG. III

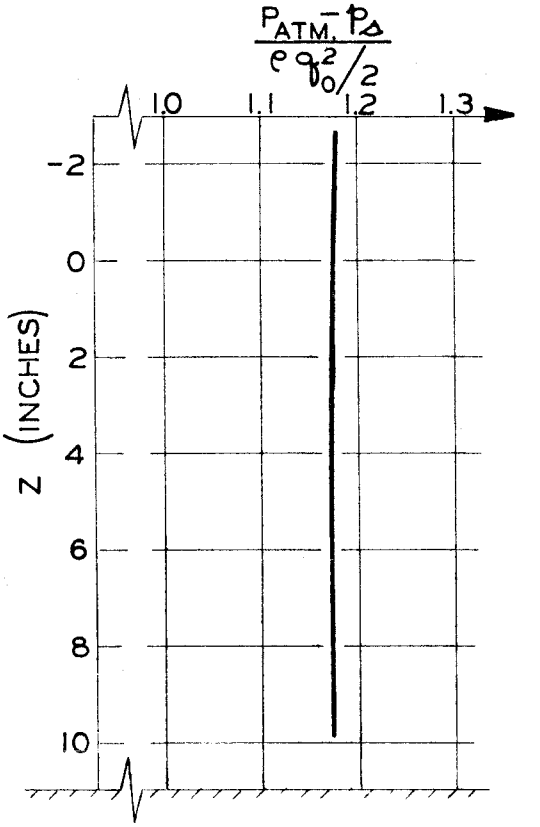

FIG. 36 UPSTREAM STATIC PRESS. DISTRB., CONFIG. III

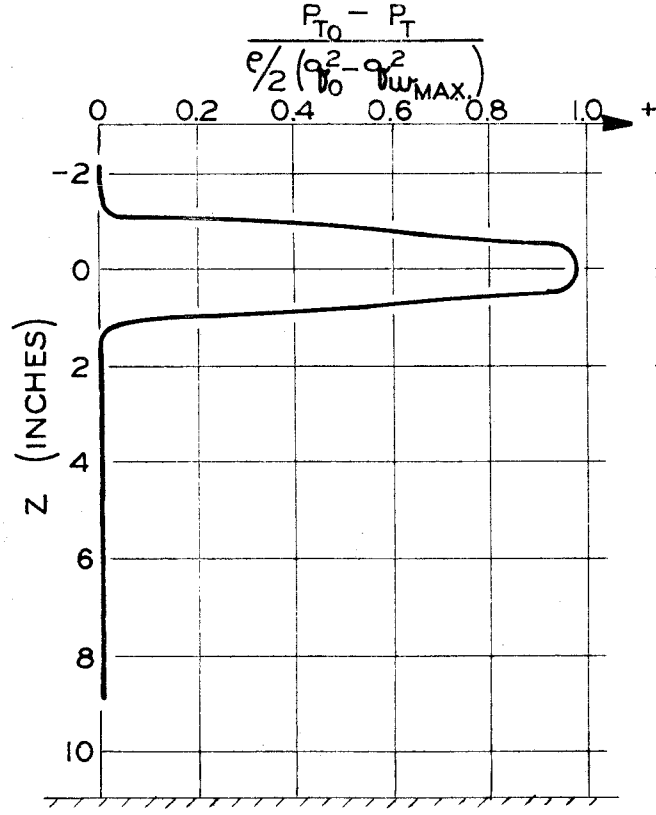

FIG. 37 UPSTREAM TOTAL PRESS. DISTRB., CONFIG. III

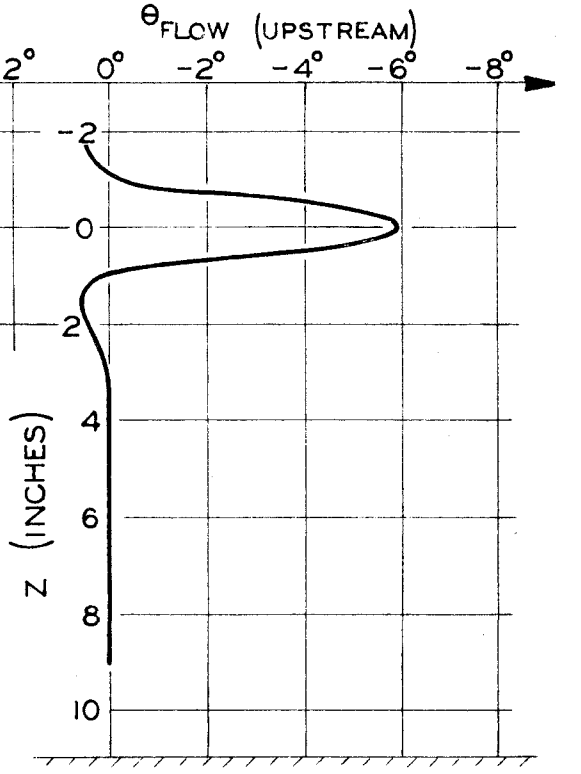

FIG. 38 UPSTREAM LATERAL FLOW ANGLE, CONFIG. III

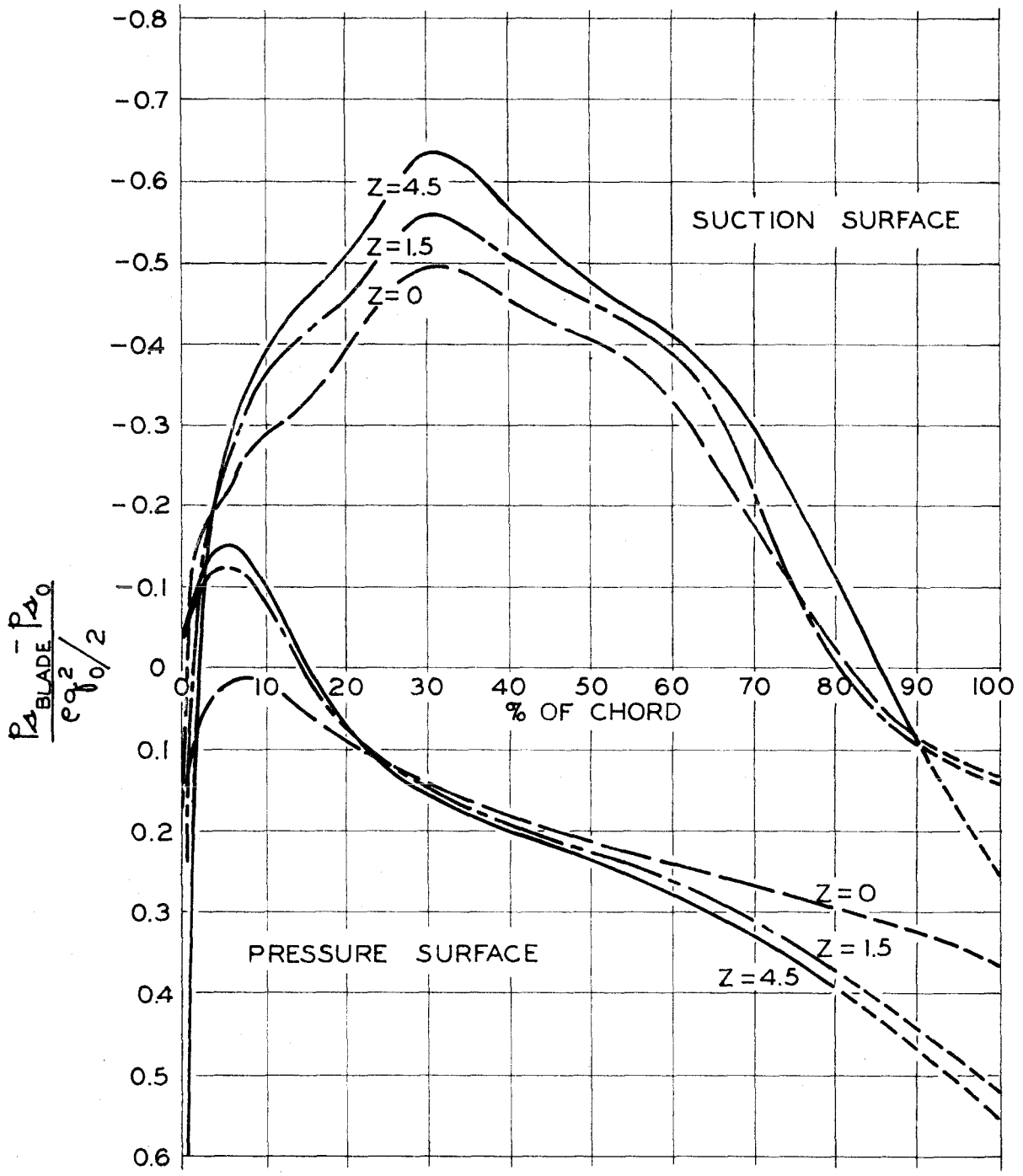

FIG. 39
BLADE PRESSURES
CONFIGURATION III

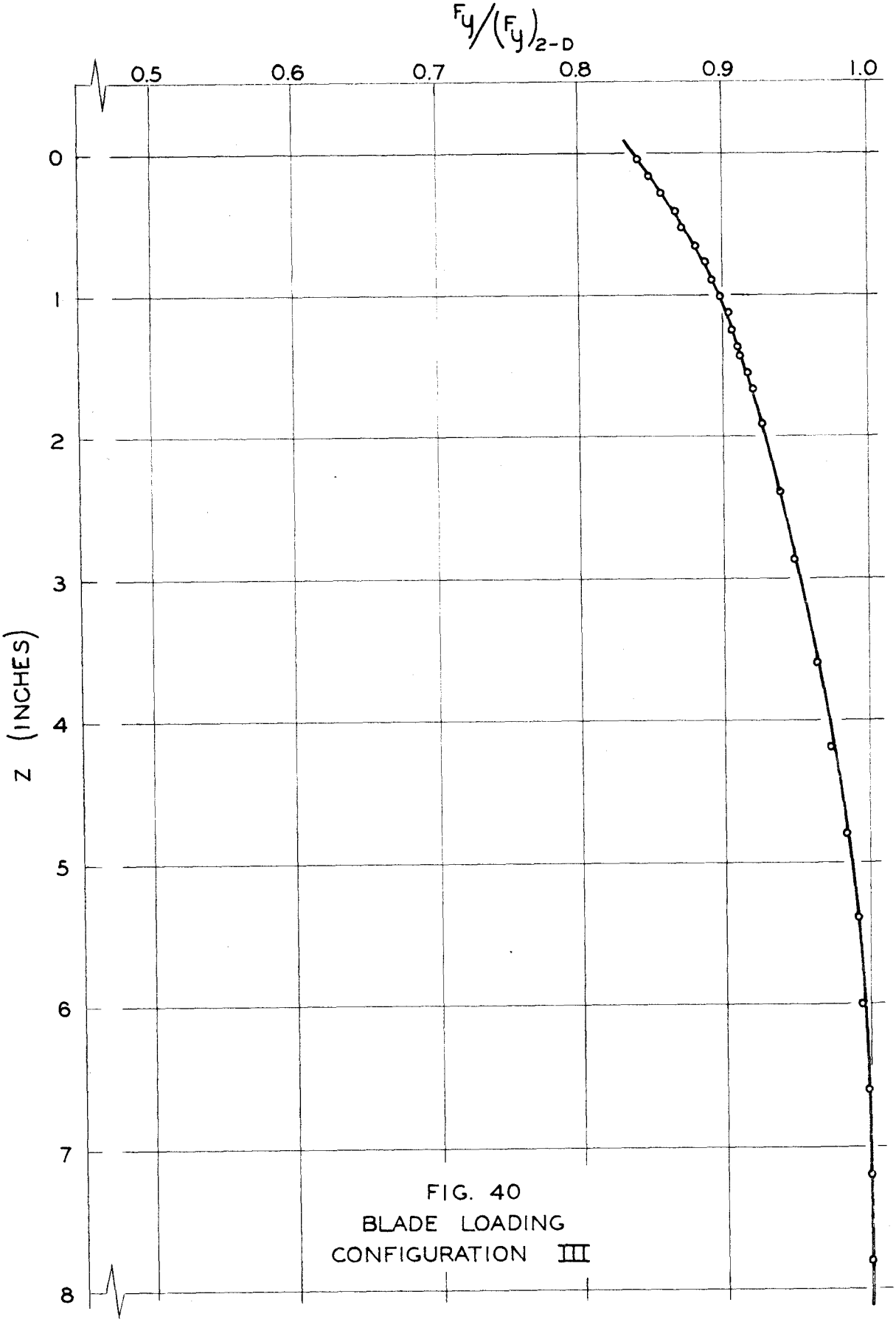

FIG. 40
BLADE LOADING
CONFIGURATION III

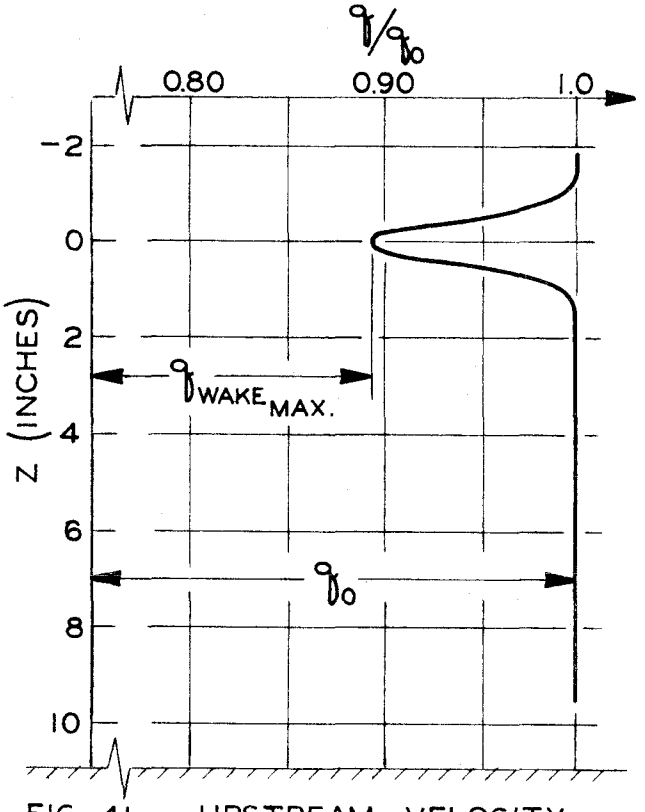

FIG. 41 UPSTREAM VELOCITY DISTRIBUTION CONFIG. IV

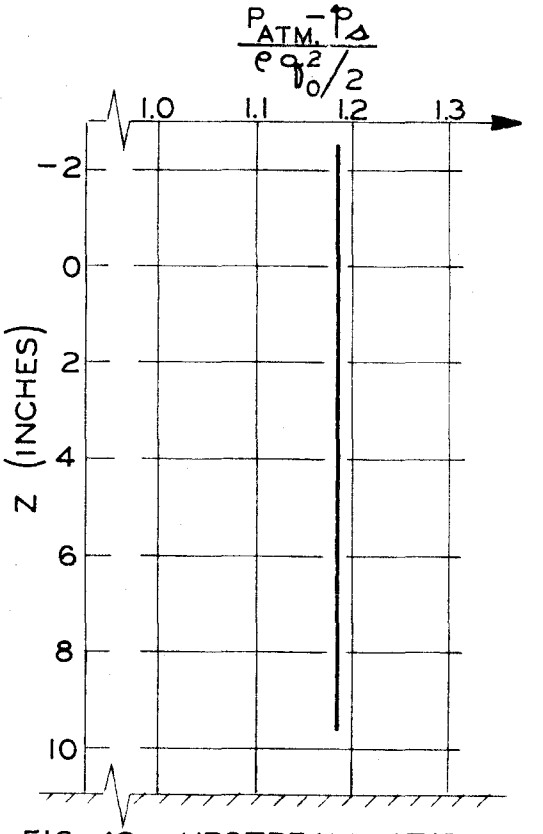

FIG. 42 UPSTREAM STATIC PRESS. DISTRB. CONFIG. IV

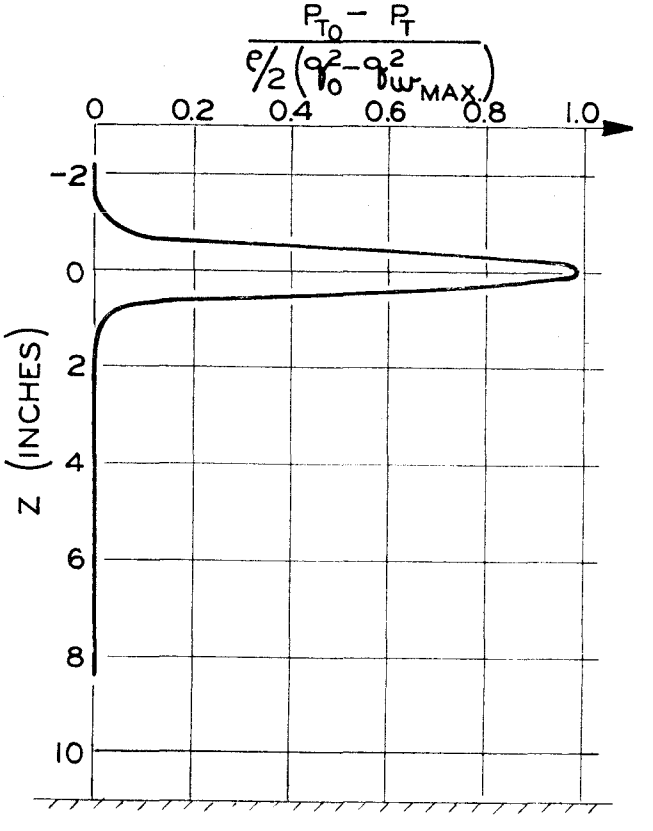

FIG. 43 UPSTREAM TOTAL PRESS. DISTRB. CONFIG. IV

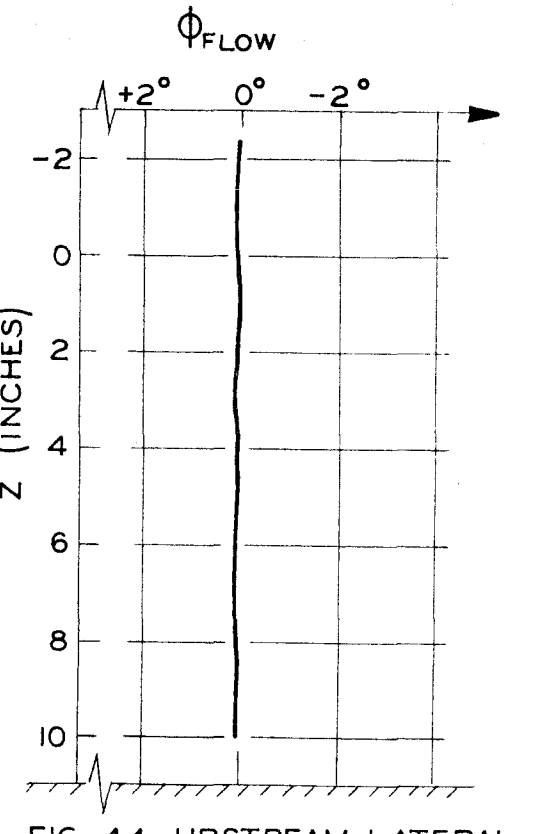

FIG. 44 UPSTREAM LATERAL FLOW ANGLE CONFIG. IV

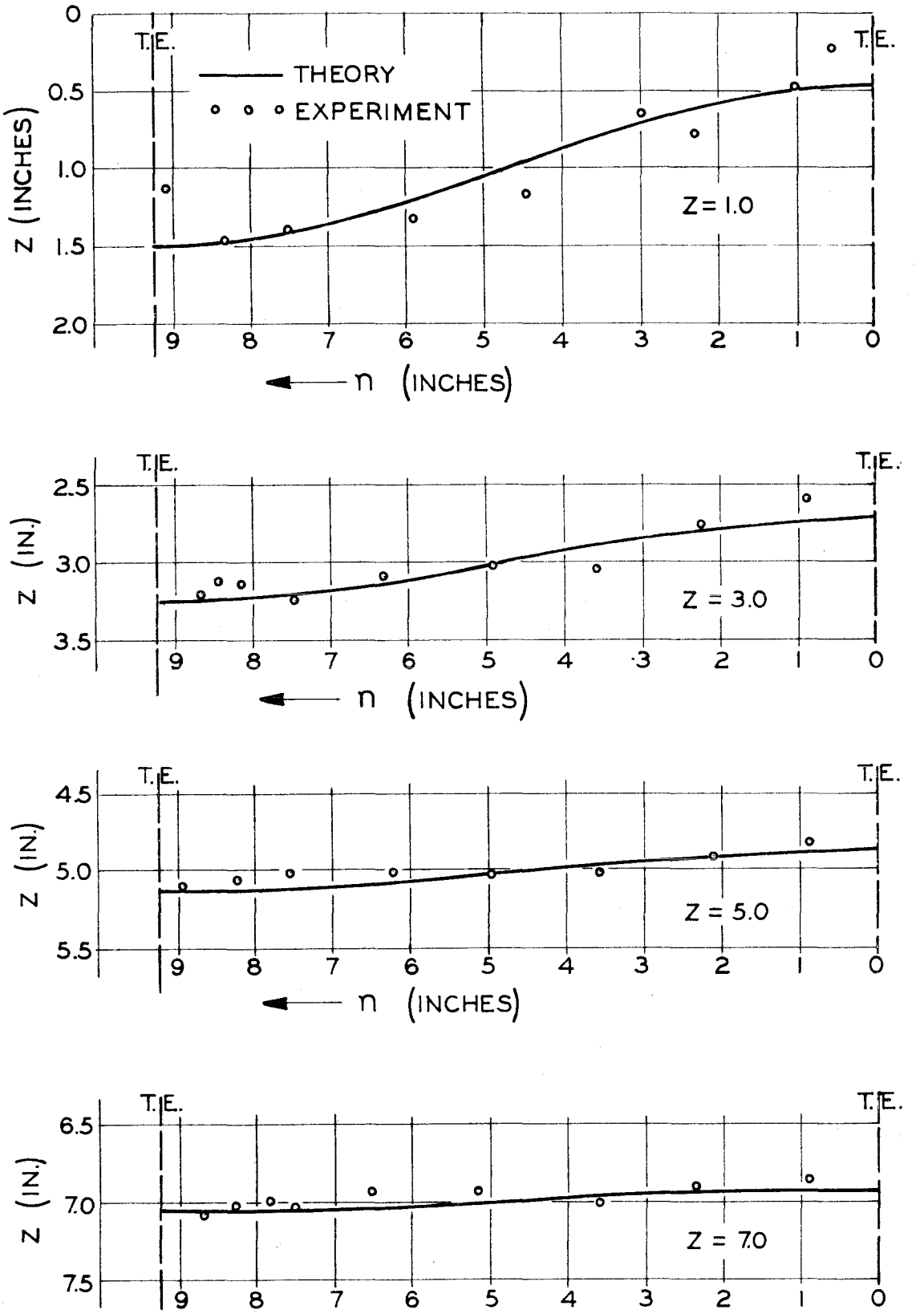

FIG. 45
STREAMSURFACE DISTORTION AT TRAILING EDGE
CONFIGURATION II

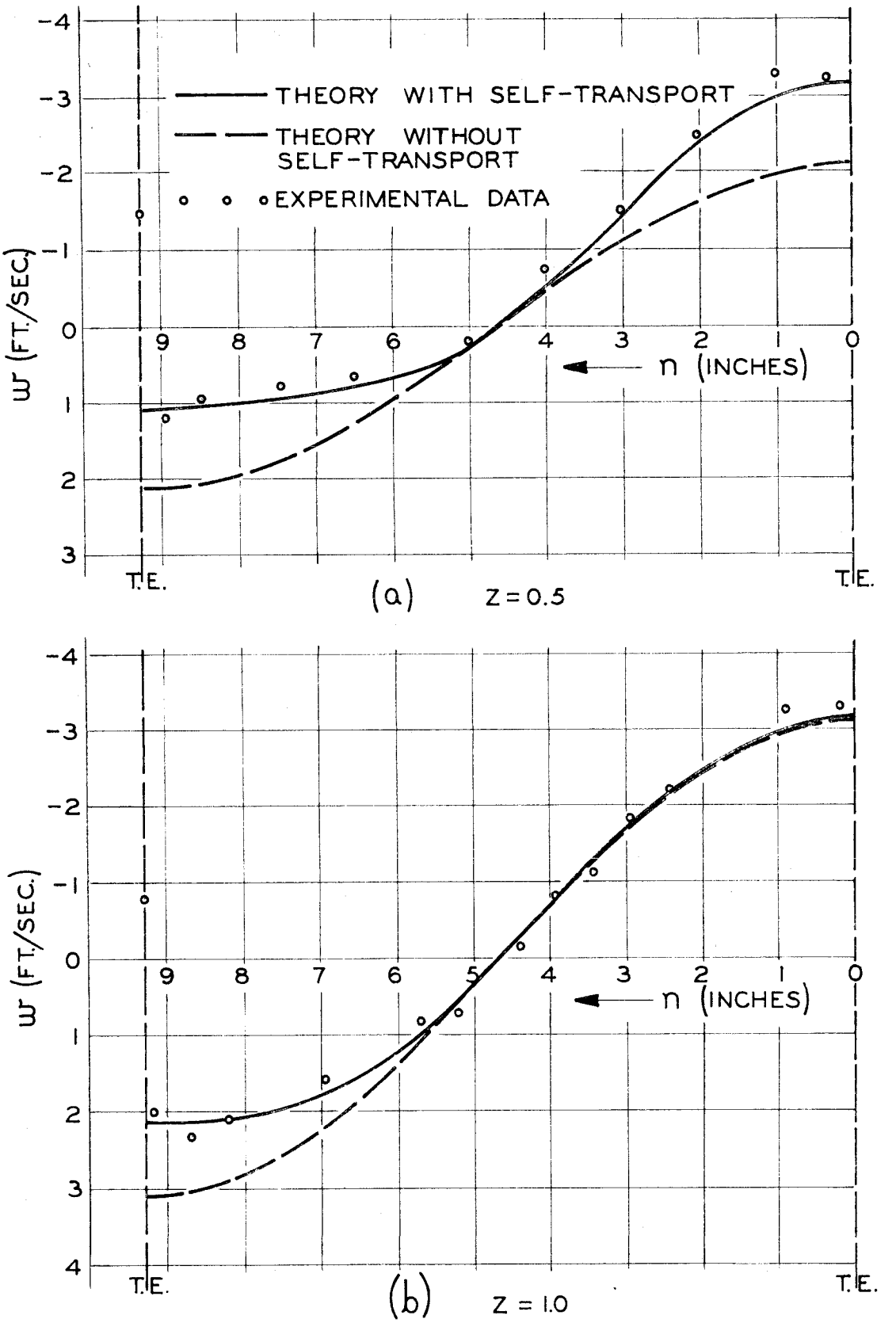

FIG. 46
INDUCED SPANWISE VELOCITIES DOWNSTREAM
CONFIGURATION II

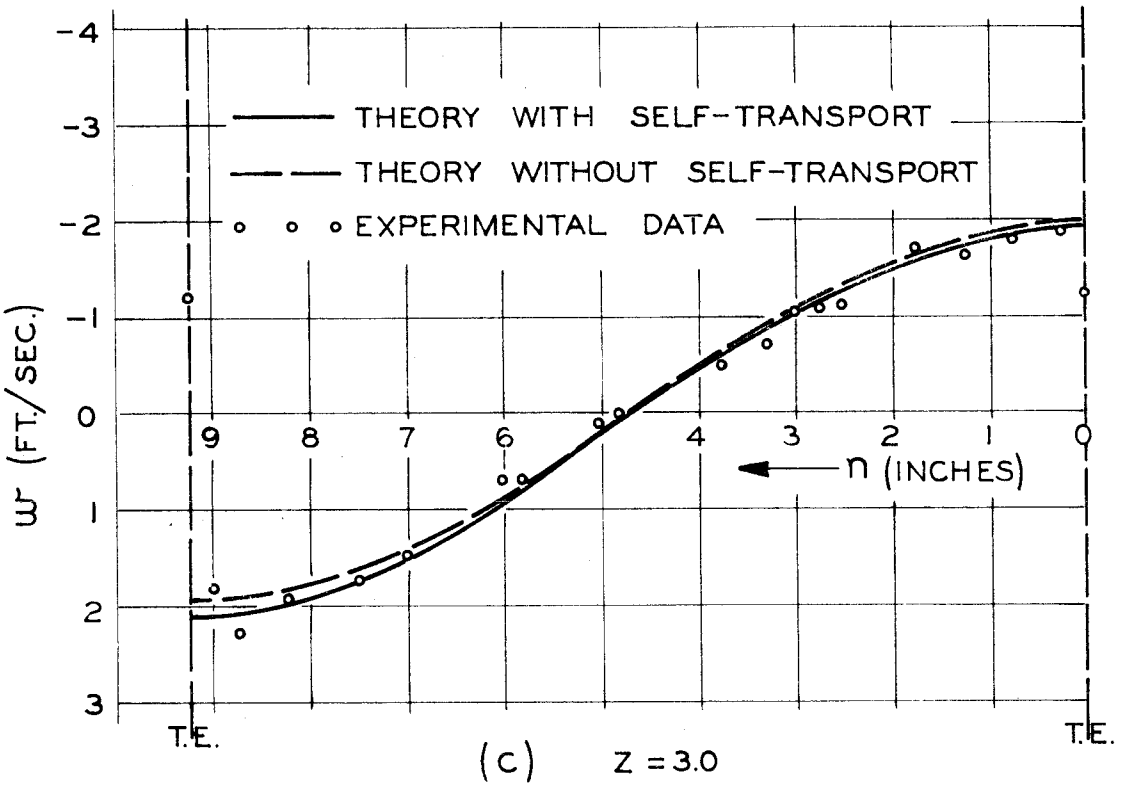

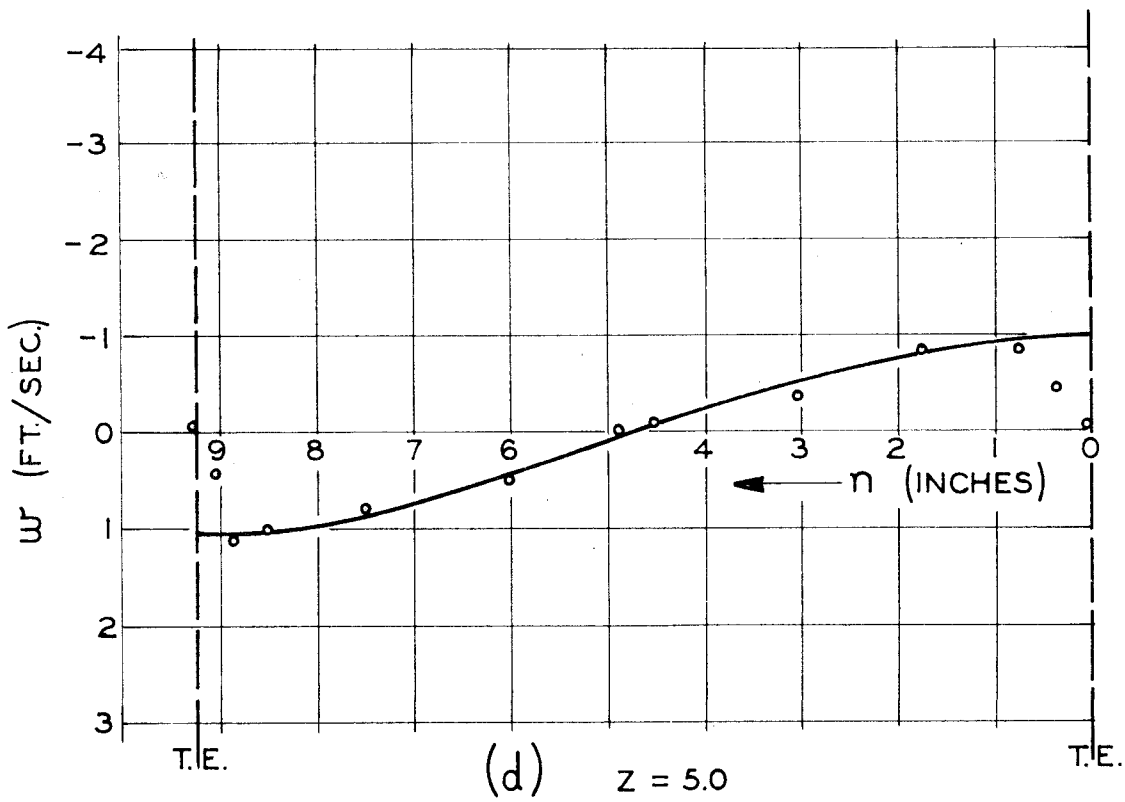

FIG. 46 CONCLUDED
INDUCED SPANWISE VELOCITIES DOWNSTREAM
CONFIGURATION II

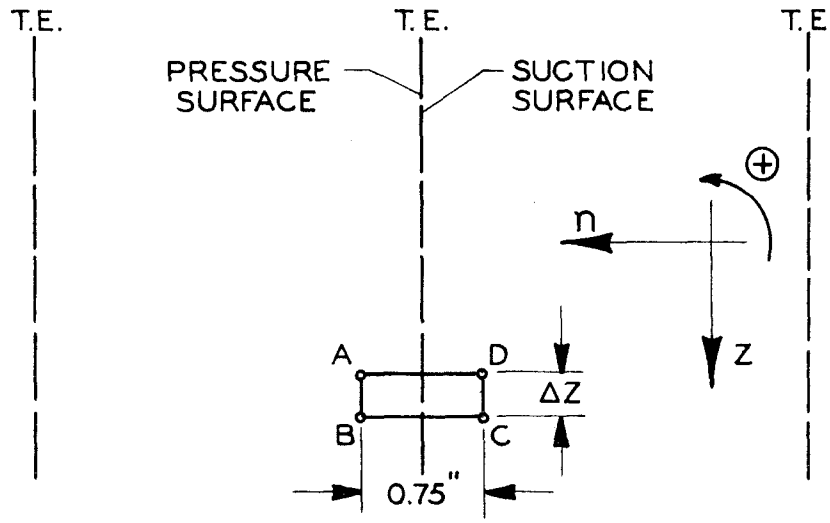

FIG. 47 TRAILING EDGE CIRCULATION

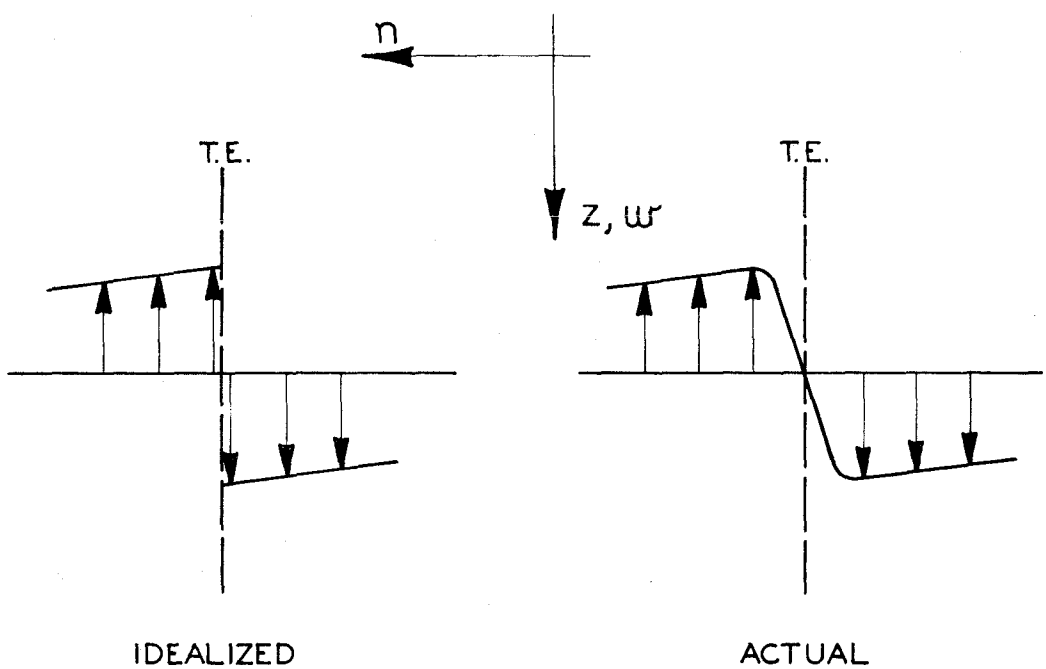

FIG. 48 TRAILING EDGE VELOCITY

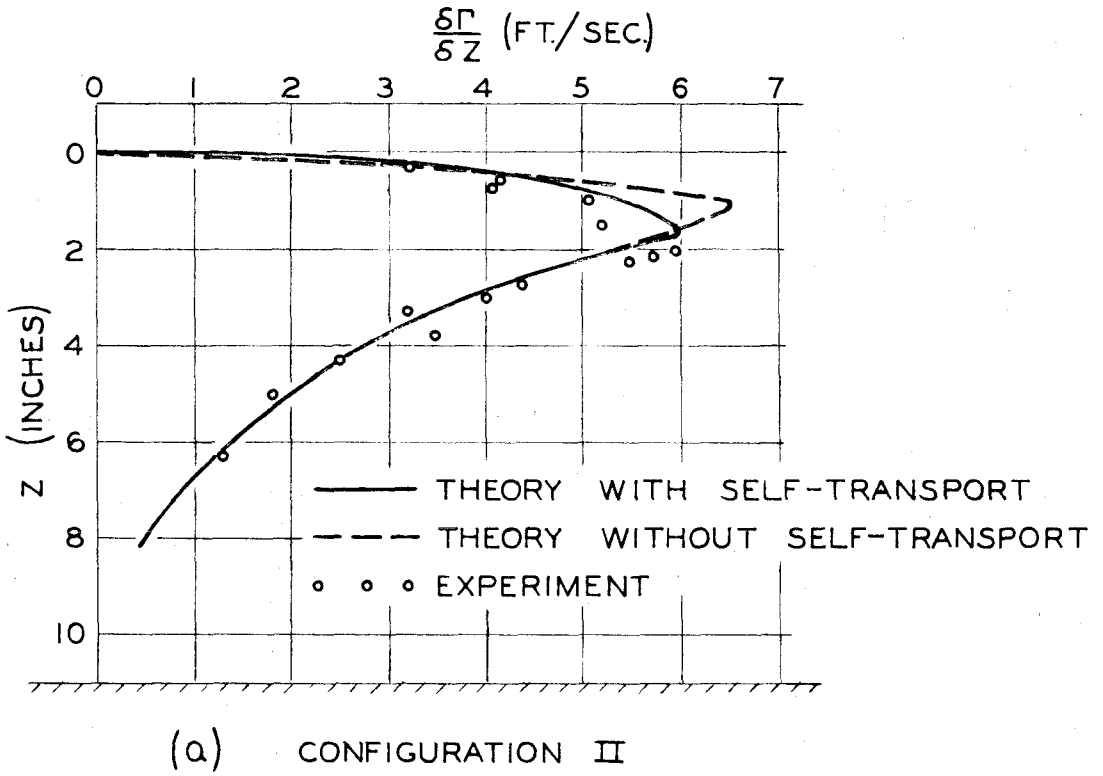

(a) CONFIGURATION II

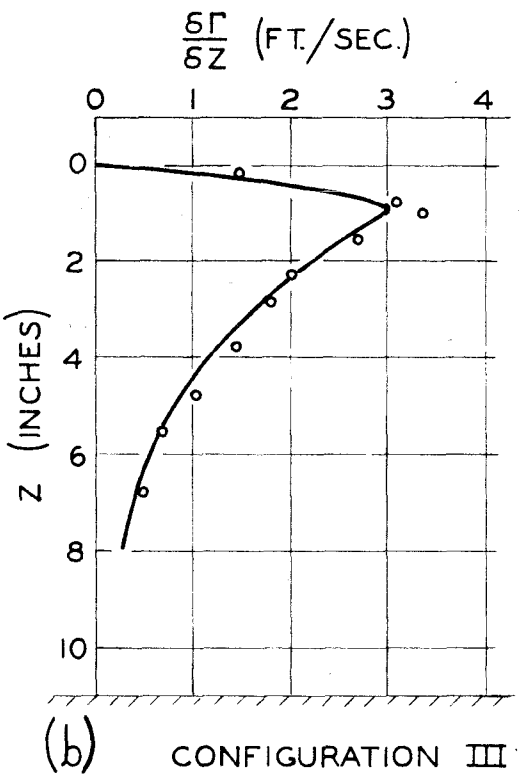

(b) CONFIGURATION III

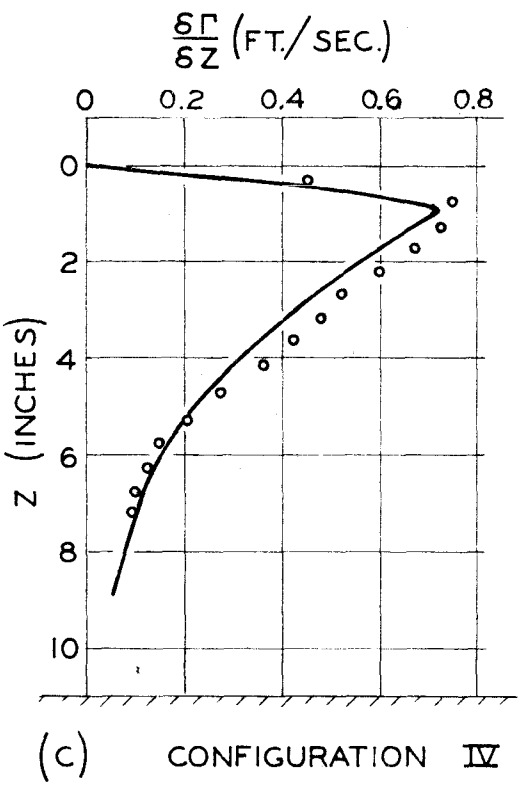

(c) CONFIGURATION IV

FIG. 49
TRAILING EDGE CIRCULATION

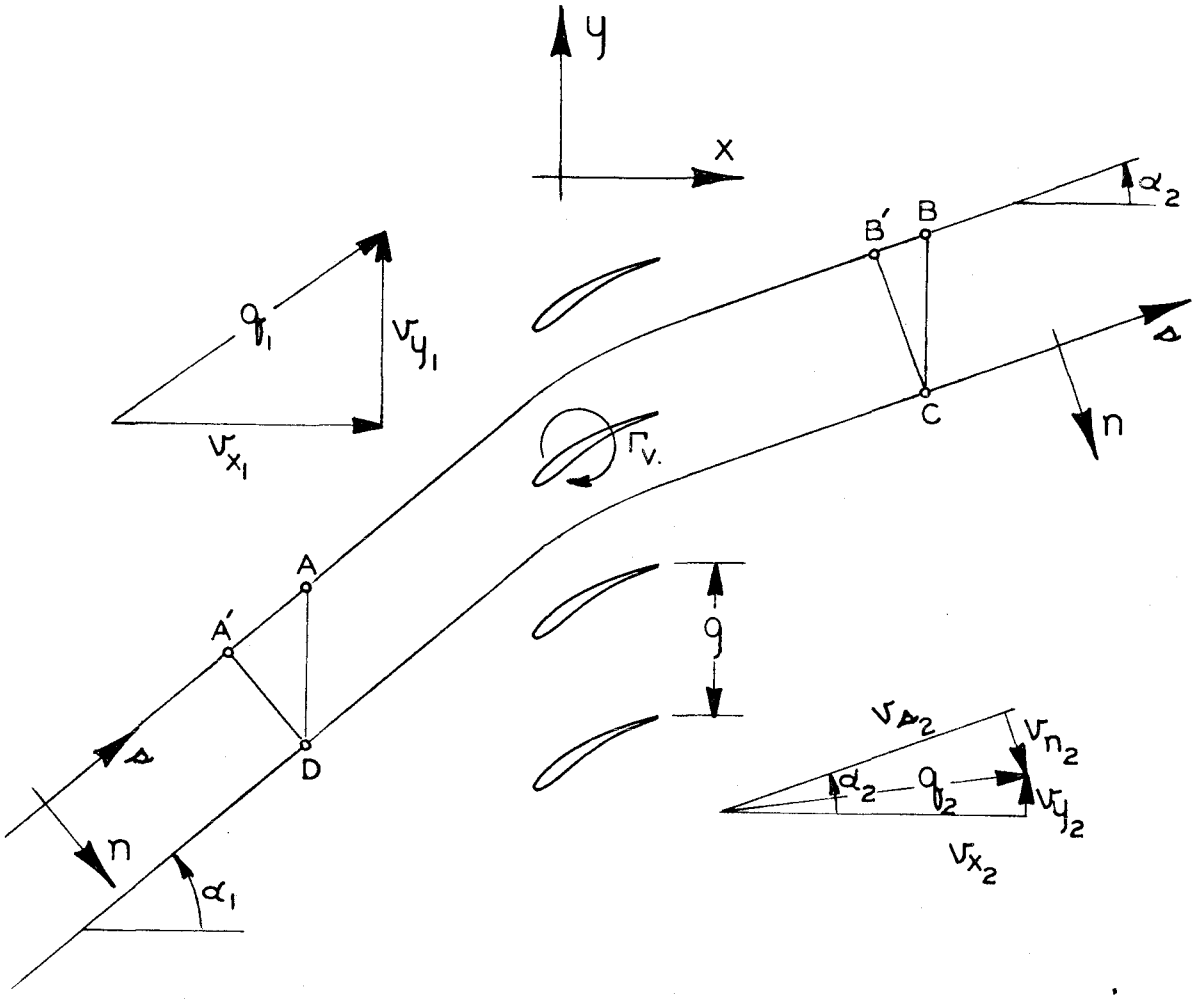

FIG. 50 TWO DIMENSIONAL CIRCULATION PATH

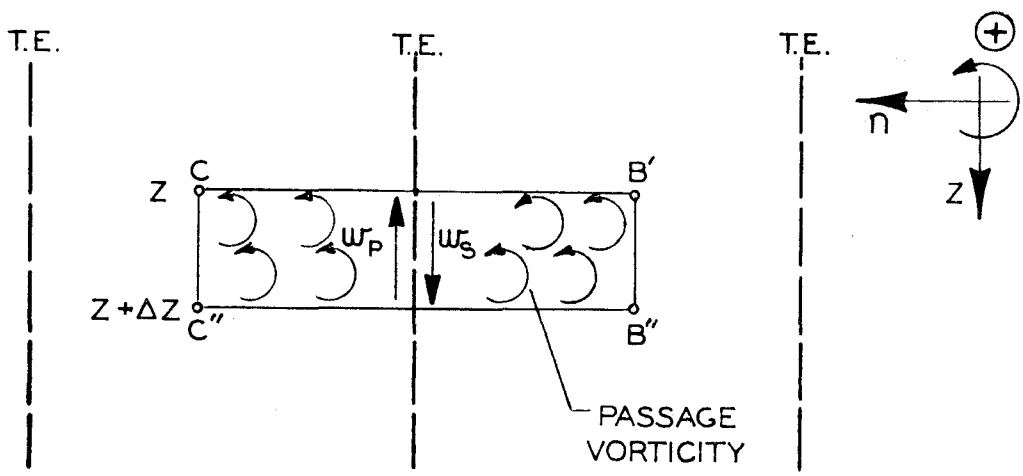

FIG. 51 CIRCULATION AT STN. 2

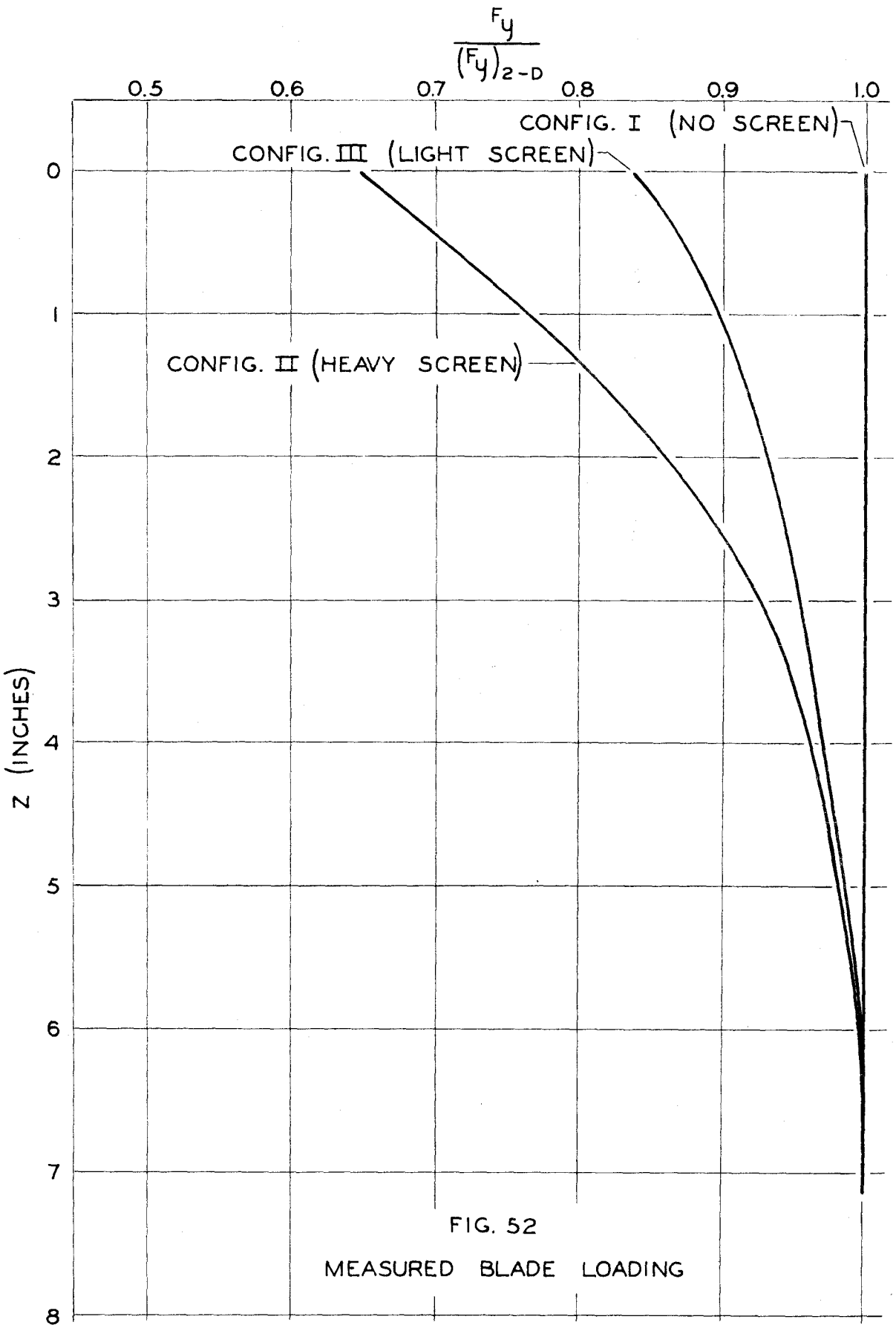

FIG. 52

MEASURED BLADE LOADING

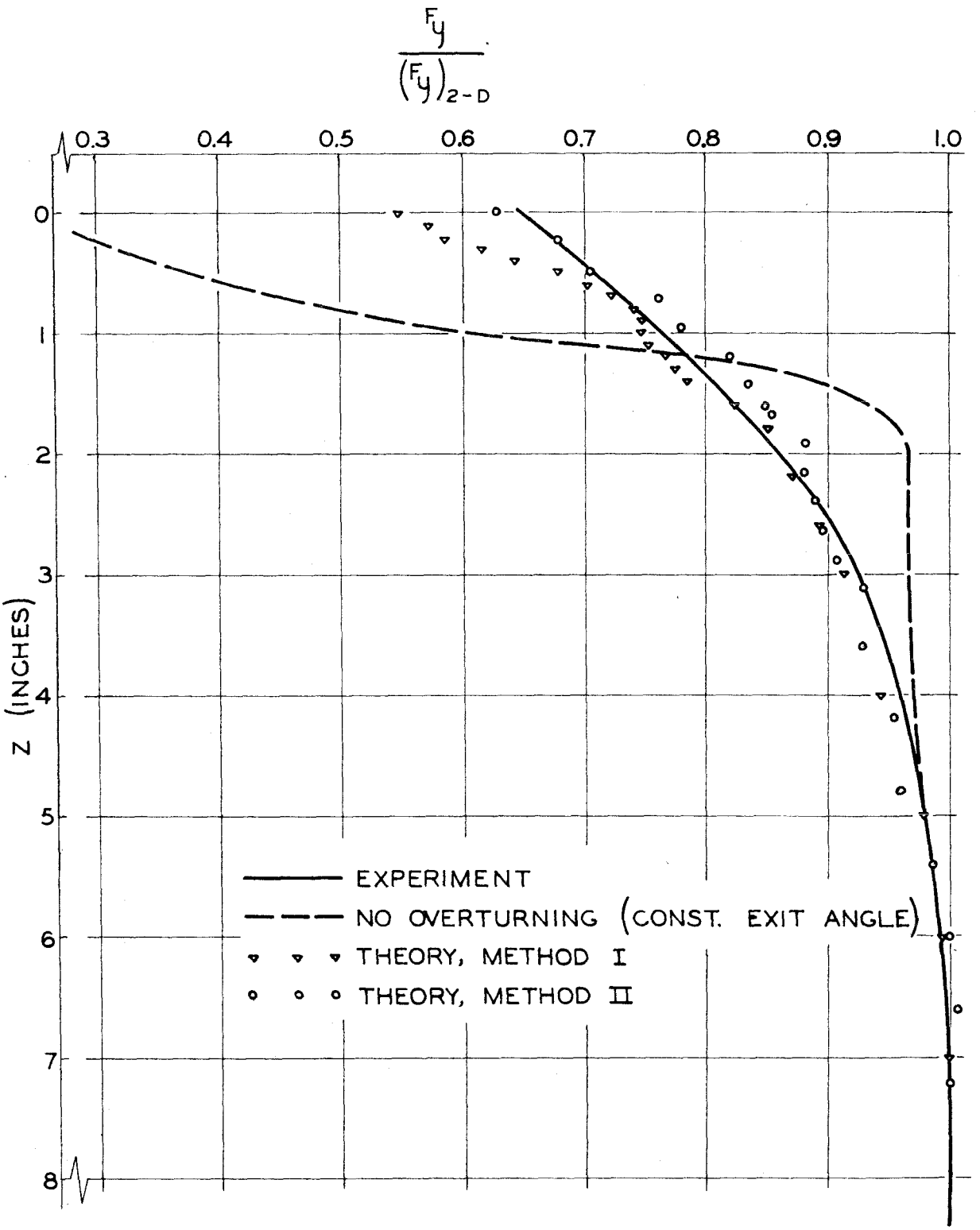

FIG. 53

BLADE LOADING, CONFIGURATION II

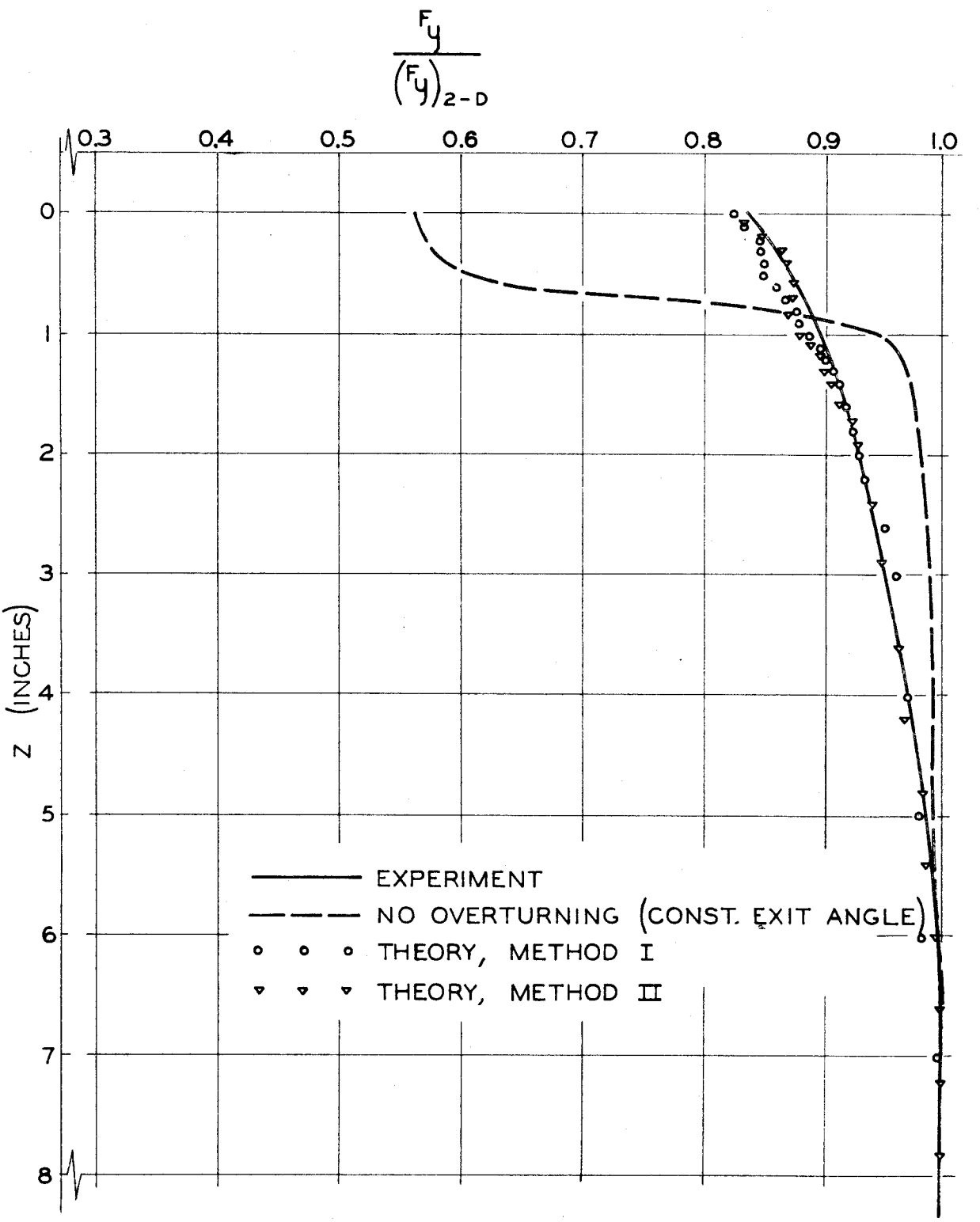

FIG. 54

BLADE LOADING, CONFIGURATION III

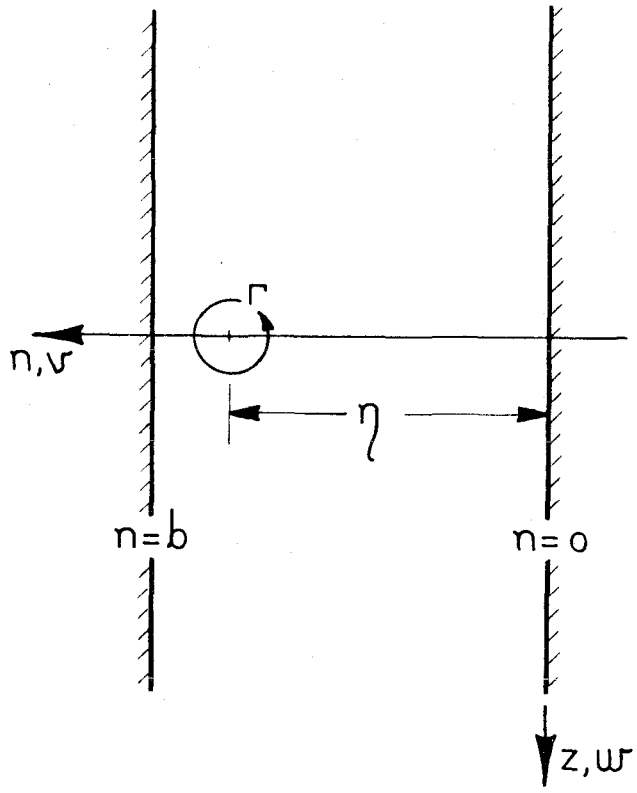

FIG. 55 CHANNEL CONFIGURATION